A MAGNETIC RESONANCE STUDY OF THE VANADIUM-CHROMIUM SYSTEM AND OF THE NÉEL TEMPERATURES OF THE CHROMIUM-RICH ALLOYS

by

Thomas Peter Graham

A Dissertation Submitted to the
Graduate Faculty in Partial Fulfillment of
The Requirements for the Degree of
DOCTOR OF PHILOSOPHY

Major Subject: Physics

Approved:

Signature was redacted for privacy.

In Charge of Major Work

Signature was redacted for privacy.

Head of Major Department

Signature was redacted for privacy.

Dean of Graduate College

Iowa State University
Of Science and Technology
Ames, Iowa

1967

TABLE OF CONTENTS

I. INTRODUCTION

Nuclear magnetic resonance (NMR) has been used extensively in the study of the properties of solids. One can regard a nuclear moment embedded in a solid as a probe of its surroundings. When the values of the pertinent nuclear properties--spin, magnetic and electric moments--are known, the resonance parameters--position, resonance width and shape and relaxation times--can be interpreted to provide information about the nuclear environment.

A nuclear magnetic moment interacts with its surroundings in a variety of ways. In general, an interaction which produces a magnetic field at the nuclear site (or an electric field gradient if we are considering the quadrupole moment of the nucleus) will change the resonant frequency from the value obtaining for a "bare" nucleus. Some of the mechanisms of interest for metallic solids are magnetic dipolar couplings between nuclei which are usually the dominant source of resonance linewidth and magnetic hyperfine interactions between a nucleus and surrounding electrons which generally determine the position (in frequency or field) of a resonance.

In metallic substances, the hyperfine interaction with the electrons in the conduction band are of prime importance. In addition to determining resonance position, these electrons are efficient in transporting energy from the nuclear spin system to the lattice, i.e. providing the mechanism for

spin-lattice relaxation. For transition metals, core electrons must also be included in the interpretation of the effect of hyperfine interactions. These interactions are usually sensitive to the details of the electronic structure and, in turn, so are the resonance parameters. The number of electronic states at the Fermi level is one property which is strongly reflected in the resonance parameters. If a rigid band (or two band, for transition metals) scheme is appropriate, the variation of this density of states with the number of conduction electrons per atom can be studied by alloying. Other changes in the internal magnetic fields, for example, those accompanying the insertion of impurities into a metal or resulting from magnetic or crystallographic phase changes, will also be evidenced by changes in the resonance parameters.

The system under investigation here, the vanadium-chromium system, forms a complete solid solution of body-centered-cubic alloys which show no evidence for the formation of intermetallic compounds (1). Here, then, one can vary the electron per atom ratio from five to six maintaining the bcc crystal structure. The vanadium-51 isotope is approximately 100% abundant, possesses a large magnetic moment and a small quadrupole moment. The chromium isotope with non-vanishing moment, chromium-53, is only 10% abundant and has a small magnetic moment. Consequently, the vanadium-51 resonance can be observed essentially throughout the alloy system (i.e. from

100% to 0.25% vanadium in chromium) at room temperature. Because of its small magnetic moment and relatively large quadrupole moment, the chromium-53 resonance is weak and can only be observed over a small range of alloy composition. In this case, then, one can use the vanadium resonance as a probe of the system.

The elements vanadium and chromium are known to exhibit anomalies in their magnetic (2, 3), thermal (4, 5, 6) and transport properties (7, 8, 9). In addition, the anomalies in chromium have been shown by neutron diffraction (10) to be associated with a magnetic phase transformation from a non-magnetic state to an antiferromagnetic state. Several investigators (11, 12) have indicated that the ordering temperature is extremely sensitive to the presence of small alloying concentrations of other transition metals. The vanadium-51 resonance and to a lesser extent the chromium-53 resonance can be used to investigate the occurrence of antiferromagnetism in these alloys.

II. THEORY

A. Basic Ideas of Nuclear Magnetic Resonance

A nucleus possessing spin angular momentum $\hbar\vec{I}$ will have associated with it a magnetic moment $\vec{\mu}$. These are related by

$$\vec{\mu} = \gamma_n \hbar \vec{I} \tag{1}$$

where $\vec{I}$ is the nuclear spin operator and γ_n is the gyromagnetic ratio which depends on the nuclear state involved. In NMR, one is only concerned with the nuclear ground state. In the presence of an external magnetic field $\vec{H}_o$, the Hamiltonian can be written as

$$\mathcal{H} = -\gamma_n \hbar \vec{I} \cdot \vec{H}_o \tag{2}$$

The nuclear magnet thus has 2I + 1 equally spaced energy levels

$$E = -\gamma_n \hbar H_o m \; ; \; m = I , I - 1 , \ldots , -I \tag{3}$$

where m is the magnetic quantum number. The frequency of a transition between adjacent levels is

$$\nu = \frac{\gamma_n H_o}{2\pi} \tag{4}$$

These transitions can be induced by the application of an alternating magnetic field perpendicular to $\vec{H}_o$ (13).

In thermal equilibrium, the level populations of a system of nuclear spins are governed by the Boltzmann factor, $\exp(-E/k_B T)$, where E is the energy of a level, T the absolute temperature and k_B the Boltzmann constant. The absorption of energy from the alternating magnetic field requires a net

population difference between levels, otherwise the absorption would equal the emission. This difference is maintained through the interaction of the spin system with the lattice. The spin-lattice relaxation time T_1 is a measure of the efficiency of the interaction and is closely related to the resonance shift in metals.

B. Magnetic Hyperfine Interaction

Fermi (14) has shown that the Hamiltonian describing the magnetic hyperfine interaction between a nucleus and its electrons is given by

$$\mathcal{H} = \gamma_e \gamma_n \hbar^2 \vec{I} \cdot \sum_i \left(\frac{8\pi}{3} \vec{S}_i \, \delta(\vec{r}_i) + \frac{\vec{L}_i}{r_i^3} - \frac{\vec{S}_i}{r_i^3} + \frac{3(\vec{S}_i \cdot \vec{r}_i)\vec{r}_i}{r_i^5} \right) \quad (5)$$

where the sum is over the electrons. $\vec{I}, \vec{L}, \vec{S}$ represent, respectively, the nuclear spin, electron orbital and electron spin angular momentum operators. γ_e and γ_n are the electronic and nuclear gyromagnetic ratios respectively, $\vec{r}$ the electron's position relative to the nucleus and $\delta(\vec{r})$ the Dirac delta function. The first term is called the (Fermi) contact term. It accounts for the interaction of the nucleus with the s-electrons which have non-vanishing wave-functions at the nuclear site. The second term arises from the interaction of the nucleus with the magnetic field due to orbital currents. The last two terms represent the spin-dipolar interaction between the nuclear moment and the electronic moments. The diagonal matrix elements of this Hamiltonian give rise to the

Knight shift which is the shift of resonance position with respect to a non-magnetic, non-metallic reference. The off-diagonal matrix elements contribute to the spin-lattice relaxation time. We shall discuss these two aspects of the hyperfine interaction separately at first and then exhibit the relationship between the shifts and relaxation times.

1. Knight shift

The original explanation of Knight's observations (15) that, in simple metals, the resonance occurred at smaller external fields than the resonance in diamagnetic compounds, measured at the same frequency, assumed that only the contact part of the hyperfine interaction was operative (16). In a magnetic field, the electrons at the Fermi surface acquire a net spin polarization. Since the s-electrons wave-functions do not vanish at the nucleus, they will provide a spin polarization and hence a magnetic field at the nucleus in addition to the external field. The relative shift in resonance position due to the contact term can be written as

$$K_s = \left(\frac{\Delta H_s}{H_o}\right) = \frac{8\pi}{3}\chi_s \, \Omega \langle |u_k(o)|^2 \rangle_{FS} \qquad (6)$$

where the Pauli susceptibility per volume is given by

$$\chi_s = 2\mu_B^2 \, N_s(E_F). \qquad (7)$$

μ_B is the Bohr magneton, $N_s(E_F)$ is the density of s-electron states per unit energy range per volume for one direction of

spin at the Fermi level, Ω is the atomic volume and $<|u_k(o)|^2>_{FS}$ is the s-electron probability density at the nuclear site (r=o), averaged over the electrons at the Fermi surface. A detailed derivation can be found in Milford (17) or Slichter (18). This expression is consistent with the usual observations for simple metals that a) at constant frequency the metal resonance occurs at a lower field than that of a non-magnetic reference; b) the shift is independent of the external field; c) the shift is essentially independent of temperature; d) the shift increases with atomic number due to the increase of $<|u_k(o)|^2>_{FS}$.

When considering a metal having a partly filled band, as in the transition metals, the second term of Equation 5 has been shown to provide a significant contribution to resonance shifts (19). In the metal the angular momentum is quenched and thus there is no first order contribution. However, an appreciable contribution can be induced by the external field in second order. Clogston, Yafet and Jaccarino (20) have shown, in the tight binding limit, that this orbital contribution can be written as

$$K_{orb} = \left(\frac{\Delta H_{orb}}{H_o}\right) = 2\Omega<r^{-3}>_{metal}\chi_{orb} \qquad (8)$$

where $<r^{-3}>_{metal}$ is the average of r^{-3} over the band electron wave-functions in the metal (d-band in this case) and χ_{orb} is the analogue of the Van Vleck temperature independent

contribution to the susceptibility. This has been given by Kubo and Obata as (19)

$$\chi_{orb} = \mu_B^2 \sum_{n,n'} \int \frac{d^3k}{(2\pi)^3} \frac{f(E_{n\vec{k}}) - f(E_{n'\vec{k}})}{E_{n'\vec{k}} - E_{n\vec{k}}} \langle n\vec{k}|\vec{L}|n'\vec{k}\rangle \quad (9)$$

where f(E) is the Fermi distribution, n and n' label the filled and unfilled orbital levels respectively and $\vec{k}$ is the wavevector. Evaluation of this relation requires a detailed knowledge of the electronic structure. At present such knowledge is lacking and χ_{orb} must be obtained or estimated from experimental data. It might be remarked that this source of shift is the same as that which is responsible for the paramagnetic contribution to the chemical shifts in atoms and molecules.

The third and fourth terms in Equation 5 give rise to an anisotropic shift of the resonance as discussed by Bloembergen and Rowland (21). For cubic metals however, the contribution from these terms vanishes and so will not be discussed here.

Another contribution to the shift arises from core polarization (22). This mechanism is believed to be responsible for the occurrence of negative Knight shifts and strongly temperature dependent shifts in rare-earth and transition metal compounds (23). It is also responsible for the large, negative, internal magnetic fields at an iron or cobalt nucleus in those metals. Core polarization arises from the electrostatic exchange-coupling between the d-electrons and the inner shell

electrons. The coupling for an inner shell electron with spin parallel to the d-electron spin is different than that of an inner electron in the same shell but with spin antiparallel to the d-electron spin. As a consequence, the spatial part of the wave-functions will differ for the two spin states. For s-electrons this gives rise to a non-vanishing spin density at the nucleus and therefore a magnetic field via the contact interaction. Thus, in a magnetic field, a shift of the resonance occurs. Yafet and Jaccarino (24) have given, in the tight binding limit, the following expression for the relative shift due to core polarization

$$K_d = \left(\frac{\Delta H_d}{H_o}\right) = - \frac{8\pi}{3} \chi_d \Omega \langle |\varphi_{cp}(o)|^2 \rangle \qquad (10)$$

where χ_d is the d-band susceptibility per volume

$$\chi_d = 2\mu_B^2 N_d(E_F), \qquad (11)$$

$N_d(E_F)$ is the density of d-electron states per volume at the Fermi level for one direction of spin and $\langle |\varphi_{cp}(o)|^2 \rangle$ is the s-electron probability density due to the exchange interaction. As can be seen, this contribution to the total shift is negative and in addition χ_d is usually temperature dependent and leads to a temperature dependent Knight shift.

2. Spin-lattice relaxation time

The spin-lattice relaxation time, T_1, is a measure of the coupling of the nuclear spin system to the lattice. It is

defined as the time characteristic of the approach of the spin system to thermal equilibrium. It can be defined quantitatively by

$$\frac{dn}{dt} = \frac{n_o - n}{T_1} \tag{12}$$

where n is the population difference between adjacent energy levels and n_o is the value of this difference at thermal equilibrium. In terms of the macroscopic magnetization of a sample we may write (25)

$$\frac{d\vec{M}}{dt} = \frac{\vec{M}_o - \vec{M}}{T_1} \tag{13}$$

In metals, the most important relaxation mechanisms are due to coupling between the electrons at the Fermi surface and the nuclear spin via the magnetic hyperfine interaction given in Equation 5. Only the electrons near the Fermi surface are involved because the separation in energy between the nuclear magnetic levels is only about 10^{-4} electron volts. Energy conservation can be maintained by a change in the wavenumber of the electron involved.

The relaxation due to the contact term proceeds via a simultaneous spin flip of the nucleus and electron. Korringa (26) has shown this contribution to be

$$(T_1)_s^{-1} = \frac{64}{9}\pi^3\hbar^3\gamma_e^2\gamma_n^2 \langle|u_k(o)|^2\rangle_{FS}^2 \; N_s^2(E_F)k_BT \tag{14}$$

He was also able to show that T_1 is simply related to the Knight shift by

$$(T_1T)_s = \frac{\hbar}{4\pi k_B} \left(\frac{\gamma_e}{\gamma_n}\right)^2 \frac{1}{K_s^2} \qquad (15)$$

where T is the absolute temperature. The constancy of the product T_1T is well established for most metals which have been studied. For non-transition metals, the T_1's predicted from the Knight shifts on the basis of this equation are too short. This discrepancy cannot be removed by invoking additional relaxation mechanisms. For the alkali metals, much improved agreement is found by using Pines' correction to the free electron model which includes the interactions of the electrons with one another (27). For transition metals, however, the other terms in Equation 5 must be considered.

Obata (28) has shown that the orbital term in Equation 5 provides a relaxation mechanism in which the nuclear spin is flipped with a consequent change in the orbital momentum of the electron. The contribution to T_1 from this source can be written as

$$(T_1)^{-1}_{orb} = 4\pi\hbar^3 \gamma_e^2 \gamma_n^2 \langle r^{-3}\rangle^2_{metal} N_d^2(E_F) k_BT \left[\frac{2}{3} f\left(2 - \frac{5}{3} f\right)\right] \qquad (16)$$

where f is the fraction of $3d(\Gamma_5)$ states at the Fermi level and $\langle r^{-3}\rangle_{metal}$ is the average of r^{-3} over the d-electron wavefunction in the metal for those electrons near the Fermi level. This average differs from $\langle r^{-3}\rangle_{metal}$ in Equation 8. For χ_{orb} all the d-electron states contribute, here only those near the

Fermi surface can enter into the relaxation process. Since these averages are different and K_{orb} does not depend on $N_d(E_F)$, a Korringa-like relation does not exist between $T_{1\ orb}$ and K_{orb} (24).

The spin-dipolar terms in the hyperfine Hamiltonian can also provide a relaxation mechanism even in cubic metals. Korringa (26) and Obata (28) have discussed this. The contribution can be written as

$$(T_1)^{-1}_{dip} = 4\pi\hbar^3\ \gamma_e^2\ \gamma_n^2\ \langle r^{-3}\rangle^2_{metal}\ N_d^2(E_F)\ k_BT$$

$$[\tfrac{1}{49}\ (\tfrac{5}{3}f^2 - 2f - 2)] \qquad (17)$$

This contribution is approximately 1/25 of the orbital contribution and is expected to be small.

The core polarization mechanism can also provide a relaxation path. The d-electrons at the Fermi surface are coupled to the nuclei via the inner shell s-electrons and can take up energy from the nuclear spin system. Yafet and Jaccarino (24) have derived an expression for T_1. They give

$$(T_1)^{-1}_{d} = \frac{64}{9}\ \pi^3\hbar^3\ \gamma_e^2\ \gamma_n^2\ \langle|\varphi_{cp}(o)|^2\rangle^2_{FS}\ N_d^2(E_F)\ k_BT$$

$$[\tfrac{1}{3}f^2 + \tfrac{1}{2}(1-f)^2] \qquad (18)$$

A Korringa-like relation can be written as

$$(T_1T)_d = \frac{\hbar}{4\pi k_B}\ \left(\frac{\gamma_e}{\gamma_n}\right)^2\ \left[K_d^2\ [\tfrac{1}{3}f^2 + \tfrac{1}{2}(1-f)^2]\right]^{-1} \qquad (19)$$

Figure 1. The approach to equilibrium of the magnetization for a system of spin 7/2 nuclei with unequal level spacings in a magnetic field as a function of time in units of T_1. Case I -- all transitions initially saturated. Case II -- only the $1/2 \leftrightarrow -1/2$ transition initially saturated

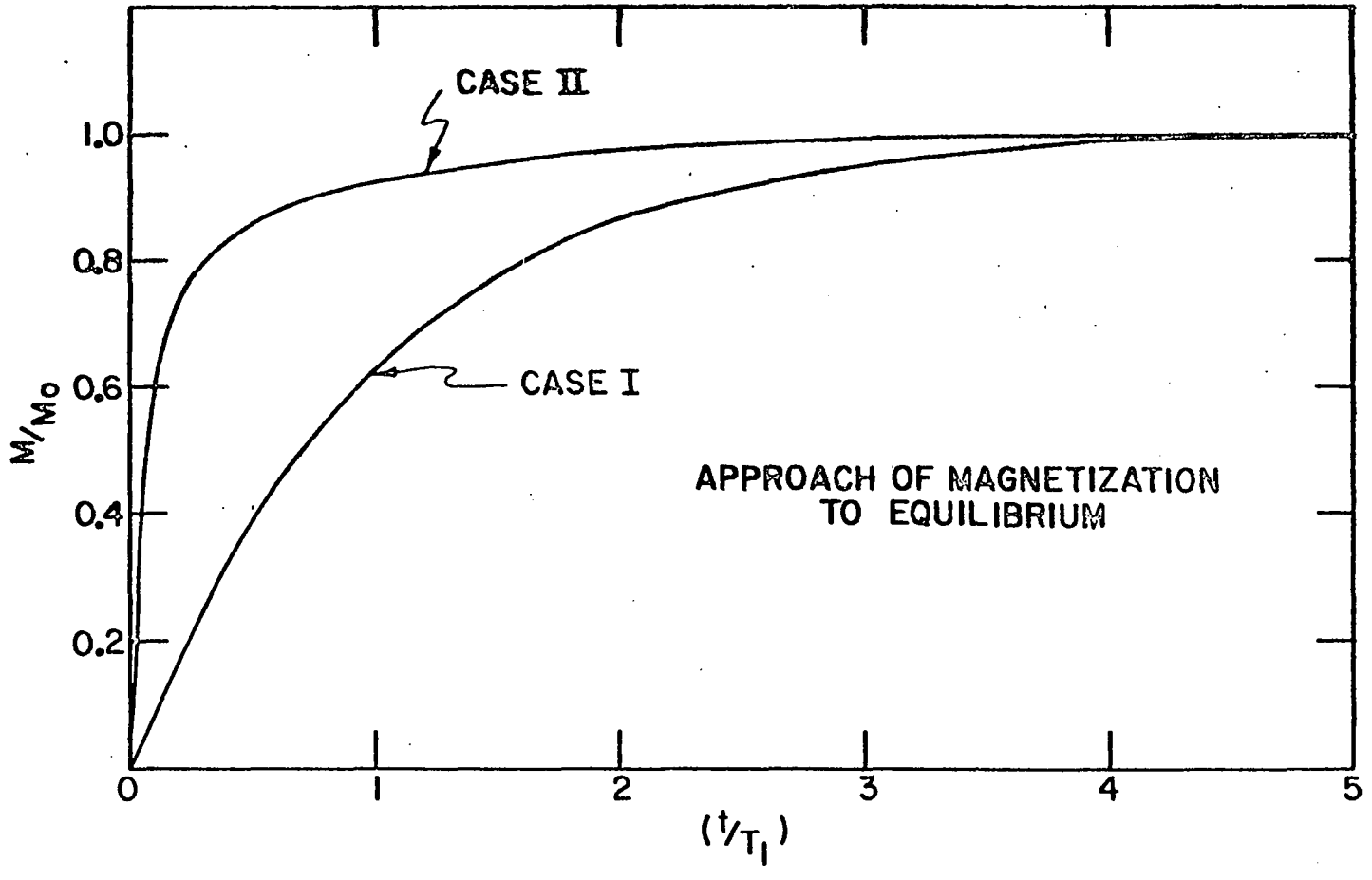
CASE II
CASE I
APPROACH OF MAGNETIZATION
TO EQUILIBRIUM
M/Mo
1.0
0.8
0.6
0.4
0.2
0
1
2
3
4
5
(t/T1)

The relation is quite similar to Equation 15 with the exception of the factor f involving the fraction of Γ_5 wave-function at the Fermi surface. This factor varies between 0.2 and 0.5 and thus tends to increase T_1 relative to a simple Korringa relation.

The mechanisms we have discussed are expected to be the important ones for the vanadium-chromium system. Another mechanism, which involves the electrons via the electric hyperfine interaction, is that between the nuclear quadrupole moment and the electric field gradient produced by the electrons (29). Because of the extremely small quadrupole moment of vanadium-51, this is not expected to be of importance.

Since the $(\frac{1}{T_1})$'s are essentially transition rates for the various processes, the total relaxation rate can be written as

$$(T_1)^{-1}_{ToT} = (T_1)^{-1}_{s} + (T_1)^{-1}_{orb} + (T_1)^{-1}_{dip} + (T_1)^{-1}_{d} + \ldots \quad (20)$$

In the above discussion, we have tacitly assumed that the energy levels of the spin system are equally spaced so that a single relaxation time is appropriate. If the energy levels are not equally spaced, perhaps due to a quadrupole interaction, the same mechanisms would be operative but the approach to equilibrium would not, in general, be described by a single characteristic time. It may be described by as many as 2I (I is nuclear spin here) relaxation times depending upon the initial conditions and the type of relaxation mechanism--magnetic or electric. Figure 1 illustrates this for a nuclear

spin equal to 7/2 and with magnetic relaxation (the type discussed above). In Case I, the levels are initially equally populated and the equilibrium magnetization M is approached with a single relaxation time. In Case II, the central transition ($1/2 \leftrightarrow -1/2$) is initially saturated while the other levels are in thermal equilibrium. In this case, the growth of magnetization for the central line is described by four relaxation times. The initial relaxation rate is fourteen times faster than in Case I. This indicates that some care must be exercised in comparing experimental relaxation times with theoretical predictions when there are quadrupole interactions present, as might be the case in our alloys. In Appendix A we have sketched the derivation of these effects.

C. Line Width

A number of physical processes may contribute to the line width of a resonance. For example, spin-lattice processes limit the lifetime of a nucleus in a given Zeeman state. From the Uncertainty relation, the resonance has a broadening of the order of $(2\pi\gamma T_1)^{-1}$. This is negligible for vanadium (0.06 Oe), but it can preclude detection of a resonance in a system with very short T_1. Other sources of broadening can be external to the sample: magnet inhomogeneity, usually a few tenths of an oersted; modulation broadening, for which a correction can be made (30); the presence of ferromagnetic impurities. These contributions can be minimized and the width ascribed to

mechanisms peculiar to the sample itself. We shall now discuss some of these mechanisms.

1. Dipolar broadening

In a system of nuclei, each nucleus experiences, in addition to an external field, a local field due to dipolar interactions with surrounding nuclei. This local field is on the order of μ/r^3, approximately a few oersteds. To obtain the shape and width of a resonance line it would be necessary to solve the problem of N nuclei in a magnetic field coupled to one another via the dipolar interaction, the Hamiltonian of which is (18)

$$\mathcal{H} = \frac{1}{2} \sum_{\substack{i,j \\ i=j}} \left[\frac{\vec{\mu}_i \cdot \vec{\mu}_j}{r_{ij}^3} - \frac{3(\vec{\mu}_i \cdot \vec{r}_{ij})\ (\vec{\mu}_j \cdot \vec{r}_{ij})}{r_{ij}^5} \right] \qquad (21)$$

For N of the order of 10^{23} the calculation is prohibitive. However, Van Vleck (31) has calculated the second moment of the resonance line from which useful information can be extracted. The dipolar second moment for like nuclei in a powdered sample is

$$\langle \Delta H_d^2 \rangle = \frac{4}{15} \gamma^2 \hbar^2 I(I+1) \sum_k r_{jk}^{-6} + \frac{1}{3} \gamma^2 \hbar^2 I(I+1) \sum_k r_{jk}^{-6} \qquad (22)$$

where the sum is over the nuclear sites. If another nuclear species is present in the sample, an additional term

$$\frac{4}{15} \gamma'^2 \hbar^2 I'(I'+1) \sum_k r_{jk}^{-6} \qquad (22')$$

is included. The sum is now over the sites appropriate to the particular nucleus. In a vector model, in which the magnetic moment precesses about the direction of the applied field (the z direction), the first term in Equation 22 comes from the static z-component of the field of the other moments. The second term arises from the oscillating x and y components of the precessing moments. These components induce transitions, thereby limiting the lifetime of the spin states. This type of process contributes to the width as previously mentioned. This second term is missing in the case of unlike nuclei since they are not precessing at the frequency necessary to cause transitions.

It is appropriate here to introduce a second relaxation time, T_2, which is reciprocally related to the line width. It is variously called the total or transverse relaxation time. To illustrate this, consider the net nuclear magnetization along the z-axis produced by putting a system of spins in a magnetic field in the z direction. If the magnetization is given a component perpendicular to the field, the transverse magnetization will decay at a rate described by (25)

$$\frac{dM_x}{dt} = \frac{-M_x}{T_2} \quad ; \quad \frac{dM_y}{dt} = \frac{-M_y}{T_2} \tag{23}$$

This decay is caused by the dipolar interactions among the spins and the relaxation back along the z-axis characterized by T_1. The first cause (usually the more important one),

results in a dephasing of the moments in the x-y plane. The individual nuclear spins precess around the external magnetic field. If initially the magnetization is perpendicular to the external field, then in a time of the order of T_2, the phase relationships among the nuclei will be lost. This is brought about by the different local z-fields produced by the static part of the interaction and by the mutual spin-flipping part which changes the local fields and hence the precession frequencies. The dipolar part of T_2 is designated T_2' and called the spin-spin relaxation or phase memory time. T_2 can be written as (32)

$$(T_2)^{-1} = (T_2')^{-1} + (2T_1)^{-1} \qquad (24)$$

and is related to the line width by

$$T_2 = a\,\gamma\Delta H \qquad (25)$$

where a is a number of the order of 1 and depends on the shape of the resonance line.

2. Quadrupolar broadening

A nucleus with spin greater than 1/2 possesses a quadrupole moment and, in an electric field gradient, no longer has its 2I+1 magnetic energy levels equally spaced in the presence of a magnetic field. The quadrupole interaction shifts the levels unequally and splits the resonance into its 2I components. For a gradient with axial symmetry, the Hamiltonian is given by (33)

$$\mathcal{H} = \frac{e^2qQ}{4I(2I-1)} [3I_z^2 - I(I+1)] \qquad (26)$$

where the z direction is along the symmetry axis of the gradient. The resonant frequency is given in the first order of perturbation theory by

$$\nu_{m\rightarrow m-1} = \nu_o + (2m-1) \frac{3e^2qQ}{8I(2I-1)h} (3 \cos^2\theta - 1) \qquad (27)$$

where $\nu_{m\rightarrow m-1}$ is the transition frequency between the m and m-1 magnetic levels, Q is the quadrupole moment of the nucleus, ν_o is the unperturbed resonance frequency, θ is the angle between the symmetry axis of the gradient and the magnetic field and q is the electric field gradient due to the extranuclear charge. For m = 1/2 there is no shift in the transition frequency. The m = 1/2 to m = -1/2 transition is called the central transition or line while the others are termed the satellites. In the second order of perturbation the central line is shifted. Its position is given by

$$\nu_{1/2\rightarrow -1/2} = \nu_o + \frac{9}{64} \frac{2I+1}{4I^2(2I-1)} \frac{e^4q^2Q^2}{h^2\nu_o} (1 - 9 \cos^2\theta)(1 - \cos^2\theta) \qquad (28)$$

In working with metals powdered samples are used. Thus the satellite absorption is spread over a frequency region for which $-1 < (3\cos^2\theta - 1) < 2$ due to the random distribution of crystallite orientations. The peak absorption occurs for $\cos^2\theta = o$. The intensity of the central line, if affected, will be spread over a frequency region for which $-16/9 <$

$(1 - 9\cos^2\theta)(1 - \cos^2\theta) < 1$. Absorption peaks occur for $\cos^2\theta = 0, 5/9$. The broadening of the central line is proportional to ν_o^{-1} in a powder since the shift given above has this dependence. The changes in the line width will depend upon the amount of satellite intensity remaining under the resonance line when the first order theory is appropriate. In second order the satellites are far removed and the width is proportional to the square of the quadrupole interaction divided by the working frequency. Kambe and Ollom (34) have given the corrections to the second moment for the case where the satellites are removed from the central line but the central line is unaffected. In this case, one can put limits on the strength of the quadrupole interaction. If we require that the inner satellite peaks are at least a line width $\delta\nu$ away from the line center, then from Equation 27

$$\frac{e^2qQ}{h} \geq \frac{4I(2I - 1)}{3} \delta\nu \qquad (29)$$

Similarly, if we require that the second order broadening be at most equal $\delta\nu/2$ then, using Equation 28

$$\frac{e^2qQ}{h} \leq \left[\nu_o \delta\nu \frac{128}{25} \frac{I^2(2I - 1)}{2I + 3}\right]^{1/2} \qquad (30)$$

The above discussion holds for a well defined gradient such as is found in a non-cubic metal. However, in cubic metals one is also able to observe quadrupole effects. These are due to the random gradients produced by defects such as dislocations

and impurities. Because defects have a profound effect on the resonance intensity via quadrupole interactions, we defer further discussion until we treat resonance intensity. A more complete discussion of quadrupole effects is found in Rowland (35).

3. Inhomogeneous Knight shift broadening

When one introduces an impurity into a metal, as in alloying, the potential, or excess charge, is screened off by a redistribution of the conduction electrons. If this charge redistribution alters the density of charge of electrons at the Fermi level at neighboring nuclei, then one expects the Knight shift to change. Early experiments (36) indicated that the shift was approximately constant in dilute alloys. This was interpreted in terms of Mott's theory of impurity scattering which gave a short range exponential screening of the impurity (37). Recent experiments, however, indicate that an impurity atom will affect a hundred or so neighbors. The early experiments appear now to have been complicated by quadrupole effects. Drain (38) has studied silver-cadmium alloys (both spin 1/2, so no quadrupole effects) and to explain the line widths, found it necessary to include the effects of the impurity out to at least the second nearest neighbors. He also found that the Knight shifts decreased linearly with increasing cadmium concentration throughout the alpha phase (0-40% Cd). Rowland (39) has studied silver alloys containing many different

solutes and finds that his results are well described by the electron distribution proposed by Friedel and his co-workers (40, 41, 42).

The impurity is considered as a spherical square well and the scattering from it analyzed by the partial wave method. The relative change in charge density at the Fermi level is found to fall off at large distances from the impurity as

$$\frac{\Delta\rho}{\rho} \propto \frac{\sin(2k_F r + \Phi)}{(k_F r)^2} \qquad (31)$$

As a result of this distribution, each shell of nuclei around an impurity will, in general experience a different charge distribution and hence have a different Knight shift. Blandin and Daniel (41) have shown that this leads to an average Knight shift proportional to the impurity concentration and a contribution to the second moment quadratic in the concentration and external field.

4. Miscellaneous sources of broadening

Drain (43) has considered the effect of the bulk magnetism of the sample on the resonance line width in powders. The demagnetizing field of a given particle and the field due to its neighbors change the field experienced by the nuclei in the particle. The overall effect is to produce a contribution to the line width which is estimated to be

$$\Delta H_{demag} = 3\chi_v H_o \qquad (32)$$

where χ_v is the volume susceptibility.

Ruderman and Kittel (44) have shown that nuclei can be coupled to one another via the conduction electrons. One process, called indirect exchange coupling, will cause a broadening of the resonance if unlike nuclei are present. In this process an s-electron interacts with a nucleus via the contact interaction, then interacts with a second nucleus also via the contact interaction. This, in effect, couples the nuclei with a coupling constant proportional to the product of the respective hyperfine coupling constants. For elements of mass 100 or more this mechanism provides a substantial portion of the resonance width. Other electron-coupled interactions are possible but are weaker than the indirect exchange.

If a nucleus is situated at a non-cubic site in a metal, it is possible to have an anisotropic Knight shift. The nucleus interacts through the dipolar part of the hyperfine interaction, Equation 5, with the non-s-electrons present at the Fermi surface. Bloembergen and Rowland (21) have shown that the absolute shift in field for axial symmetry and a single crystal is

$$\Delta H_{anis} = \mu_B^2 \, \Omega \, N(E_F) \, q \, (3 \cos^2\theta - 1) \, H_o \qquad (33)$$

where q is a measure of the charge anisotropy at the Fermi surface. In a powder the angle function gives rise to an asymmetric line. The line width increases with the external field.

D. Resonance Intensity

Resonance transitions are induced by the application of an oscillatory magnetic field perpendicular to H_o. The resonance intensity, $I(\nu)$, is proportional to the imaginary part of the nuclear susceptibility induced by this field. The total intensity is proportional to

$$\int_o^\infty \chi_n''(\nu)\, d\nu \tag{34}$$

where (45)

$$\chi_n''(\nu) = \frac{\gamma^2\hbar^2}{4k_BT}\,\frac{\pi N\nu_o\, g(\nu)}{2I+1}\sum_{m=I}^{m=-I+1}\left|\langle m|I_+|m-1\rangle\right|^2 \tag{35}$$

where $g(\nu)$ is the normalized shape function. So we have

$$\text{Intensity} \propto \frac{\gamma^2\hbar^2}{4k_BT}\,\frac{\pi N\nu_o}{2I+1}\sum_{m=1}^{m=-I+1}(I+m)(I-m+1) \tag{36}$$

We see that the resonance intensity is proportional to the number N of nuclei present.

In practice what one obtains is the derivative of the resonance, the first moment of which is the intensity. In making relative measurements of a number of samples where the line shape does not change we can use the product of the peak-to-peak amplitude and the square of the line width of the derivative as a measure of the intensity (35). If the line width is constant then we need use only the amplitude.

We shall first discuss the effect of quadrupole interactions on resonance intensity. We have seen how a quadrupole interaction spreads the resonance absorption in a powder sample.

Consider, for example, a nucleus with spin 3/2 in a well defined gradient which is large enough to split the satellites away from the central line. We find, according to the matrix elements, that 30% of the intensity is in each satellite and that the remaining 40% is in the central line. If we do not have the same gradient at each nucleus but have a random distribution of gradients, then because the satellite splitting differs for each nucleus, we will have a further smearing out of the satellite intensity. For instance, in cubic KBr only 40% of the Bromine resonances is observed (46). In this case the gradients produced by dislocations have so smeared out the satellites that they are unobservable. If the gradients are sufficiently large the central line may also be unobservable. The presence of large, impurity induced gradients appears to be the reason for the absence of resonances in the hexagonal metals titanium and hafnium. In many cubic alloys part or all of the central line may be gone for the same reason. We shall now discuss the effect of impurities in cubic metals.

Upon introducing an impurity into a metal containing nuclei with quadrupole moments one expects the resonance of the host nuclei to be modified due to the difference in valence and size of the impurity. In the interpretation of earlier experiments (47), the valence effect was thought to be negligible. This was because the Mott theory of impurity scattering (37) gave a short range exponential screening of the

impurity. Experiments indicated that perhaps a hundred neighbors of an impurity were affected. Hence the effect of local strain which drops off as $1/r^3$ (35) was thought to be more important. However more recent work has indicated that the valence effects are predominant (except where the valence of the impurity is the same as the solvent) where now the screening behaviour is described by the ideas proposed by Friedel (40). Using the method of partial waves to analyze the scattering, he showed that the screening charge fell off with a sinusoidally modulated $1/r^3$ dependence.

Averbuch et al. (48) have shown that the gradients produced by strains in copper are not large enough to account for the quadrupole effects observed in dilute copper alloys. Rowland (49) has made an extensive study of the copper-63 resonance in alloys with many different solutes. He found a strong correlation between the number of nuclei whose resonance is made unobservable by the gradient produced by the impurity with the effective charge of the impurity. (The effective charge is the difference between solvent and solute charges.) There was little correlation with the strain due to the misfit of atomic size. Kohn and Vosko (50) calculated the charge distribution around an impurity and the gradient at lattice sites in its vicinity. The gradient is

$$q(r) = \frac{C}{r^3} \cos(2k_F r + \varphi) \qquad (37)$$

where k_F is the Fermi momentum, r the distance from the impurity, φ is a constant that depends on the phase shifts and C is a constant that depends on the phase shifts, the Sternheimer antishielding factor (51) and an enhancement factor due to the Bloch character of the electrons. This theory is in good agreement with the data of Rowland on the copper alloys.

In materials which under-go a transition from one phase to another (crystallographic or magnetic) the total resonance intensity should remain constant. As we approach a phase transition the resonance intensity in one phase will decrease and increase in the other phase (assuming that none of the mechanisms previously discussed renders either resonance unobservable). An illustration of the effect of a magnetic transition is afforded by the measurement of the proton resonances in $CuCl_2 \cdot 2H_2O$ (52). Above the Néel temperature there are four proton resonances due to the dipolar interaction with the copper ion. The dipolar field is on the order of 50 gauss. Below the Néel temperature eight resonances are observed, the doubling being due to the copper moments on two sub-lattices having oppositely directed moments. The dipolar field in this case is of the order of 1000 gauss.

MnF_2 is an example where, in contrast to $CuCl_2 \cdot 2H_2O$, the internal field is considerably larger than the external field in the magnetically ordered state. Jaccarino and Shulman (53) observed that at the Néel point the F^{19} resonance disappeared

abruptly. This was explained by the rapid rise at the Néel temperature of the average value of the manganese electron spin <S> and hence the local field at the fluorine nucleus. The fluorine resonance was thus displaced outside the range of the spectrometer. In zero external field, the effective field at a fluorine nucleus was found to be about 40,000 gauss. The above discussion indicates that at least in some cases the magnetic ordering temperature of a material can be determined by resonance methods.

Figure 2. Block diagram of the Varian V4200B NMR spectrometer system used for the steady state experiments

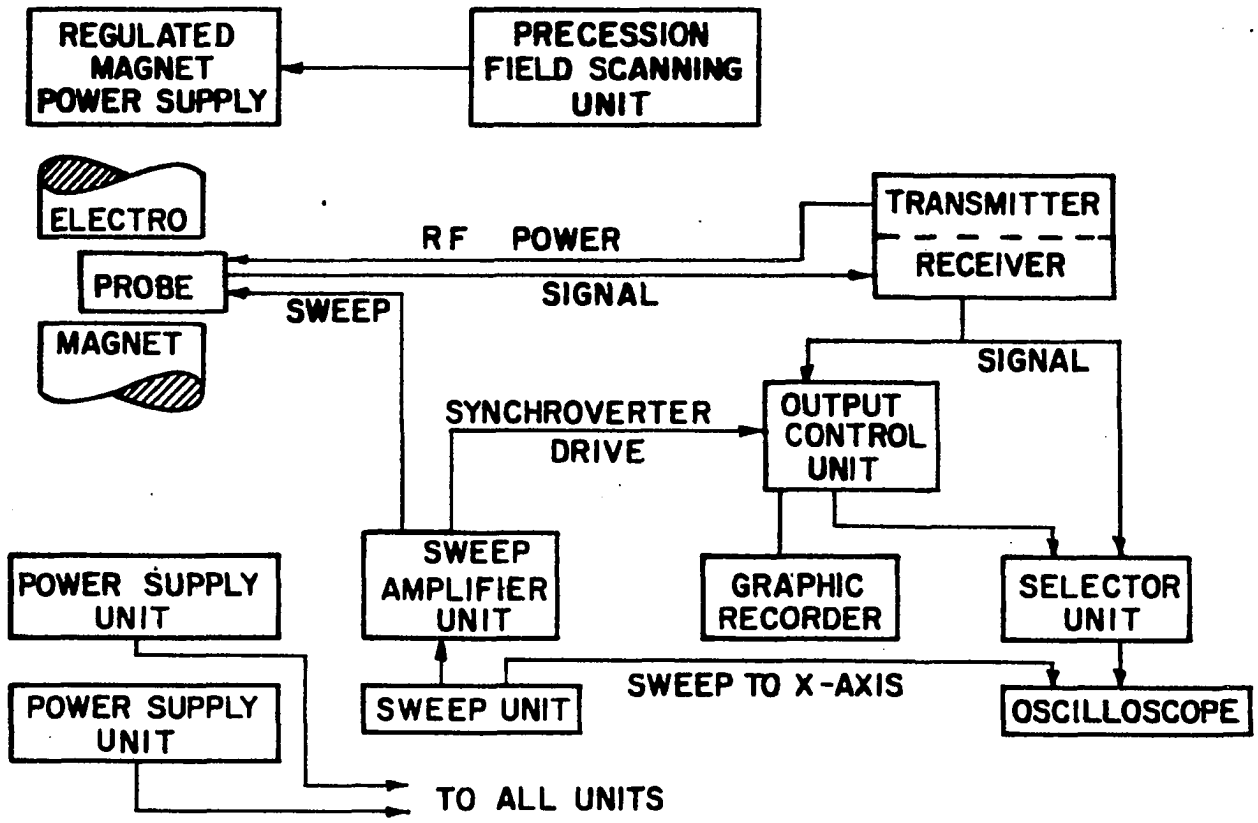
REGULATED MAGNET POWER SUPPLY
PRECESSION FIELD SCANNING UNIT
ELECTRO
PROBE
MAGNET
RF POWER
SIGNAL
SWEEP
TRANSMITTER
RECEIVER
SIGNAL
SYNCHROVERTER DRIVE
OUTPUT CONTROL UNIT
POWER SUPPLY UNIT
SWEEP AMPLIFIER UNIT
GRAPHIC RECORDER
SELECTOR UNIT
POWER SUPPLY UNIT
SWEEP UNIT
SWEEP TO X-AXIS
OSCILLOSCOPE
TO ALL UNITS

III. EXPERIMENTAL ASPECTS

A. Steady State Measurements

For the steady state measurements, a Varian V4200B variable frequency spectrometer was used in conjunction with a Varian 4012 12" electromagnet system. The spectrometer is of the crossed coil or induction type proposed by Bloch et al. (54). Bloch analysed the behaviour of the magnetization of a nuclear spin system in the presence of a strong external field and a weak radio-frequency field in a plane perpendicular to the strong field. He obtained an expression for the total nuclear susceptibility $\chi = \chi' + i\chi''$ · χ'' produces a magnetization which is out of phase with the r-f field inducing the transitions and is responsible for the energy absorption by the nuclear spin system. The component χ' produces a nuclear magnetization in phase with the r-f field and describes the dispersion accompanying the absorption. These components of magnetization are observed by the voltage they induce in a receiving coil which is placed with its axis perpendicular to both the external field and the axis of the r-f (transmitting) coil. By leaking some of the r-f voltage into the receiving coil with appropriate phase, either component of the magnetization can be observed.

The block diagram in Figure 2 depicts the major components of the spectrometer system. The transmitter contains a tunable (2-16 MHz) oscillator and r-f amplifier for driving the

transmitter coil in the probe. The probe contains three mutually orthogonal coils; the r-f coil which supplies r-f power to the spin system, the receiver coil which picks up the nuclear signal and a set of modulation coils with axis parallel to the external field. There is a cylindrical hole through the probe along the axis of the receiver coil which accepts the sample. Also in the probe are two sets of flux paddles for adjusting the leakage between the transmitter and receiver coils. The sweep unit supplies the modulation power and also provides the reference signal for the phase sensitive detector. The magnetic field is modulated at an audio frequency (40 Hz) to take advantage of the narrow bandwidths possible with phase sensitive detection. The receiver amplifies and demodulates the r-f picked up by the receiver coil. From the receiver, the audio carrier goes either to the oscilloscope for display or to the output control unit. This unit amplifies the detected audio signal from the receiver, rectifies the signal by means of a chopper-type phase detector and filters the resulting dc signal for driving a graphic recorder.

The magnet system consists of a stable, regulated high-voltage power supply and a magnet with pole caps tapered from 12" to 5" and a 1.75" air gap. The combination provides a maximum field of about 16.5 KOe. The frequency of the spectrometer is usually held constant and a field scanning unit, which controls the magnet current, is used to sweep through

resonance by slowly altering the polarizing field of the electromagnet.

Due to the detection scheme used, the derivative of the resonance is obtained. The absorption mode is used when measuring line width. The peak-to-peak width of the absorption derivative corresponds to the width between the points of maximum and minimum slope of the absorption. When the resonance line is symmetric, the center of the resonance is most easily measured using the dispersion mode since the peak of the dispersion derivative corresponds to the resonance center. When using the absorption mode, the zero crossing point is determined by comparison with the baseline above and below the resonance.

In measuring a Knight shift, the dial position on the scan unit at which the metal resonance center occurs is determined. The same is done for a diamagnetic reference solution. The difference in resonance fields is then determined by calibrating the dial of the scan unit in oersteds using the reference solution. Since the gyromagnetic ratio of the reference nuclei is known and the experiment is done at a fixed frequency determined by an electronic counter (CMC or H-P), the resonance field of the reference nuclei can be determined. With this calibration the shift can be determined. The same calibration procedure is used for the line width measurements. For making intensity measurements, the absorption derivative is used. The

line width and peak-to-peak amplitude are measured. The number of nuclei present is determined by weighing the sample so that comparisons among different samples, of the intensity/nucleus can be made. In comparing different nuclei, account must be taken of the differing spin etc. according to Equation 36.

Prior to taking measurements, the magnetic field was cycled over the range of the scan to avoid hysterisis effects. Usually 6 to 8 measurements were made to determine a shift or a line width. The modulation amplitude was usually kept to 1/5 the line width for the line width measurements to avoid modulation broadening. For the intensity measurements, the modulation and r-f field were held constant from sample to sample. Usually 3 to 4 separate determinations of intensity were made.

For measurements at temperatures other than room temperature, various techniques were used. At liquid helium temperature, a double dewar was used. It consisted of an inner dewar for helium and an outer dewar jacket containing liquid nitrogen. The inner dewar projected 18" below the nitrogen jacket, the last 6" being a single dewar which fitted into the NMR probe. For liquid nitrogen temperature, a single dewar with a long tip which fitted into the probe was used. For temperatures between 77° K. and room temperature, cold nitrogen gas was blown across the sample which was in a dewar tube placed in

the probe. The cold gas was provided either by putting a heater in liquid nitrogen and boiling off the gas or by passing nitrogen gas under pressure through copper coils immersed in liquid nitrogen. The temperature could be varied by changing the heater voltage in the first case and by varying the flow rate of the nitrogen gas in the latter case. Low temperatures, approaching that of liquid nitrogen, could be attained more easily using the gas system. The temperatures above liquid nitrogen temperature were measured with a copper-constantan thermocouple which was embedded in the sample. With this system the temperature could usually be kept constant to within a degree during a measurement.

For temperatures above room temperature (up to about 250° C.), the nitrogen gas was passed through a pyrex tube filled with glass chips which was in an oven. As in the above, the temperature was controlled by the flow rate of the nitrogen gas.

B. Pulse Measurements

A pulsed NMR system in conjunction with a Harvey-Wells L-128A magnet system was used for these measurements. Bloch (25) has pointed out that if an intense r-f pulse is applied to the spin system at equilibrium in an external field the macroscopic moment acquires a non-equilibrium orientation. Following the pulse the macroscopic moment precesses around the external field and a transient signal can be observed as a

voltage in a pickup coil. In our system a single coil is used, acting both as the transmitter and receiver coil. As previously discussed the z component of the moment will decay back along the external field with characteristic time T_1 and the transverse components will decay to zero with characteristic time T_2. By using two pulses of appropriate width these relaxation times can be measured. For a given r-f field, the pulse width (duration of the pulse) determines the angular displacement of the moment during the pulse. The r-f field produces a torque which, acting for a time t rotates the components of the moment perpendicular to the r-f field through an angle $\theta = \gamma H_1 t$. H_1 is the magnetude of the r-f field. By using so-called 90° pulses and 180° pulses we can measure T_1 and T_2.

T_2 is usually determined by the echo technique introduced by Hahn (55). In this method a 90° pulse is followed at a later time τ by a 180° pulse. At time 2τ a spontaneous echo is observed. The height of the echo is described by

$$h = h_o \exp(-2\tau/T_2) \qquad (38)$$

By varying τ, T_2 can be obtained. The echo is formed in the following manner. At equilibrium the moment is parallel to the somewhat inhomogeneous external field (z axis). On applying a 90° pulse along the x axis the moment is flopped into the x-y plane along the y axis. As discussed in connection with Equation 23 there will be a dephasing and the moment in

the x-y plane will decay to zero. This decay is reflected in the voltage induced in the coil. When the 180^{o} pulse is applied at time τ the y components of the moments are rotated 180^{o} but remain precessing with the same sense. As a result at time 2τ they are back in phase and produce a moment which induces a voltage, the echo, in the coil. As an example consider the moment to be composed of two groups of moments in slightly different fields and hence precessing at different frequencies. At time τ one group has precessed through an angle $\omega_1\tau$ and the second through $\omega_2\tau$ in the x-y plane. After the 180^{o} pulse their angular positions are $180^{o} - \omega_1\tau$ and $180^{o} - \omega_2\tau$. From τ to 2τ they precess through angles $\omega_1\tau$ and $\omega_2\tau$ and thus at 2τ are both in phase. During the period from 0 to 2τ some of the nuclei have been dephased randomly due to the dipolar interaction and hence are not rephased. The echo height decreases as τ increases following Equation 38 above.

The usual method of measuring T_1 with two pulses is to use two 90 degree pulses separated by a variable time. The first pulse flops the magnetization into the x-y plane. After a certain time, part of the magnetization has relaxed back along the z-axis. The second pulse then flops this down into the x-y plane. Following a 90^{o} pulse there is a decay tail, the height of which is proportional to the magnetization. By measuring the height of the second decay as a function of the variable time between pulses, one can determine the relaxation

rate. We were unable to use this method, however, because the tail decayed so rapidly that by the time the receiver had recovered from the pulse, the tail was unobservable. The method used was to measure the height of an echo as a function of the time between applications of the 90°-180° pulse sequence which gives rise to the echo. This method has been suggested by Reich (56) as a method of obtaining crude measurements of short spin-lattice relaxation times. By keeping the time delay between the 90° and 180° pulses constant, we observe a constant fraction of the magnetization initially along the field direction (z-axis). By changing the rate of repetition of the two pulse sequence, we change the initial magnetization along the z-axis. The height of the echo is proportional to the initial magnetization so we are able to obtain the growth curve for the magnetization. We obtain T_1 by fitting the echo height data to

$$M = M_o (1 - \exp(-t/T_1)) \qquad (39)$$

or more simply by measuring the time at which M falls to 1-1/e of its equilibrium value. Here t is the time between applications of the 90°-180° pulse sequence.

The pulse system was constructed by R. A. Hultsch for his study of self-diffusion in lithium and sodium. It is based on the design of Buchta et al. (57) with minor modifications (58). Figure 3 shows a block diagram of the apparatus. The r-f source is a 5.25 MHz crystal controlled oscillator. The pulser

Figure 3. Block diagram of the spin echo spectrometer used for the pulse measurements

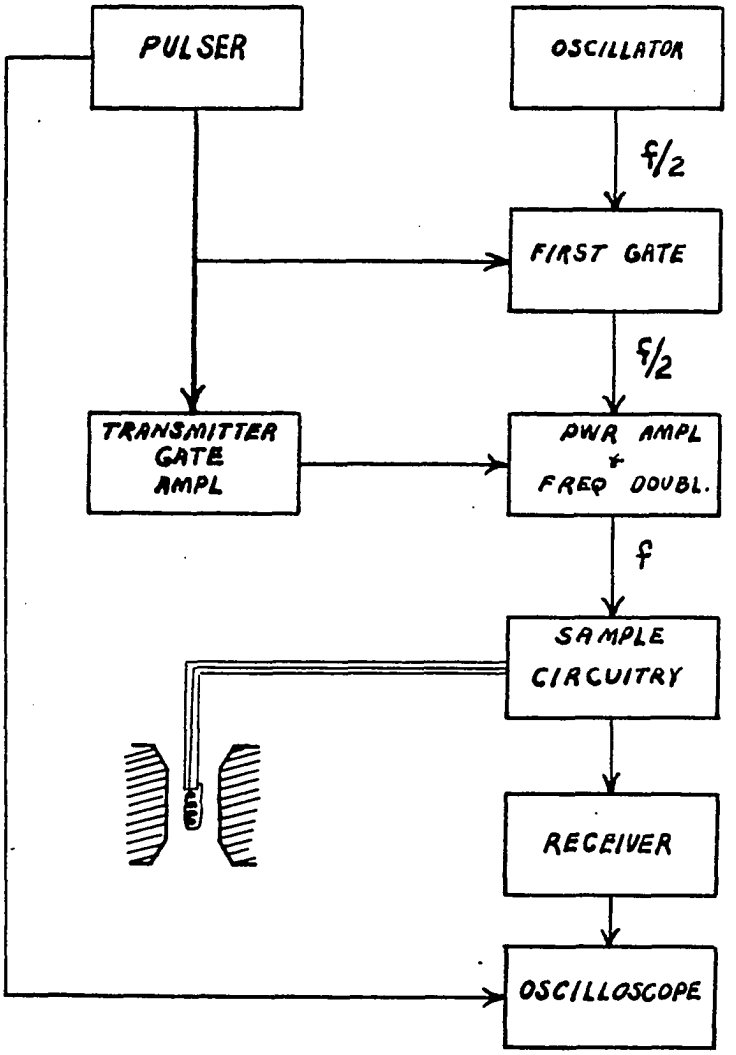
PULSER
OSCILLATOR
f/2
FIRST GATE
f/2
TRANSMITTER GATE AMPL
PWR AMPL & FREQ DOUBL.
f
SAMPLE CIRCUITRY
RECEIVER
OSCILLOSCOPE

operates the first gate allowing the 5.25 MHz signal to enter the amplifier and doubler. At the same time the pulser, after amplification, controls the frequency doubler. The pulser provides three pulses (only two of which were used here), the width of each being variable and the time interval between each being variable. The 10.5 MHz pulses are fed to the sample coil which is the tank of a tuned LC circuit. The same coil is used to detect the nuclear signal. The signal (including the transmitter pulses) is amplified and detected by the receiver and is displayed on an oscilloscope for measurement using a triggering pulse from the pulser. The echo height can be measured on the vertical axis of the oscilloscope. The horizontal axis can be calibrated in units of time. The pulse that initiates the two-pulse sequence can be used to trigger a H-P electronic counter operating in the time-interval mode. This enables us to measure the repetition rate.

The Harvey-Wells magnet system used for the pulse measurements consisted of a stable regulated high current power supply and a magnet with 12" cylindrical pole caps and a 3" air gap. The magnetic field used for these experiments was about 9325 oersteds.

C. Samples

The alloy samples were arc melted buttons prepared from high purity vanadium, chromium and manganese by Dr. O. N. Carlson's group of the Ames Laboratory. Pure vanadium and

Table 1. Nuclear properties[a]

Nucleus	Vanadium-51	Chromium-53	Manganese-55	Aluminum-27	Potassium-39
NMR frequency (MHz/10^4 Oe)	11.193	2.406	10.553	11.094	1.987
Natural abundance (%)	99.75	9.54	100	100	93.08
Magnetic moment (in eħ/2Mc)	5.1392	-0.47354	3.4611	3.6385	0.39094
Spin (in ħ)	7/2	3/2	5/2	5/2	3/2
Quadrupole moment (barns)	-0.04[b]	-0.03[c]	0.35[d]	0.149	0.07

[a]NMR Table, Varian Associates, Palo Alto, Calif., Fifth Edition (1965).

[b]Kiyoshi Komura, J. Phys. Soc. Japan 21, 1466 (1966).

[c]R. W. Terhune et al., Phys. Rev. 123, 1265 (1961).

[d]H. Walther, Z. Physik 170, 507 (1962).

Table 2. Typical impurity concentrations in the starting materials (ppm)

Impurity	Vanadium	Chromium
O	40	22
H	10	1
N	<5	1+
C	150	10
Cr	70	--
Al	--	3
Ca	<20	1
Fe	150	29
Cu	30	1
Mg	<20	1
Mn	--	1
Mo	--	1
Ni	20	2
Si	<50	20
Ti	<20	--
V	--	1

chromium metals were also provided. The buttons were remelted a number of times to ensure homogeneity. Some of the buttons containing 5% or less vanadium were given homogenizing anneals at 1650° C. for one hour. The samples were filed and passed through sieves to obtain small particles. This is necessary in order to avoid eddy current distortion of the resonance line shape which occurs when the particle size is larger than the skin depth (59). Iron introduced in the filing process was removed with a strong magnet. The samples were usually annealed for about four hours at 550° C. in an argon atmosphere to relieve any strains that may have been introduced on filing.

A sample of pure chromium enriched to 98.5% Cr^{53} was obtained from the Oak Ridge National Laboratories. It was in powdered form with particle size about 5 microns.

The Al^{27} nuclei in a solution of $AlCl_3$ were used as a reference for the V^{51} resonance. The measurements are converted to measurements with respect to the V^{51} resonance in $VOCl_3$ by using the measured ratio of the V^{51} and Al^{27} resonant frequencies in the same field (60) and using 1109.4 Hz/Oe for Al^{27}. In the early measurements of the chromium (using the unannealed samples) the shift was determined relative to that in Na_2CrO_4 (61) by determining the frequency ratio of the Cr^{53} resonance in the metal to the K^{39} resonance in HCOOK and using their reported magnetic moment ratios (61, 62). The measurements on the homogenized and annealed samples were made with

respect to Na_2CrO_4 directly. The Mn^{55} shift was measured with respect to $NaMnO_4$. Pertinent nuclear properties and typical impurity concentrations in the vanadium and chromium metals are given in Tables 1 and 2 respectively.

Figure 4. The resonance intensity of the V^{51} resonance in the vanadium-chromium system as a function of the chromium concentration. The intensity is expressed as the fraction of the intensity expected when all transitions contribute to the resonance

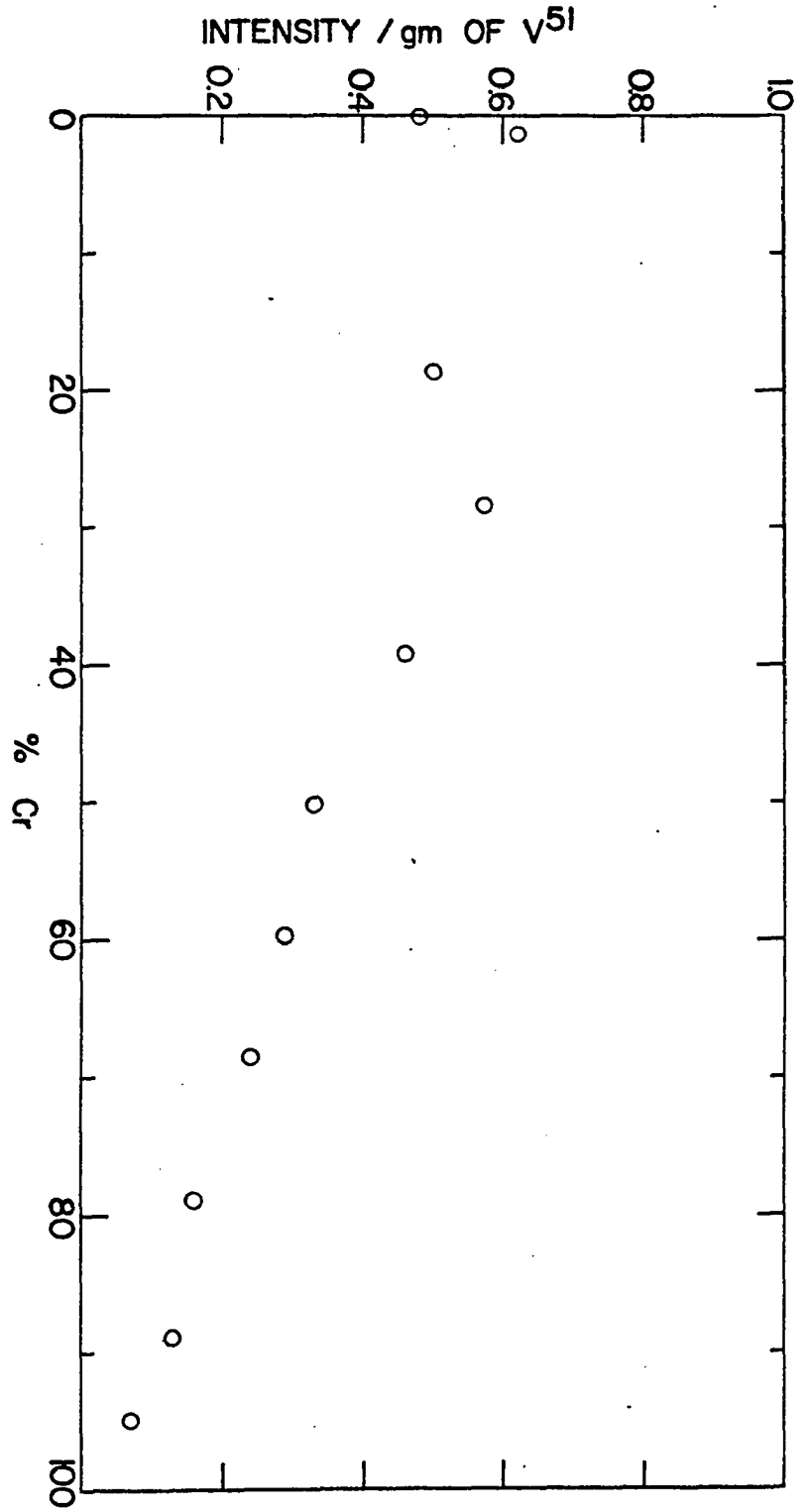
INTENSITY / gm OF V51
0.2
0.4
0.6
0.8
1.0
0
20
40
60
80
100
% Cr

Table 3. Estimates of the quadrupole interaction strength from intensity and zero field line width and from the echo half-width of the V^{51} resonance

Vanadium concentration %	Intensity nucleus ± 10%	Transitions present[a]	e^2qQ/h Oe	echo half-width microseconds	e^2qQ/h Oe
100	0.48	(±3/2,±1/2)& (1/2,-1/2)	134	8	112
98.86	0.62	"	146		
81.32	0.50	"	108		
71.57	0.57	"	118		
60.78	0.46	"	100		
49.93	0.33	"	82	9	99
		(1/2,-1/2)	164		
40.36	0.29	(±3/2,±1/2)& (1/2,-1/2)	79		
		(1/2,-1/2)	158		
31.30	0.24	"	132		
21.06	0.16	"	98[b]	10	89
11.10	0.13	"	64[b]		
5.36	0.07	"	30[b]	25	36
3.41	0.05	"			
1.17	0.10	"			

[a]Assumed on the basis of the intensity measurement.

[b]Since the intensity is below 0.19, some nuclei have been removed from the resonance and thus the interaction would be ∝ 100 times larger for them.

IV. RESULTS AND DISCUSSION

A. Intensity

In Figure 4 we present the intensities of the V^{51} resonance at 15.234 MHz in the vanadium-chromium system as a function of chromium content. The intensities are expressed as the fraction of the intensity expected when all the transitions contribute to the resonance. The data is found in the second column of Table 3. The scatter of the measurements is about 10%. The intensity of pure vanadium was obtained by comparing its integrated intensity with that of aluminum. Using Equation 36, where the sum is written as 2/3 I(I+1)(2I+1), the intensity per nucleus ratio is found to be 0.55. Experimentally we find an aluminum to vanadium intensity ratio of 1.15. Dividing this into the theoretical value we find that only about 48% of the full intensity of the V^{51} resonance is observed. Aluminum metal was chosen because its resonant frequency is conveniently close to that of vanadium and on the basis of previous experiments (63), it does not show any diminution of intensity with cold work (filing). (If, as Lecander has recently noted (64), aluminum does not contribute fully to the resonance, the intensity of the vanadium resonance would be even smaller.) Since the line shape of aluminum differs from that of vanadium, it was necessary to compare the integrated intensities. The vanadium resonances in the alloys were compared with pure vanadium on the basis of the approximate intensity $J'(\Delta H)^2$

where J' is the peak-to-peak amplitude of the resonance derivative and ΔH is the peak-to-peak width. (The line widths are given in the next section.) This method was used for the alloys because their line shapes were about the same--somewhere between Lorentzian and Gaussian--while the shape of the aluminum resonance was somewhat squarer than Gaussian. Freshly filed, unannealed vanadium also gave a shape somewhat squarer than Gaussian. For alloys containing 90% or more chromium, the resonance shape was quite asymmetric whereas, in the other alloys, the shape was essentially symmetric.

The shape and asymmetry characteristic of second order quadrupole interactions were not observed except perhaps for the dilute alloys at the chromium-rich end of the alloy system. In all cases the line width increased as the frequency (and field) of measurement was increased. This is in contrast to what is expected for second order quadrupole interactions; the line-width would decrease as the frequency increased.

The behaviour of the intensity in pure vanadium was anomalous. In the freshly filed (unannealed) vanadium the intensity was dependent on the particle size of the sample. The sample with larger particles gave a more intense resonance than a sample with smaller particles. This is thought to be due to the fact that the centers of the filings are not as distorted as the outer layers. However, annealing of the smaller particles at a temperature above the recrystallization

temperature changed the intensity but slightly. Contrary to the expectation that full intensity would be restored, the intensity remained at roughly 50% of full intensity.

Experiments, mainly on copper and aluminum, have indicated, at least for dilute solute concentrations, that an "all or nothing" description adequately accounts for the intensity measurements (47). In this model it is assumed that there is a critical radius beyond which the solute has no influence. The intensity will be proportional to the number of solvent nuclei unaffected by the impurity. If c is the concentration of impurity, 1-c is the probability that a site is occupied by a solvent atom. The probability that a solvent atom is surrounded by n other solvent atoms is $(1-c)^n$. The intensity should then be proportional to $(1-c)^n$. The number of nuclei n affected by the impurity is termed the "wipe out number ". If an impurity causes both first and second order quadrupole effects care must be taken in separating these effects. If the central line is unaffected, then by subtracting its theoretical contribution from the observed intensity, the effect of the impurity on the satellites can be determined. If for some reason (cold work for example) the satellites are absent, the diminution of the intensity of the central line can be observed. The numbers n obtained for these two cases are considerably different. Since the gradient necessary to affect the central line is roughly 20 times that necessary to remove the

Figure 5. A doubly logarithmic plot of the intensity of the V^{51} resonance in the vanadium-chromium system as a function of the probability that a site is occupied by a solvent nucleus, 1-c. The solid lines indicate the behaviour expected on the basis of a "wipe out number" description with n equal to 8 and 56

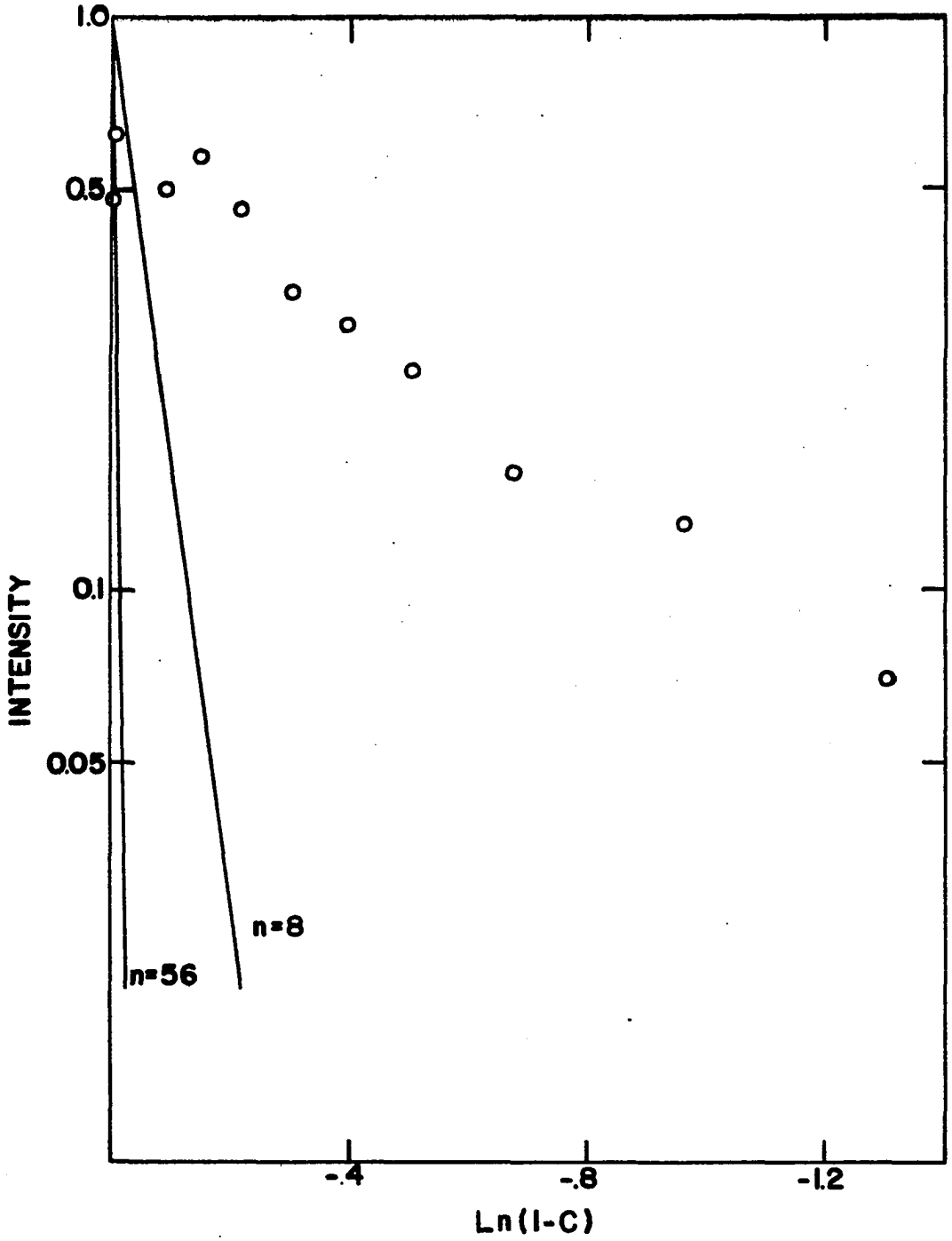
1.0
0.5
0.1
0.05
INTENSITY
n=8
n=56
-.4
-.8
-1.2
Ln(1-C)

Figure 6. A doubly logarithmic plot of the satellite intensity of the V^{51} resonance in the vanadium-chromium system as a function of the probability that a site is occupied by a solvent nucleus. The satellite intensity was obtained by subtracting the theoretical intensity of the central transition from the observed intensity. The solid lines are discussed in the text

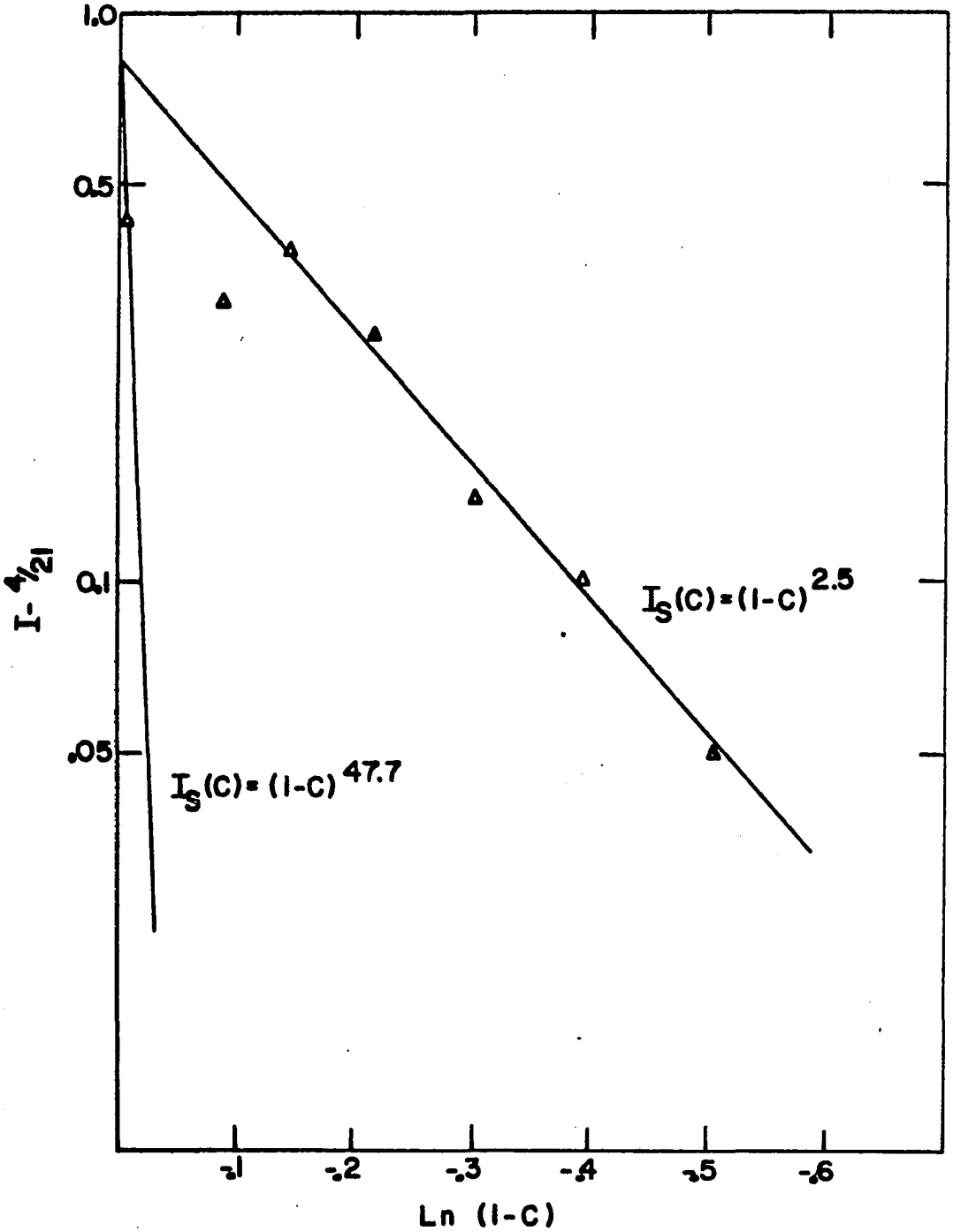
1.0
0.5
0.1
.05
I- 4π/21
$I_S(C) = (1-C)^{2.5}$
$I_S(C) = (1-C)^{47.7}$
-.1
-.2
-.3
-.4
-.5
-.6
Ln (1-C)

satellites (based on Equations 29 and 30) the number affected in first order is larger than in second order.

The application of these ideas to the case at hand is not very fruitful. In Figure 5 we show the concentration dependence of the total intensity on a doubly logarithmic plot. A few lines with slope n corresponding to the number of atoms in the first few shells around an impurity are included for comparison. In Figure 6 is plotted the satellite intensity obtained after subtracting the theoretical intensity of the central line. From the square of the matrix element of the transition, $I(I-1) + m(m-1)$, the relative intensities of the transitions for spin 7/2 are in the ratios 7:12:15:16:15:12:7. We have subtracted 16/84 from the normalized intensity to obtain the intensities used in Figure 6. The initial slope indicates that the first four shells (48 atoms) are affected in first order. However for the more concentrated alloys the intensity decreases very slowly with $n = 2.5$ being an average interaction number. The intensity as shown in both Figures 5 and 6 is considerably larger than is to be expected with an "all or nothing" approach.

One possible reason for lack of agreement with the simple model is that the majority of the alloys can not be considered as dilute. In the more concentrated alloys the spheres of influence of the solutes will overlap resulting in a relatively larger intensity. Weinberg and Bloembergen (65), using a

Figure 7. The spatial dependence of the electric field gradient around an impurity atom in a metal as discussed in the text. The arrows denote the positions appropriate to the first 17 shells of neighbors in the vanadium lattice

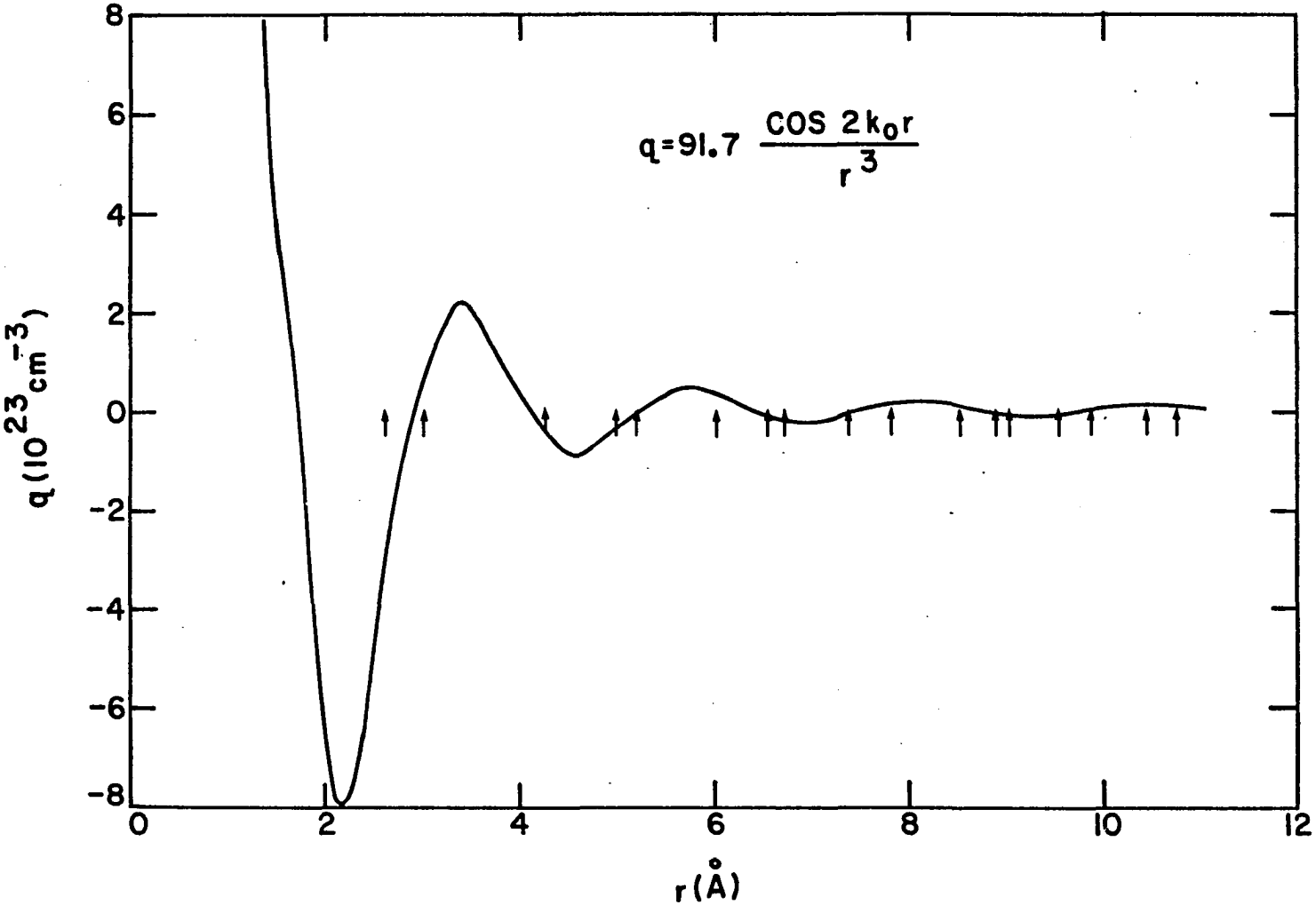
q=91.7 COS 2k0r / r3
q(10^23 cm^-3)
r(Å)
8
6
4
2
0
-2
-4
-6
-8
0
2
4
6
8
10
12

gradient of the form C/r^3, took into account solute configurations which produced no net field gradient although they might be within the critical radius. For example the first shell surrounding a solvent nucleus could be filled with impurities and still contribute to the resonance. For the case where n = 54 (in a fcc lattice) there was a 25% increase of the theoretical intensity at c = 0.25. An increase of this magnitude is much too small to account for our results, factors of ten are needed. There are additional configurations of solutes which can produce small gradients at a solvent nucleus. These nuclei could be expected to contribute to the resonance intensity. Weinberg and Bloembergen suggest that these contributions may be comparable to the contributions due to the zero gradient configurations. If the gradient is modulated as mentioned in Section II.D, then a further increase in theoretical intensity might be expected.

We have shown, for illustrative purposes, in Figure 7 the spatial dependence of a gradient of the form of Equation 37. The Fermi energy was chosen to be 7 electron volts and the angle φ equal to π (π was the angle obtained by Langer and Vosko using many-body perturbation theory (66)). The constant C is a scale factor in this example. The distances of the first few shells from an impurity are indicated by the arrows (using the lattice constant appropriate to vanadium). As can be seen from the figure, it is possible that the positions of

Figure 8. An experimental trace of the V^{51} resonance in a chromium alloy containing 0.267% vanadium depicting the asymmetry of the resonance

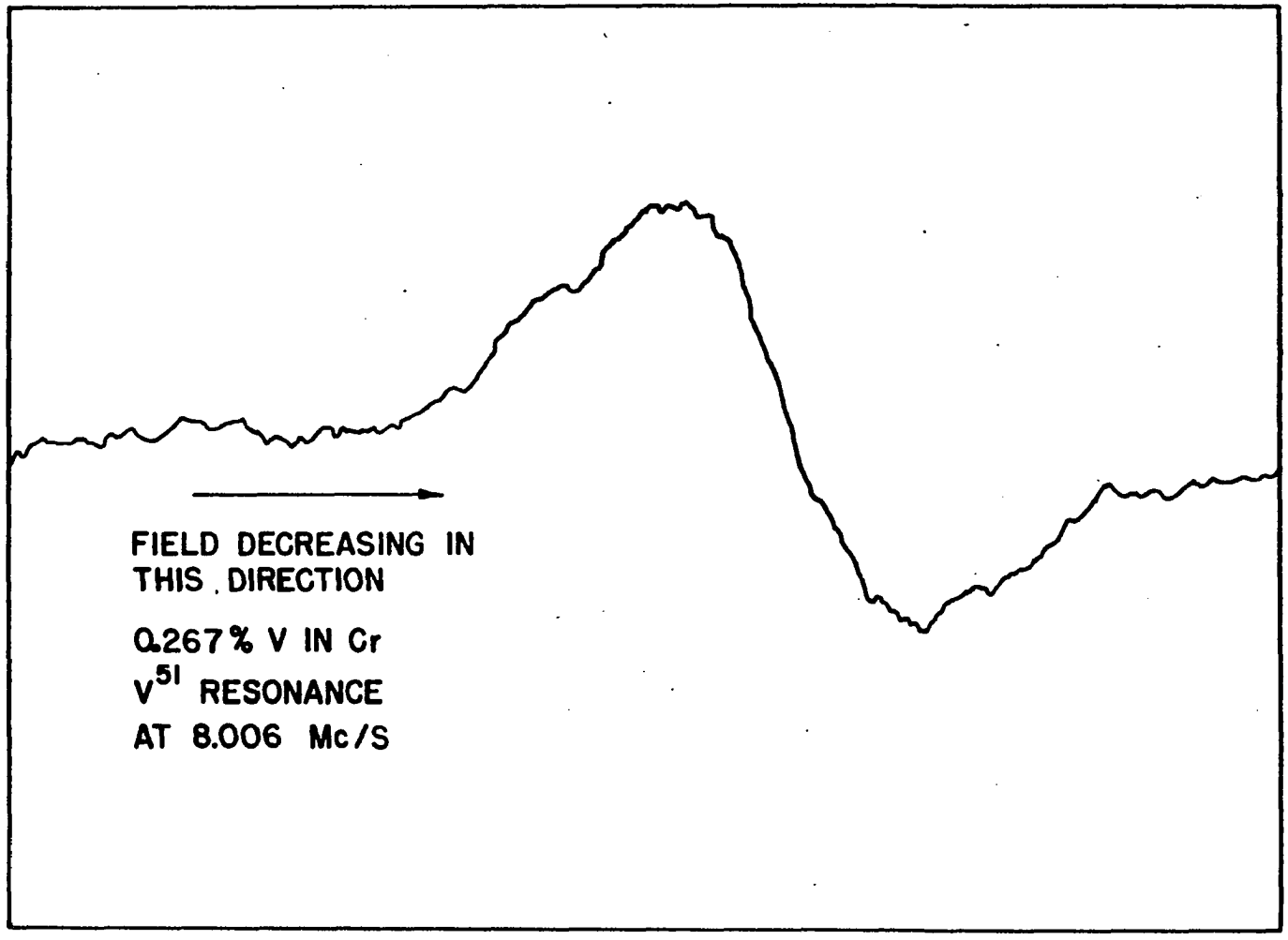
FIELD DECREASING IN
THIS DIRECTION
0.267% V IN Cr
V51 RESONANCE
AT 8.006 Mc/S

the closest nuclei coincide with a node in the gradient. These nuclei would then contribute fully to the resonance. Furthermore, at high concentrations (say 10% and above) there would be a certain amount of interference among the gradients produced by different solutes, this again tending to increase the intensity.

The above discussion gives an indication of some of the difficulties which would be encountered in attempting to calculate the intensity variation. An additional complication in a transition metal such as vanadium is the presence of two bands, the s-band and the d-band. The phase shifts obtained on the basis of pure s-band screening would be vastly different from those obtained on the basis of pure d-band screening. As a result of this difference the nodal points would differ in the two cases. The truth probably lies between these two extremes.

As seen from Figure 5 the intensity falls below 16/84, the contribution from the central transition, at the chromium-rich end of the system. This indicates that there are second order quadrupole effects taking place. However the line-width does not indicate this; there is no inverse frequency dependence. In the dilute chromium alloys the line shape is severely distorted. Figure 8 shows one of the experimental traces of the V^{51} resonance in a sample containing .267% vanadium. The area above the baseline must equal the area below but this does not

appear to be the case. This means that some of the resonance intensity is lost in the baseline noise, the low field side being the more deficient. We shall discuss this point further when we consider imhomogeneous Knight shift effects. Here we shall just say that at the chromium-rich end of the system there are second order quadrupole effects. A gradient which renders the central transition unobservable is approximately three times larger than that which just starts to affect the central line. It is thus conceivable that, with the modulated gradient given above, the first one or two shells are "wiped out" whereas the gradient at the more distant shells is insufficient to cause second order affects. This is probably the reason why the characteristic field dependence is not observed.

The Cr^{53} resonance was observed in the dilute chromium alloys. The resonance was very weak and only the center of the dispersion mode resonance was measured. The Cr^{53} isotope is only 9.54% abundant, its magnetic moment is small and its resonant frequency correspondingly low. These facts partly account for the weakness of the resonance. With more than 3% vanadium in the alloy the chromium resonance is unobservable. At this composition the concentration of Cr^{53} has only dropped to about 9%. We would still expect to see a resonance in a sample containing half this amount. It thus appears that the impurities are having a profound effect upon the Cr^{53} resonance.

This observation is a further indication of rather strong quadrupole interactions at the chromium rich end of the alloy system. The quadrupole moments and Sternheimer antishielding factors are not reliably known for vanadium or chromium so we cannot estimate the magnitude of the gradients or even the relative strengths of the quadrupole interactions of vanadium and chromium.

With regard to the vanadium resonances at the chromium-rich end of the system we must remember that here vanadium is the impurity and not chromium. The modulated gradient given above holds at distances somewhat removed from the impurity. When one is looking at the resonance of the impurity, in addition to the gradients produced by the other impurities, there can be a gradient due to the screening charge on the impurity itself. That is to say, heretofore we have been discussing the gradient due to the screening charge outside the impurity potential (approximated by a square well) but when looking at the impurity resonance the screening charge inside the potential must be considered. Daniel (42) and Clogston (67) have considered this screening effect on the electronic magnetic susceptibility (and hence the Knight shift) at the impurity but the electric gradient has not been considered.

In view of the preceding discussion we can give the following qualitative description of the experimental observations. The lack of full intensity in pure vanadium is due to the

impurities present in the starting materials. This is thought to be analogous to the case of impure aluminium (63). A concentration of 0.64% magnesium in aluminium is sufficient to lock the dislocations in the lattice. Annealing brings the intensity back to only 60% of full intensity. This effect is probably present to some degree in all the vanadium-chromium alloys. As the chromium content is increased the intensity decreases slowly. The gradients produced by the chromium atoms are probably rather weak (first order effects) and there is probably a great deal of interference. At about 75% chromium the gradients become stronger. In this region the density of states (presumably d-electron states) falls to a rather low value (68). The phase shifts and Bloch character of the electrons should reflect this change. The slight rise of the intensity at about 1% vanadium in chromium is not too reliable experimentally, but such a rise is to be expected as infinite dilution is approached.

B. Line Width

In Figure 9 we present a plot of the vanadium-51 resonance line widths as a function of chromium concentration (solid lines). The measurements were made at frequencies of 15.235 and 3.985 MHz. A few measurements at intermediate frequencies were also made. The data are tabulated in Table 4. Except in the chromium-rich end of the system, the resonances were symmetric. As can be seen from Figure 9, the resonances were

Figure 9. The V^{51} line widths in the vanadium-chromium system as a function of the chromium concentration at 15.235 MHz and 3.985 MHz. X denotes the line width obtained upon extrapolation to zero field. The dashed line is the theoretical dipolar line width and the dotted line is the dipolar width obtained using a "wipe out number" description as discussed in the text

Figure 9. The V^{51} line widths in the vanadium-chromium system as a function of the chromium concentration at 15.235 MHz and 3.985 MHz. X denotes the line width obtained upon extrapolation to zero field. The dashed line is the theoretical dipolar line width and the dotted line is the dipolar width obtained using a "wipe out number" description as discussed in the text

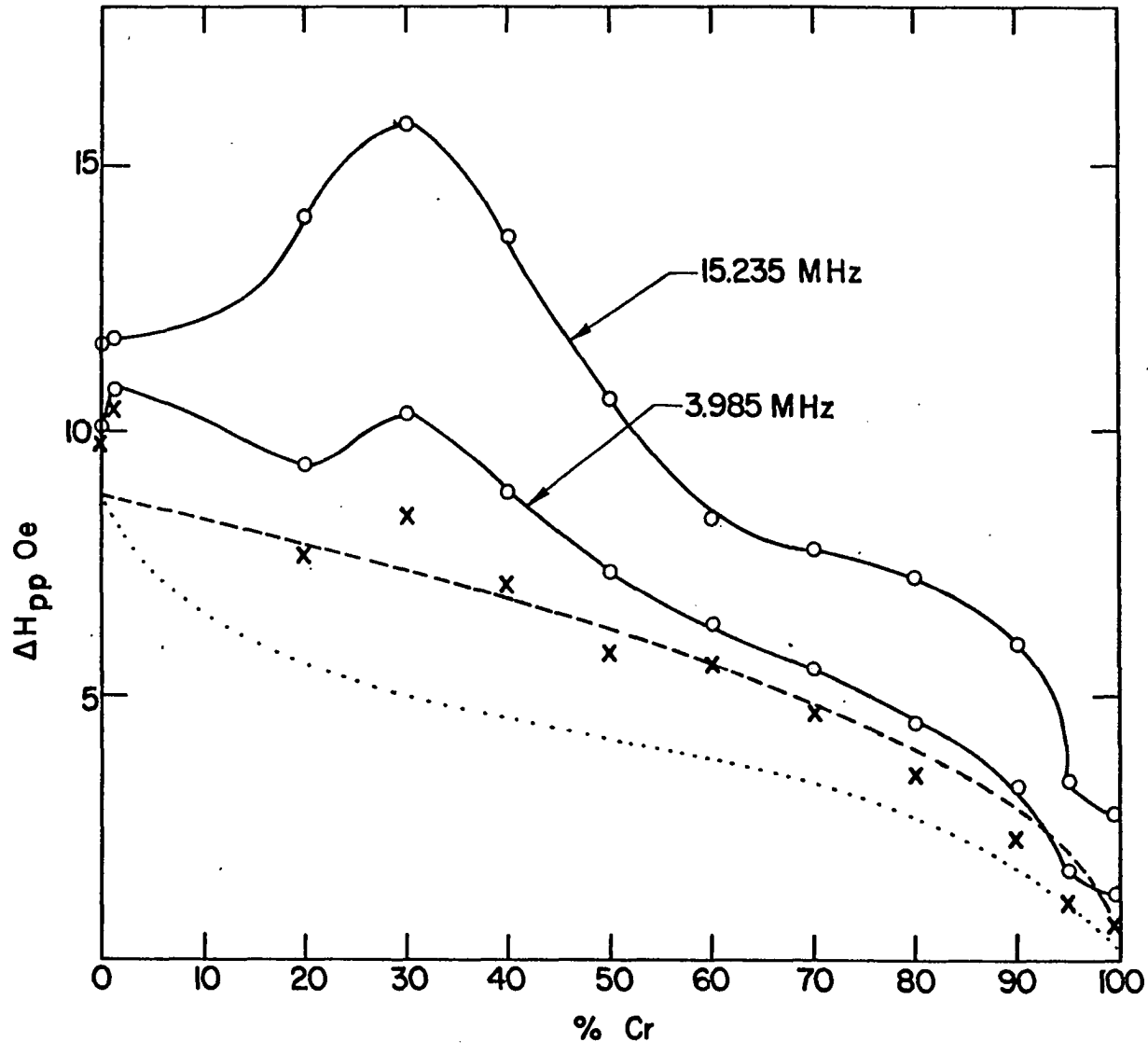
15.235 MHz
3.985 MHz
15
10
5
ΔH_{pp} Oe
0
10
20
30
40
50
60
70
80
90
100
% Cr

Table 4. Peak-to-peak line width of the V^{51} resonance in the annealed powders

Vanadium concentration %	Frequency MHz	Line width Oe ± 0.20 Oe
100	15.235	11.77
	7.500	10.70
	3.983	10.11
98.86	15.204	11.71
	3.985	10.78
81.32	15.234	14.02
	3.985	9.35
71.57	15.234	15.75
	3.986	10.34
60.78	15.234	13.65
	3.986	8.87
49.93	15.235	10.59
	3.986	7.34
40.36	15.234	8.33
	3.985	6.33
31.30	15.234	7.77
	3.985	5.51
21.06	15.235	7.22
	3.985	4.68
11.10	15.234	5.99
	3.985	3.28

Table 4. (Continued)

Vanadium concentration %	Frequency MHz	Line width Oe ± 0.20 Oe
5.36	15.235	3.38
	3.985	1.70
3.41	15.234	3.0
2.16	3.478	1.21
1.72	15.470	2.70
1.17	15.278	2.78
	11.485	2.53
	8.004	2.12
	6.020	1.75
	4.001	1.70
0.556	15.236	2.57
0.267	15.234	2.73
	3.991	1.24

narrower at the lower field. In order to analyze this data we must separate the field dependent and field independent contributions.

Of the line broadening mechanisms discussed previously, the anisotropic Knight shift interaction, inhomogeneous Knight shift effects and bulk magnetism effects would cause the line width to increase as the external field is increased. (This assumes the absence of localized moments as is thought to be

the situation in both vanadium and chromium (69,70).) The anisotropic shift interaction is ruled out for most of the alloy system because, with the magnitude of the line width changes involved, the asymmetry of the line shape would be striking. At the chromium-rich end of the system there is asymmetry but the characteristic anisotropic Knight shift splitting is absent. Also, Rowland (39) quotes an unpublished calculation of Vosko's to the effect that the anisotropic shift would contribute to the width less than 10% of the change of the Knight shift.

According to Drain (42), the paramagnetism of the powdered sample can increase the line width by approximately $3\chi_v H_o$. This contribution depends upon the shapes of the particles, and Drain considered various possibilities, took an average and arrived at the above estimate. The values appropriate to our alloys are given in the third and fourth columns of Table 5 for two values of the external field. Since the effects we are discussing contribute a broadening linear in the applied field (and frequency), we have extrapolated the line widths to zero field. These field independent widths are given in the fifth column of Table 5 and are represented by the x's in Figure 9. The last two columns in the table give that part of the field dependent width which is not accounted for by the bulk magnetism correction. It is seen that this correction essentially accounts for the field dependent width of vanadium

Table 5. Calculation of residual field-dependent line width

% V	$3\chi_v$[a] $10^{-6}\ \frac{emu}{cm^3}$	ΔH_{demag} Oe @13.63 KOe	ΔH_{demag} Oe @3.562 KOe	$\Delta H_{H=0}$ Oe	$\Delta H_{meas} - \Delta H_{H=0} - \Delta H_{demag}$ Oe @13.63 KOe	$\Delta H_{meas} - \Delta H_{H=0} - \Delta H_{demag}$ Oe @3.562 KOe
100	106.8	1.46	0.39	9.78	0.53	-0.06
98.86	98.5	1.34	0.35	10.47	-0.10	-0.04
81.32	103	1.4	0.37	7.68	4.94	1.3
71.57	104.7	1.43	0.38	8.40	5.92	1.56
60.78	93.8	1.28	0.33	7.14	5.23	1.4
49.93	94.4	1.29	0.34	5.83	3.47	1.17
40.36	81.8	1.12	0.29	5.61	1.6	0.43
31.30	73.7	1.0	0.26	4.70	2.07	0.55
21.06	67.3	0.92	0.24	3.51	2.79	0.93
11.10	68	0.93	0.24	2.30	2.76	0.74
5.36	68	0.93	0.24	1.08	1.37	0.38
1.17	68	0.93	0.24	1.15	0.7	0.31

[a]Using the data of reference (80).

and the 98.86% alloy. For the others, however a fairly large contribution remains.

The remaining source of field dependent broadening, the inhomogeneous Knight shift, is thought to be responsible for the line shape of the alloys at the chromium-rich end of the system. In the dilute vanadium alloys the line shape does not indicate the presence of this effect. In the more concentrated alloys, interference effects would tend to give a symmetric line shape. Caroli (71) has shown that, for an impurity pair, in the first approximation the charge density oscillations are just the sum of the oscillations due to a single impurity. This would tend to smear out any structure in the resonance shape but giving a broadening to the line. It is difficult to estimate the magnitude of this contribution, however, judging from Rowlands results on dilute silver alloys (39), a contribution of a few oersteds at 15 MHz does not seem unreasonable. (A more detailed discussion will be given in connection with the Knight shifts of the dilute alloys.) The reason for the large widths in the region near 30% chromium appears to be a combination of the above effects and first order quadrupole broadening. From the intensity measurements, it seems that the first pair of satellites ($\pm 3/2 \leftrightarrow \pm 1/2$ transitions) contribute to the field independent width. The above effects would broaden the satellite resonances and hence the line as a whole.

We now turn to a discussion of the field independent contributions to the line width. Ideally, what we would like to do is compare the second moment of the resonance line

$$\langle \Delta H^2 \rangle = \int_0^\infty h^2 g(h) dh \qquad (40)$$

(where h is the field relative to the resonance center and g(h) is the normalized shape function) with the second moment obtained from the Van Vleck formula. Because of the difficulty in treating the wings of the resonance in performing the above integration and since the line shapes are nearly Gaussian it will be assumed that they are Gaussian. Then, for a Gaussian shape, the peak-to-peak line width is simply related to the second moment by

$$\Delta H_{pp} = 2\sqrt{\langle \Delta H^2 \rangle} \qquad (41)$$

The dashed line in Figure 9 is the line width obtained from the dipolar second moment using Equations 22 and 22'. The lattice parameters were taken from a paper by Van Ostenburg et al. (72). Gutowsky and McGarvey (73) have calculated the lattice sum for a number of lattices including the bcc lattice. In this case the sum is equal to 29.03 a^{-6} where a is the lattice parameter. If c is the concentration of chromium, then the expression for the second moment appropriately weighted is

Table 6. Theoretical dipolar line widths

% Cr	Lattice constant Å	n	$\langle \Delta H_d^2 \rangle$ Oe^2	ΔH Oe
0	3.036	-	19.12	8.75
20	3.028	0	15.54	7.89
		8	7.69	5.55
50	3.026	0	9.76	6.25
		8	4.39	4.19
80	3.024	0	3.92	3.96
		8	1.75	2.65
100	2.878	-	0.01	0.22

$$\langle \Delta H_d^2 \rangle = [\tfrac{1}{3} I_{51}(I_{51}+1)\gamma_{51}^2 \hbar^2 p_{51}(1-c) + \tfrac{4}{15} I_{51}(I_{51}+1)\gamma_{51}^2 \hbar^2 p_{51}(1-c) + \tfrac{4}{15} I_{50}(I_{50}+1)\gamma_{50}^2 \hbar^2 p_{50}(1-c) + \tfrac{4}{15} I_{53}(I_{53}+1)\gamma_{53}^2 \hbar^2 p_{53} c] \sum_k r_{ik}^{-6} \quad (42)$$

where p is the isotopic abundance. As discussed under Equation 22', the first term above results from the mutual spin flipping among like neighbors. If, as discussed in a previous section, a solute atom not only replaces a solvent atom but also affects n other solvent nuclei (they cease to be like neighbors), then the first term will decrease more rapidly than (1-c). The number of solvent nuclei contributing to this

term will drop by an additional factor of $(1-c)^n$. Choosing n equal to eight, we obtain the dotted curve in Figure 9. The results of these calculations are in Table 6.

The simple dipolar estimate (dashed curve) seems to fit the data fairly well between 20% chromium and 70% chromium. At the chromium end there is a shift towards the lower dotted curve. This is the region where it is believed that second order quadrupole effects are becoming important as evidenced by the intensities, and consequently, a "wipeout number" description may be appropriate. The line widths of vanadium and the dilute vanadium alloy are not in good agreement with the dipolar width, possibly because of the quadrupole effects. On the whole, though, it seems that the dipolar interaction is the major source of the field independent line width.

We expect some modifications of the theoretical dipolar moment due to the quadrupole interaction. Since this interaction destroys the equal spacing of the magnetic levels, the possible number of energy conserving mutual spin flips is reduced. Thus, the quadrupole interactions will affect the theoretical second moment by altering the spin flip contribution. Kambe and Ollom (34) have discussed the case wherein the satellites are removed from the central line. A shorter discussion appears in Abragam (33). The case in which some of the satellite intensity remains in the central line has not been treated theoretically. The results of Kambe and Ollom

show that if neighboring nuclei experience the same gradient, then, for a spin of 7/2, the theoretical width is increased by a factor of 1.08. If the neighbors are in different gradients the width is reduced by a factor of 0.94. In practice a composite of these two situations is expected. We would not expect the other case to give results too far different from these. Numbers of the magnitude of these could account for the discrepancies observed.

In addition to the dipolar contribution, we have considered the indirect exchange coupling proposed by Ruderman and Kittel (44). Only the interaction between unlike nuclei contributes to the width. According to Van Vleck (31), this contribution to the second moment is

$$\langle \Delta H_{ex}^2 \rangle = \frac{I'(I'+1)}{3\hbar^2\gamma^2} \sum_j A_{ij}^2(r_{ij}) \qquad (43)$$

where γ is appropriate to the resonant nucleus and the primes refer to the non-resonant species. $A_{ij}(r_{ij})$, the exchange interaction parameter, is given and discussed by Rowland (35). For nearest neighbors at a distance R from the nucleus at the origin we have

$$A_{ij}(R) = \frac{\Omega^2 m^* \zeta\, a(s)\, \zeta'\, a(s)'\, (I+1)(I'+1)}{2\pi\, (2I+1)(2I'+1)} \cdot \frac{(2k_F R \cos 2k_F R - \sin 2k_F R)}{R^4} \qquad (44)$$

Ω is the atomic volume, m* the effective mass and the other quantities are as defined previously. We choose k_F equal to

to 1.35 $(10)^8$ cm^{-1} (E_F = 7 ev.), m = m* and ζ = 1. For V^{51} and V^{50} we used the value of a(s) calculated by Knight for V^{51} from the Fermi-Segre formula, a(s) = 0.088 cm^{-1} (36). a(s) for chromium was obtained from the measurements of Childs et al. (74), a(s) = 82.6 Mc/s = 0.0028 cm^{-1}. We find that due to the smallness of the chromium hyperfine interaction the exchange interaction with Cr^{53} is of no consequence. The interaction with V^{50} is larger but amounts to only one half of one percent of the dipolar contribution. If we consider V^{51} nuclei as unlike nuclei (due to differing gradients) we would get an exchange contribution of about the same magnitude as the dipolar contribution for n equal to eight. However this does not seem to be justified on the basis of the intensity measurements. Consequently we can regard the exchange contribution as negligible.

We can try to estimate the average strength of the quadrupole interactions in the alloy system from the extrapolated line widths using equations similar to Equations 29 and 30. We let q_1" be the gradient necessary to split the ($\pm 7/2 \leftrightarrow \pm 5/2$) transitions one line width away from the center of the line, q_1' that which splits the ($\pm 5/2 \leftrightarrow \pm 3/2$) transition and q_1 that which splits the ($\pm 3/2 \leftrightarrow \pm 1/2$). Also, we let q_2 be the gradient which just starts to split the central line (a splitting less than a line width), and q_c the gradient which removes the central line (a splitting greater than 5 line

widths). Then for a line width of 10 Oe at 15 MHz, the magnitudes of the gradients are in the ratios

$$q_1'' : q_1' : q_1 : q_2 : q_c :: 1 : 3/2 : 3 : 81 : 255. \quad (45)$$

The average interaction strengths $(e^2qQ/h)_i$ are in the same ratios. Using this scheme to estimate the strengths we find that in the region containing 0 to 60% chromium the strengths lie in the range from 80 to 300 Oe. At higher concentrations the average interaction is of the order of a few thousand Oe because the intensity falls below that of the central line (19%). These estimates give an idea of the average value of the quadrupole interactions in the alloys but do not shed much light on the actual distribution of the gradients. Recently, Redfield (75) has observed the pure quadrupole resonance of copper nuclei in dilute copper alloys. The nuclei contributing to the quadrupole resonance signal are those which are removed from the magnetic resonance signal by the strong gradients. An experiment of this type could give more detailed information about the gradient distribution.

The line width of the Cr^{53} resonance was also measured. The resonance is narrow and weak, and a relatively large modulation amplitude was required. The resonance is symmetric and approximately Gaussian. The field dependence of the line width was not determined because of insufficient field strength. The line width was temperature independent between about 50 to 105° C. As the Neel temperature is approached the line broadens.

The calculated dipolar line width for natural chromium (9.54% Cr^{53}) is 0.33 Oe. The measured line width was 2.22 Oe after correcting for excessive modulation after Andrew (30). For the enriched chromium (98.5% Cr^{53}), the calculated dipolar width is 1.07 Oe and the measured width 2.31 Oe. The contribution of the bulk magnetism to the width at 3.8 MHz (15,630 Oe) is 1.05 Oe. This correction brings the width of the enriched sample into rather good agreement with the dipolar width. For natural chromium about 0.8 Oe remains unaccounted for.

C. Spin-lattice Relaxation Time Measurements

The spin-lattice relaxation time of vanadium-51 was measured in several of the vanadium-chromium alloys. These measurements are shown in Figure 10 and the second column of Table 7. These T_1's were obtained by measuring the time between pulse sequences at which the echo height had fallen to one half of its initial value. This time is related to T_1 by $t = 0.693\ T_1$. The scatter of the data is rather large but does not obscure the fact that the T_1's of the alloys with high chromium content are considerably larger than those for the first half of the system. Subsequent to these measurements, Butterworth (76) published his measurements of T_1 which are in close agreement with ours. However, in view of the evidence presented for the presence of quadrupole interactions in this alloy system, we must convince ourselves that these measured T_1's are the ones to be compared to theory.

Figure 10. The V^{51} spin-lattice relaxation times, T_1's, in the vanadium-chromium system as a function of chromium concentration. The calculated curves are discussed in the text

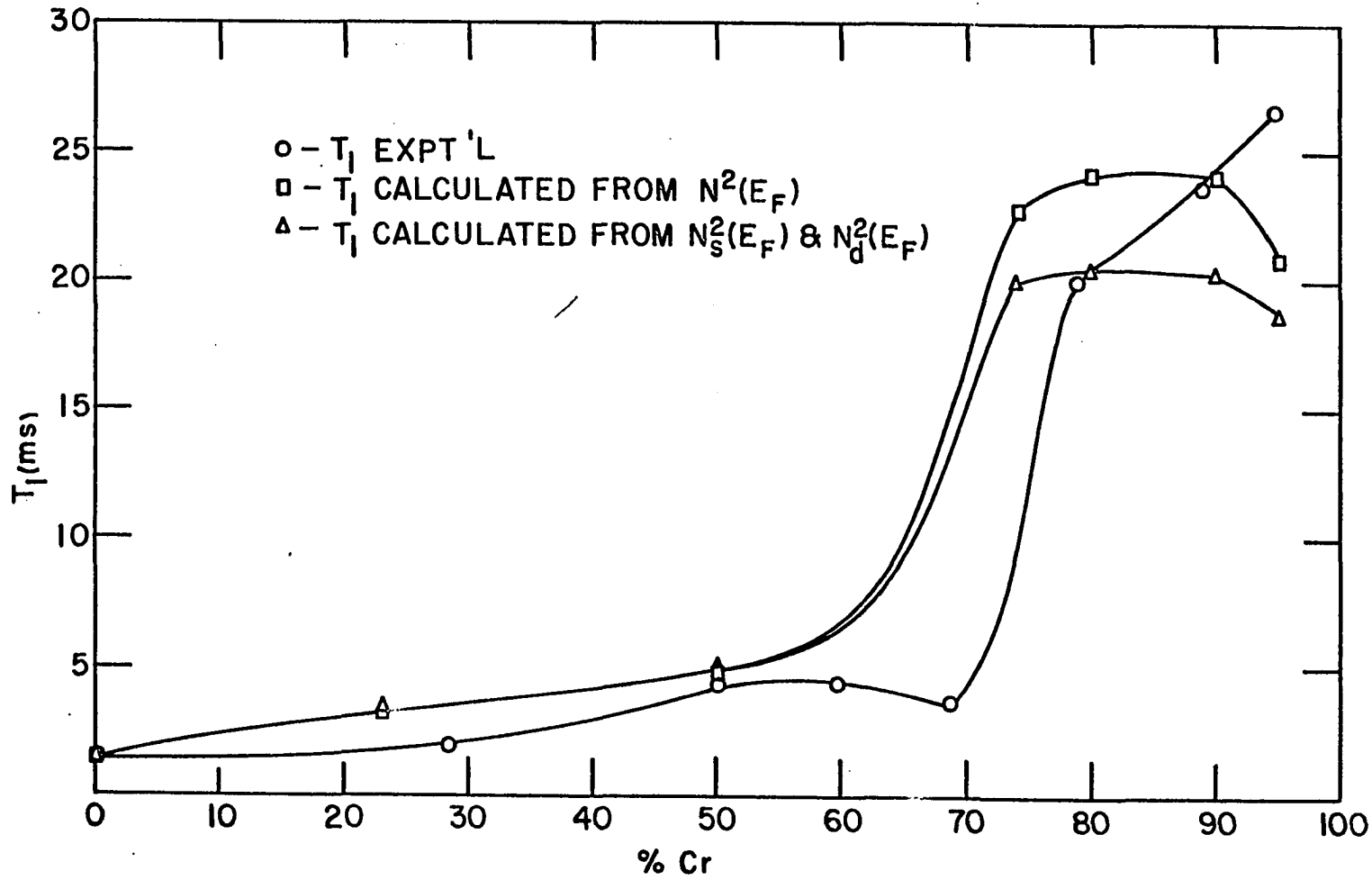
30
25
20
15
10
5
0
10
20
30
40
50
60
70
80
90
100
T_1(ms)
% Cr
o – T_1 EXPT'L
□ – T_1 CALCULATED FROM $N^2(E_F)$
Δ – T_1 CALCULATED FROM $N_s^2(E_F)$ & $N_d^2(E_F)$

Figure 11. Semi-logarithmic plot of the theoretical relative change in magnetization from equilibrium magnetization as a function of time in units of T_1.
Case I -- all transitions initially saturated.
Case II -- only the 1/2 $\leftrightarrow$ -1/2 transition initially saturated

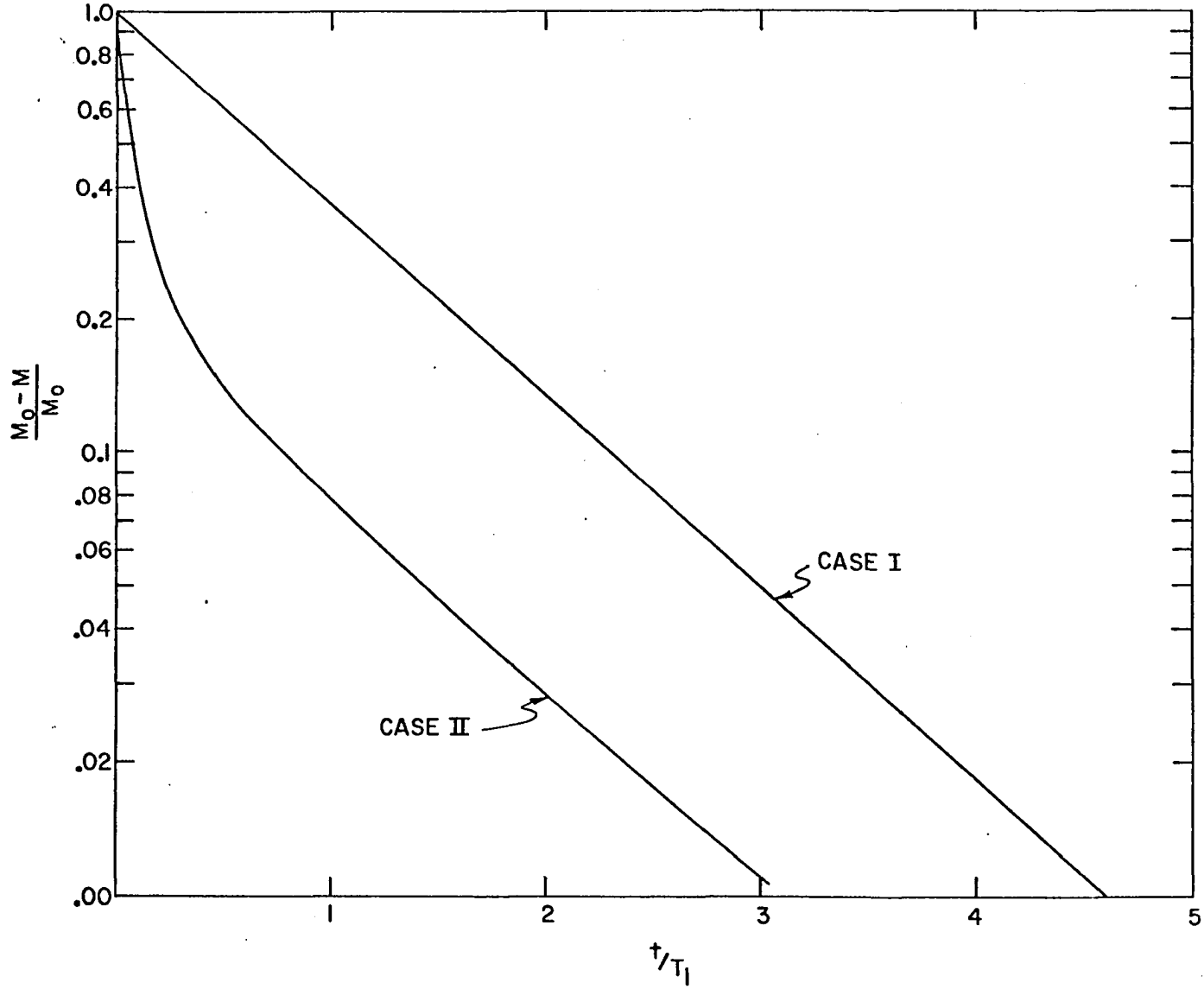
1.0
0.8
0.6
0.4
0.2
0.1
.08
.06
.04
.02
.00
$\frac{M_o - M}{M_o}$
CASE I
CASE II
1
2
3
4
5
t/T_1

Table 7. Spin-lattice relaxation times for V^{51} in the vanadium-chromium alloys

% vanadium	T_1 (measured) milliseconds	$\gamma x10^4$ [a] cal/mole deg.	$\gamma_d x10^4$ cal/mole deg.	T_1 (calculated) I[b] milliseconds	II[c]
100	1.44 ± 0.22	21.1	19.4		
77[d]		14.2	12.5	3.17	3.28
71.57	1.9 ± 0.7				
50[d]		11.6	9.9	4.75	4.95
49.93	4.3 ± 0.4				
40.36	4.3 ± 0.6				
31.30	3.6 ± 0.4				
26[d]		5.31	3.61	22.7	19.9
21.06	20 ± 1				
20[d]		5.15	3.45	24.2	20.3
11.10	24 ± 3				
10[d]		5.17	3.47	24	20.2
5[d]		5.54	3.84	20.8	18.6
5.36	25 ± 2				

[a] Data from Cheng et al. (68).

[b] Using Equation 49 in text.

[c] Using Equation 57 in text.

[d] T_1 was calculated for these concentrations as discussed in the text.

As has been noted from the intensity measurements of the steady state resonances, the satellite transitions do not contribute fully to the observed resonances. If this is the case in the pulse experiments, then one might expect to have the magnetization growth described by more than one relaxation time as discussed in Section II. In Figure 11 we have plotted the natural logarithm of the change in magnetization from equilibrium magnetization as a function of the time between successive two-pulse sequences in units of T_1. If the magnetization growth is described by a single relaxation time, the data should follow the straight line, the equation of which is

$$M = M_o[1 - \exp(-t/T_1)] \tag{46}$$

If, however, it is described by several (four, in this case) relaxation times, the other curve is appropriate. It is given by (Appendix A)

$$M = M_o[1 - 0.21 \exp(-t/T_1) - 0.243 \exp(-6t/T_1) - 0.247 \exp(-15t/T_1) - 0.298 \exp(-28t/T_1)] \tag{47}$$

In this case, the initial approach to equilibrium is more rapid, but after a time of the order of T_1 the relaxation rate becomes a constant fraction of the rate in the first case. In an attempt to decide which case was applicable, data was taken for vanadium-51 in pure vanadium and in the alloy containing 20% vanadium. The data plots are shown in Figure 12. The

Figure 12. Semi-logarithmic plot of the relative change in magnetization from equilibrium magnetization as a function of the pulse sequence repetition time for the V^{51} echo in pure vanadium and a chromium alloy containing 21.06% vanadium

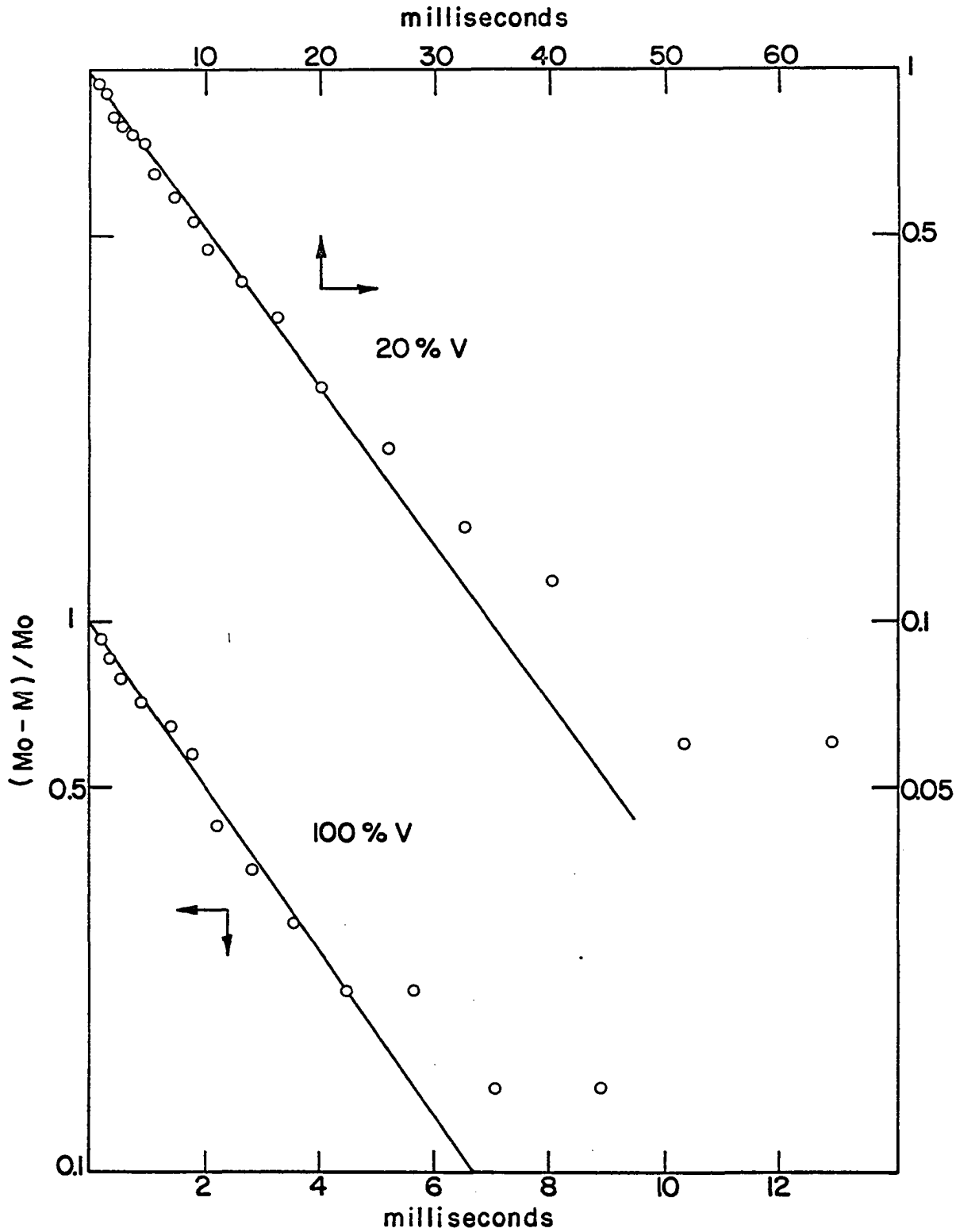
milliseconds
10
20
30
40
50
60
1
0.5
0.1
0.05
20 % V
100 % V
(Mo - M) / Mo
1
0.5
0.1
2
4
6
8
10
12
milliseconds

points at the lower right in this figure tend to hang up and give a straight horizontal line because of the difficulty in measuring M_o and small departures from M_o. This difficulty can be seen by referring to Figure 1 where it is shown that M starts to flatten out at about $t/T_1 = 2$. It is therefore difficult experimentally to tell the difference between M_o (t infinite) and M at $t = 3T_1$ or greater. One notes from Figure 11 that in order definitively to establish the second case we should have about a factor of 50 variation in the echo heights. We were only able to achieve a factor of 10 variation. At this point we will tentatively conclude that the straight line behaviour, and hence a single T_1, is more appropriate to the data.

Some further observations tend to corroborate this conclusion. In the discussion above, of the formation of the echo, we mentioned the use of a 90^o-180^o pulse sequence. However, in our experiment, the pulse widths were not simply related. This does not affect the measurement of T_1 but does indicate that interactions other than dipolar may have to be considered with regard to echo formation. Solomon (77) has considered the case where there are no dipolar interactions but there are random quadrupolar interactions. (Our case seems to be intermediate to these extremes.) Under these circumstances a number of echoes is found, all but one of which are weak. Solomon showed that the shape of the echo is the Fourier

transform of the distribution of quadrupole interactions and that the average interaction (in oersteds) is related to the half-width of the echo, t', by

$$\Delta H = (\gamma_n t')^{-1}. \qquad (48)$$

We can use the findings of Solomon in the interpretation of the observations made on the vanadium-chromium alloys, in particular the alloy containing 20% vanadium. This alloy is chosen because we were able to make a good measurement of the transverse relaxation time T_2 by measuring the echo height as a function of the pulse separation (Equation 38). T_2 is reciprocally related to the line-width of the steady-state resonance line and when only dipolar couplings are present, T_2 is the half-width of the echo. For the 20% alloy, T_2 was 0.3 milliseconds and the echo half-width was 10 microseconds. These measurements were made at the center of the magnet so there would be no narrowing of the echo due to gradients of the external field. The T_2 measurement corresponds to a line-width of about 3 oe which is about the same as the line-width measured by the steady-state method. The echo half-width gives about 90 oe. From the echo half-width we can also obtain the average interaction for pure vanadium--112 oe, the 50% alloy--99 oe and the 5% alloy--36 oe. The estimates for vanadium and the 50% alloy are in reasonable agreement with the line-width estimates. We cannot compare the other two directly because the previous estimate was based on the fact

that a large number of nuclei were entirely removed from the resonance--hence the very large interaction. If, for these cases, we assume that the satellites of the remaining nuclei are outside the central line, then for the 20% and 5% alloys we obtain interaction strengths of 100 oe and 30 oe respectively. These comparisons are included in Table 3. This relatively good agreement gives further support to the presence of quadrupole interactions in the alloys. From the foregoing it thus appears that, in the pulse experiments, we are exciting all the transitions of the nuclei which contribute to the main line. We can thus say that a single time characterizes the spin-lattice relaxation process.

It is difficult to make a detailed comparison of the experimental T_1's with Equation 20. The quantities $\langle|u_k(o)|^2\rangle_{FS}$, $\langle|\varphi_{cp}(o)|^2\rangle_{FS}$, $\langle r^{-3}\rangle_{metal}$, and f are not well known for the metals nor is it known how they vary throughout the alloy system. However, if these quantities are relatively constant throughout the alloy range, then the proportionality to the square of the density of states should be evident as long as the electrons provide the primary relaxation path. This essentially amounts to making a rigid band approximation. As a first, crude check, we have plotted T_1's, obtained by using the low temperature electronic specific heat constants (γ's) measured by Cheng, Wei and Beck (68), vs. composition. Using the equation

$$T_1 = \text{constant}/\gamma^2 \qquad (49)$$

and normalizing to the T_1 of pure vanadium, we obtain the behaviour shown by the squares in Figure 10. This correlates rather well with the experimental data, indicating that the variation in T_1 depends primarily on the density of states. A more realistic comparison could probably be made by considering the s and d-electrons as making up separate bands as is often assumed. Then Equation 20 could be written as

$$(T_1)^{-1}_{tot} = AN_s^2(E_F) + BN_d^2(E_F) \qquad (50)$$

where the s-electron contribution is approximated by using the γ for copper (1.7×10^{-4} cal mole^{-1} deg^{-2} (68)). The determination of A and B are discussed later in connection with the analysis of the Knight shifts where a more detailed breakdown of the various contributions is made. Again the results are fairly well described by the variation in the density of states. With the assumptions made, $N_s(E_F)$ is much smaller than $N_d(E_F)$ so we can say that the relaxation is largely determined by the d-electrons. As chromium is added to vanadium, $N_d(E_F)$ falls slowly until it has reached about one-half its initial value at 50% chromium. This is reflected in the gradual rise of T_1. Between about 50% to 70% chromium there is about a 55% drop in $N_d(E_F)$. This is mirrored in the rapid rise of T_1 in this region. Then both $N_d(E_F)$ and T_1 are roughly constant for the remainder of the alloy range.

Figure 13. The measured Knight shifts of V^{51} in the vanadium-chromium system at 15.235 MHz as a function of the chromium concentration

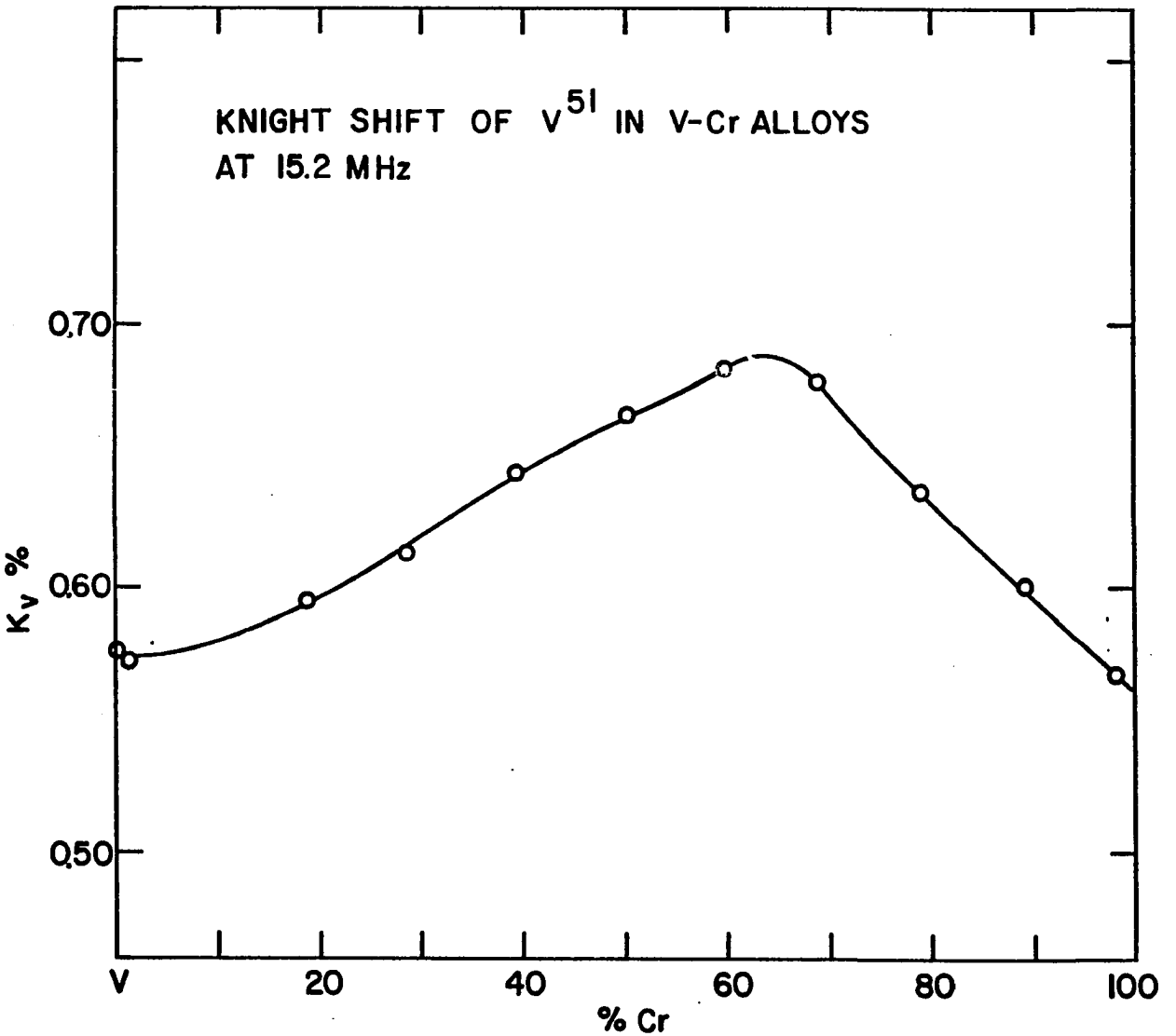
KNIGHT SHIFT OF V^{51} IN V-Cr ALLOYS
AT 15.2 MHz
0.70
0.60
0.50
K_V %
V
20
40
60
80
100
% Cr

Figure 14. The measured V^{51} Knight shift at 6 MHz and the density-of-states in the vanadium-chromium system as a function of chromium concentration. The density-of-states was calculated from the data of reference 68

2

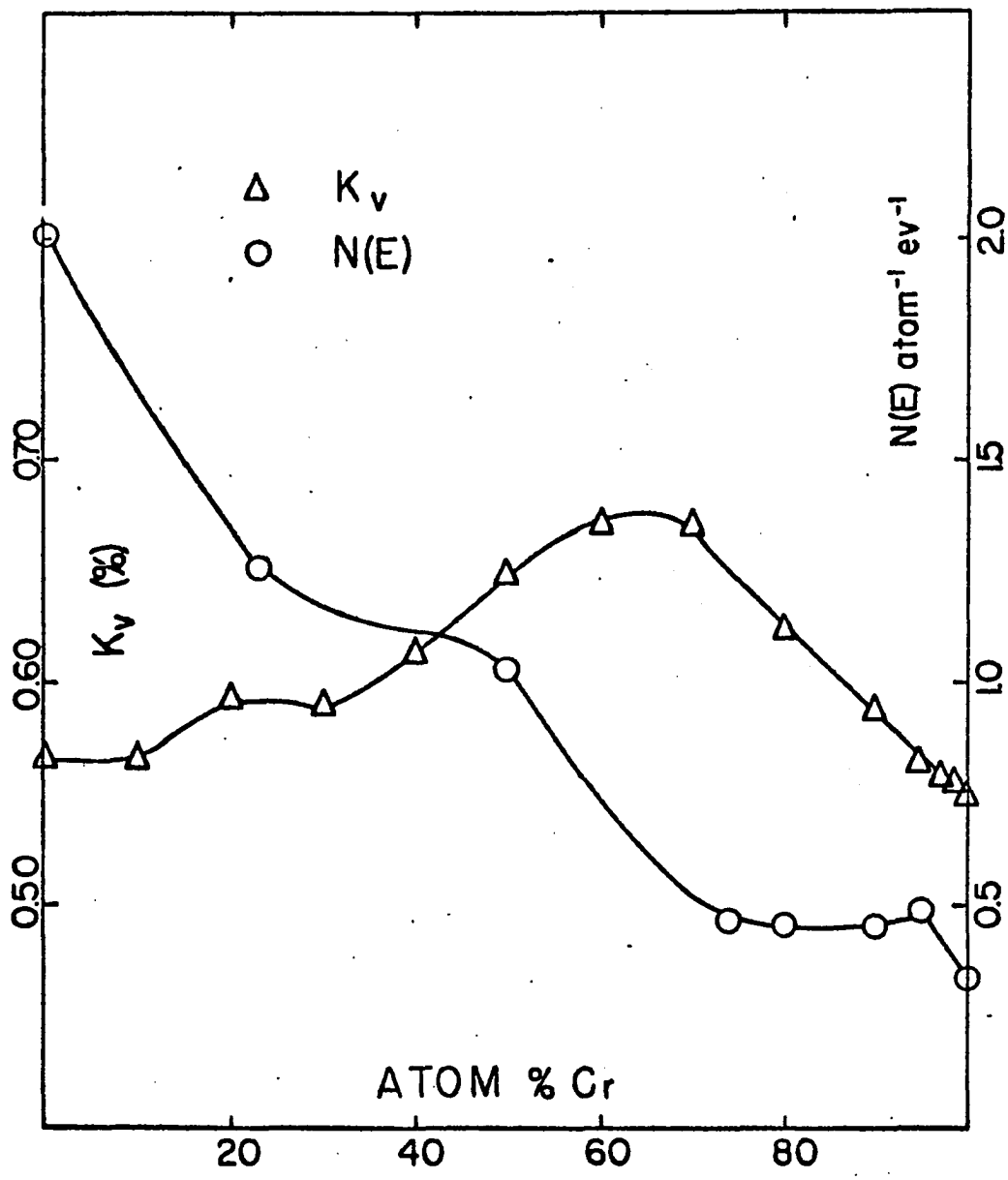

Table 8. V^{51} Knight shifts in the vanadium-chromium system

Vanadium concentration (%)	Frequency MHz	V^{51} Knight shift (%)	Comments
100	3.986	0.578 ± 0.010	AR
	6.149	0.567 ± 0.005	UR
	6.143	0.536 ± 0.011	ULN
	15.206	0.575 ± 0.003	AR
98.86	3.985	0.576 ± 0.009	AR
	6.081	0.566 ± 0.004	UR
	6.081	0.555 ± 0.003	ULN
	15.204	0.572 ± 0.003	AR
81.32	3.985	0.590 ± 0.009	AR
	6.081	0.592 ± 0.004	UR
	6.081	0.576 ± 0.009	ULN
	15.234	0.594 ± 0.003	AR
71.57	3.986	0.626 ± 0.10	AR
	6.143	0.590 ± 0.004	UR
	6.143	0.557 ± 0.013	ULN
	15.234	0.613 ± 0.004	AR
60.78	3.986	0.642 ± 0.009	AR
	6.143	0.614 ± 0.003	UR
	6.143	0.596 ± 0.004	ULN
	15.234	0.643 ± 0.003	AR

Table 8. (Continued)

Vanadium concentration (%)	Frequency MHz	V^{51} Knight shift (%)	Comments
49.93	3.986	0.656 ± 0.010	AR
	6.082	0.649 ± 0.003	UR
	6.082	0.651 ± 0.006	ULN
	15.235	0.665 ± 0.004	AR
40.36	3.985	0.669 ± 0.004	AR
	6.081	0.673 ± 0.003	UR
	6.082	0.660 ± 0.002	ULN
	15.234	0.683 ± 0.004	AR
31.30	3.985	0.666 ± 0.014	AR
	14.154	0.670 ± 0.002	UR
	6.082	0.658 ± 0.004	ULN
	15.234	0.678 ± 0.002	AR
21.06	3.985	0.619 ± 0.008	AR
	6.115	0.624 ± 0.002	UR
	6.082	0.609 ± 0.004	ULN
	15.235	0.636 ± 0.003	AR
11.10	3.985	0.592 ± 0.005	AR
	6.122	0.589 ± 0.004	UR
	6.082	0.569 ± 0.003	ULN
	15.234	0.600 ± 0.003	AR
4.94	6.081	0.565 ± 0.002	UR
	6.081	0.558 ± 0.002	ULN

Table 8. (Continued)

Vanadium concentration (%)	Frequency MHz	V^{51} Knight shift	Comments
3.0[a]	14.128	0.559 ± 0.002	UR
1.5[a]	6.082	0.556 ± 0.002	UR
0.5[a]	6.082	0.553 ± 0.003	UR
0.25[a]	14.130	0.551 ± 0.002	UR
5.36	8.006	0.573 ± 0.007	HAR
	15.235	0.576 ± 0.002	HAR
3.41	15.233	0.573 ± 0.002	HAR
2.16	3.985	0.565 ± 0.009	HAR
	8.004	0.567 ± 0.002	HAR
	15.235	0.567 ± 0.002	HAR
1.72	8.004	0.567 ± 0.006	HAR
	15.234	0.567 ± 0.002	HAR
1.17	15.234	0.561 ± 0.002	HAR
0.556	15.234	0.561 ± 0.002	HAR
0.267	15.234	0.560 ± 0.002	HAR
1.03[b]	15.230	0.568 ± 0.004	HAR

AR - Sample annealed after filing; measurement made at room temperature.
UR - Sample not annealed after filing; measurement made at room temperature.
ULN - Sample not annealed after filing; measurement made at 77° Kelvin.
HAR - Sample given homogenizing anneal before filing, annealed after filing; measurement made at room temperature.

[a]Nominal concentration.

[b]Sample contained 0.28% manganese.

D. Knight Shift Measurements

1. Vanadium-51

The Knight shift, K_V, was measured at room temperature as a function of composition at three frequencies. It was also measured at 77° K at a frequency of 6 MHz throughout the composition range with the exception of those alloys containing 3% or less vanadium. In these latter alloys, the vanadium-51 resonance was not detectable at 77° K. (The measurements on the alloys at the chromium end of the system will be discussed more fully later.) The shift is only slightly temperature dependent, being about 0.01% to 0.03% smaller at 77° K than at room temperature. For the 4 MHz and 15.2 MHz measurements in samples containing 5% or less vanadium, the samples which had been given an homogenizing anneal prior to filing were used. The data is presented in Table 7 and the 15.2 MHz data is displayed in Figure 13. Subsequent to the publication of our initial measurements (78), Van Ostenburg *et al.* (72) and Drain (79) published their measurements which are in substantial agreement with those reported here.

Comparison of the 4 MHz data with the 15.2 MHz data indicates a slight frequency dependence with the low frequency shifts being somewhat smaller. Second order quadrupole effects would have this effect. However, for most of the alloys, the uncertainties overlap. The 6 MHz data, obtained from the as-filed samples are essentially the same with the exception of

the shifts of the alloys containing 30% and 40% chromium. These deviations are thought to be due to quadrupole interactions caused by the lattice strain, due to filing, present prior to annealing.

The major item of interest here is the behaviour of the shift as a function of composition. We can see readily that the simple theory (Equation 6) is not appropriate. In Figure 14 we have plotted the composition dependence of the Knight shift for the 6 MHz data and the density of states as obtained from the low temperature specific heat data (68). The Knight shift does not reflect the behaviour of the density of states and it is difficult to believe that $<|u_k(o)|^2>_{FS}$ changes in the manner required for good agreement. In addition, the Korringa relation is not obeyed; it implies shifts of the order of 25% of those observed. To proceed to analyze the shift data in terms of contact, orbital and core polarization contributions, we must separate the various contributions to the susceptibility. In previous studies, (the V_3X compounds (23) for example), this has been achieved on the basis of the temperature dependence of the shift and susceptibility. When the d-electrons have a localized moment these quantities are temperature dependent. The orbital contributions are expected to be independent of temperature and so the orbital effects can be separated from the d-electron spin effects. However, neither vanadium nor chromium (above the Néel temperature) possess a local moment according to neutron diffraction

studies (69, 70) and the essentially temperature independent shift and susceptibility (80) observed are consistent with these results. Based on their measurements on the V_3X compounds, Clogston et al. (81) have estimated the contributions to the shift and susceptibility of vanadium. Shull and Ferrier (82) have studied, by neutron diffraction, the magnetization induced in vanadium when a magnetic field is applied. Their results are well represented by a theoretical form factor based on the distribution proposed by Clogston et al. We shall attempt to analyze our data in a fashion similar to these authors.

We write the total Knight shift as the sum of the contact, core polarization and orbital contributions. The shifts are proportional to the susceptibilities so we have

$$K_v = \alpha\chi_s + \beta\chi_d + \delta\chi_{orb} \tag{51}$$

We then determine (estimate) the various contributions to the shift of pure vanadium, determine the constants α, β and δ and use them in conjunction with the susceptibilities to obtain K_v throughout the alloy system.

Writing the contact part of the shift in terms of the free atom hyperfine constant a(s)

$$K_s = \frac{a(s)\,\chi_s\,\zeta\,\Omega\,I}{2\mu_B\mu_n} \tag{52}$$

where

$$a(s) = \frac{16\pi}{3}\,\frac{\mu_n\mu_B}{I}\,|\Psi_A(o)|^2 \tag{53}$$

Figure 15. The measured susceptibility from reference 80, the susceptibility calculated from the specific heat data of reference 68 and their difference, the orbital susceptibility, of the vanadium-chromium system as a function of the chromium concentration

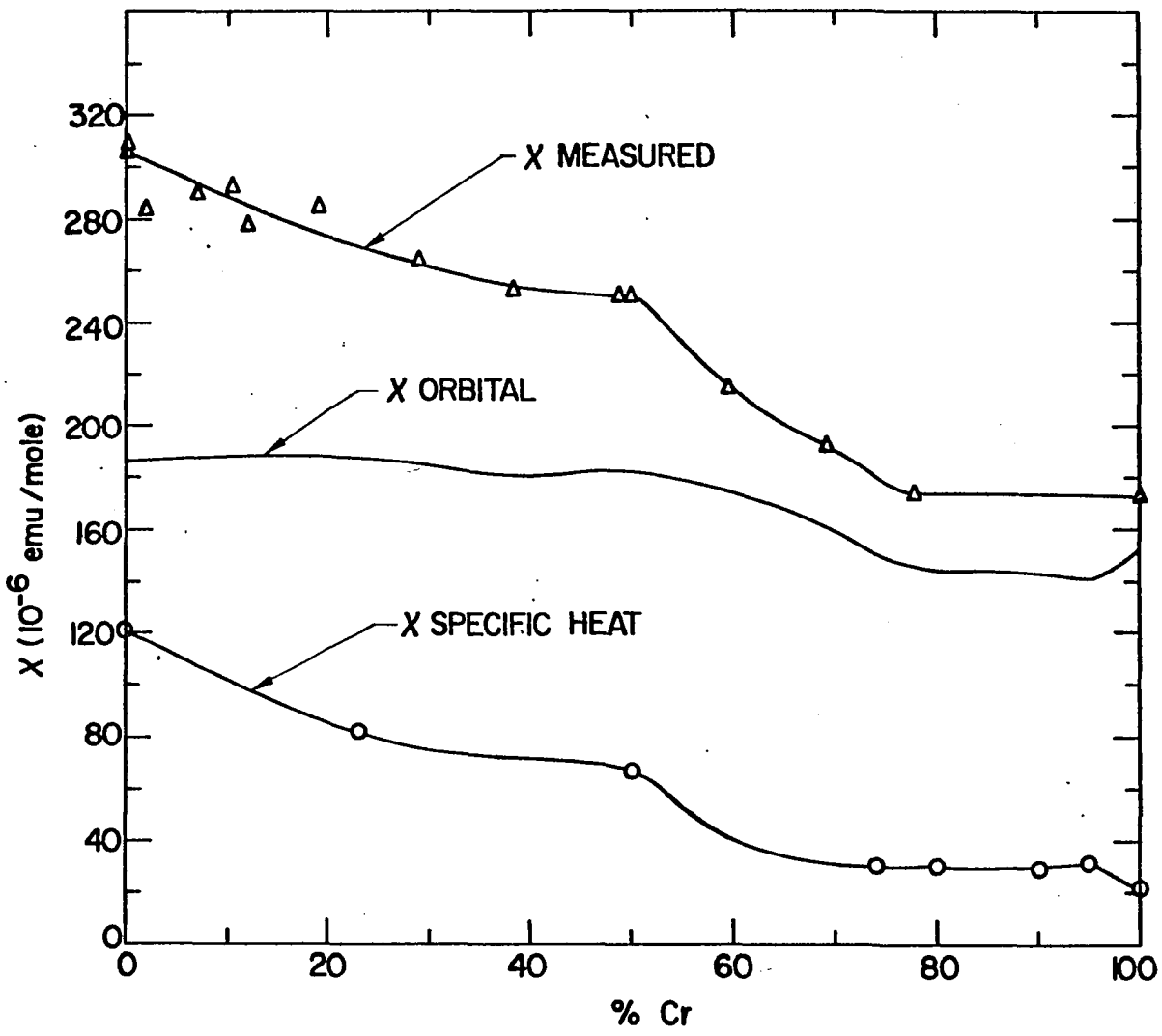
χ MEASURED
χ ORBITAL
χ SPECIFIC HEAT
χ (10⁻⁶ emu/mole)
% Cr
0
40
80
120
160
200
240
280
320
0
20
40
60
80
100

assuming $\zeta = 1$ (the ratio of the probability density in the metal to that in the free atom) and using data from Knight's review (35), we estimate this contribution to be 0.06%.

Initially it was believed that orbital effects made no contribution to the relaxation (81). On this basis, K_d was estimated to be -0.218% using the Korringa relation and the T_1T of Butterworth (83). (Although our T_1 measurements agree well with his, they were rather crude as previously stated; in addition he measured T_1 as a function of temperature.) Using the results of Yafet and Jaccarino (24) and including orbital relaxation (28), one obtains $K_d = -0.24\%$. This is not significantly different from the estimate of -0.218% which is used in the subsequent analysis and which was obtained prior to the appearance of the above papers. With these values for K_s and K_d we obtain, by subtraction from the measured Knight shift, $K_{orb} = 0.733\%$.

We next separate the susceptibility into its component parts according to

$$\chi_{meas} = \chi_s + \chi_d + \chi_{orb} = \chi_{sp\ ht} + \chi_{orb} \qquad (54)$$

where χ_{meas} has been corrected for diamagnetism. In Figure 15 we show the susceptibility measurements of Childs et al. (80), the susceptibility calculated from the low temperature specific heat measurements (68) by use of the equation

$$\chi_{sp\ ht} = \frac{3\ u_B^2}{\pi^2\ k_B^2} \qquad (55)$$

Figure 16. The calculated contributions to the V^{51} Knight shift in the vanadium-chromium system from the contact interaction, k_s, core polarization, k_d, and the orbital interaction, k_{orb}, as a function of the chromium concentration

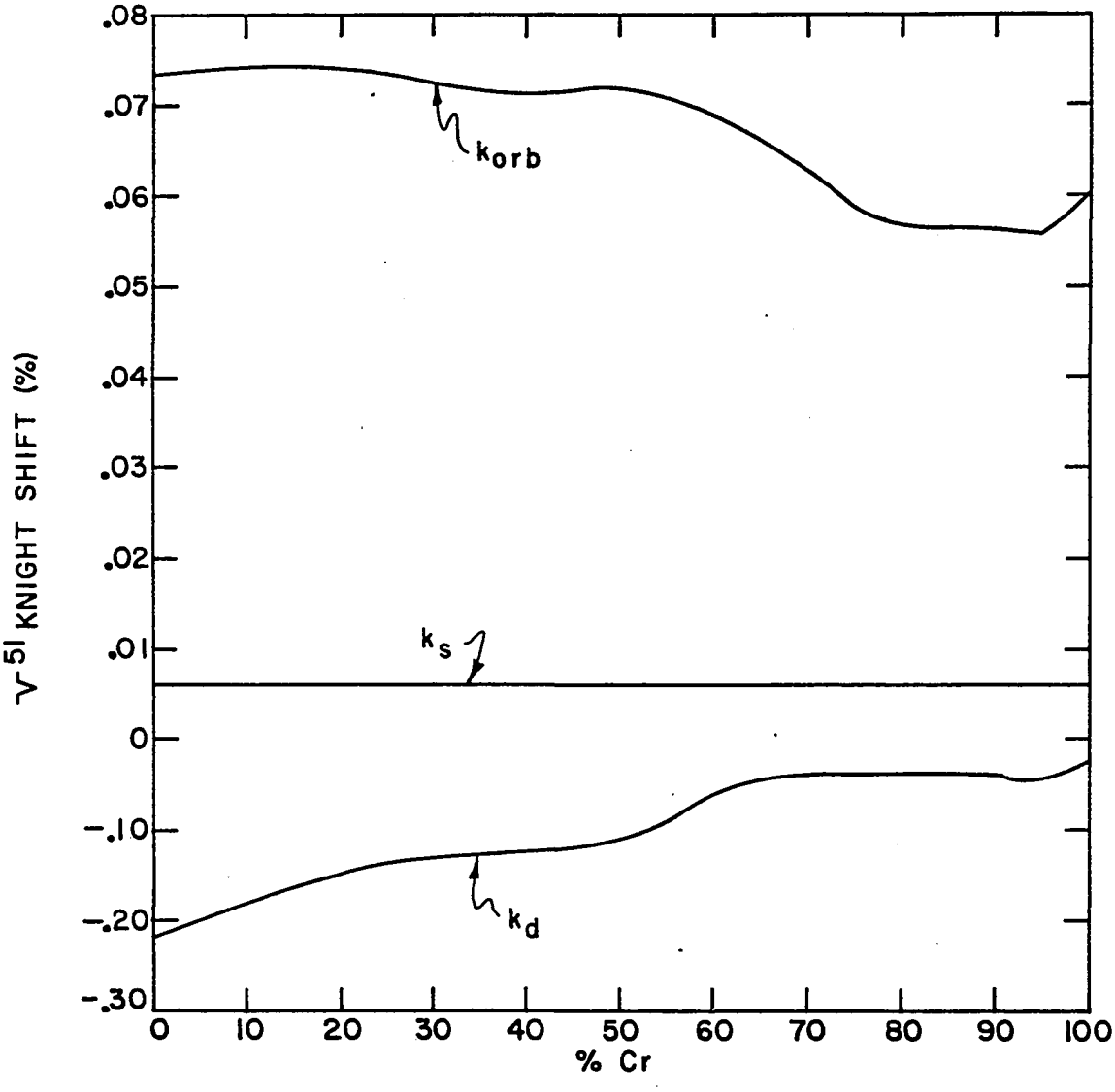
.08
.07
.06
.05
.04
.03
.02
.01
0
-.10
-.20
-.30
K^{51} KNIGHT SHIFT (%)
k_{orb}
k_s
k_d
0
10
20
30
40
50
60
70
80
90
100
% Cr

Figure 17. Comparison of the Knight shift measured at 15.235 MHz with the shift calculated in the manner described in the text

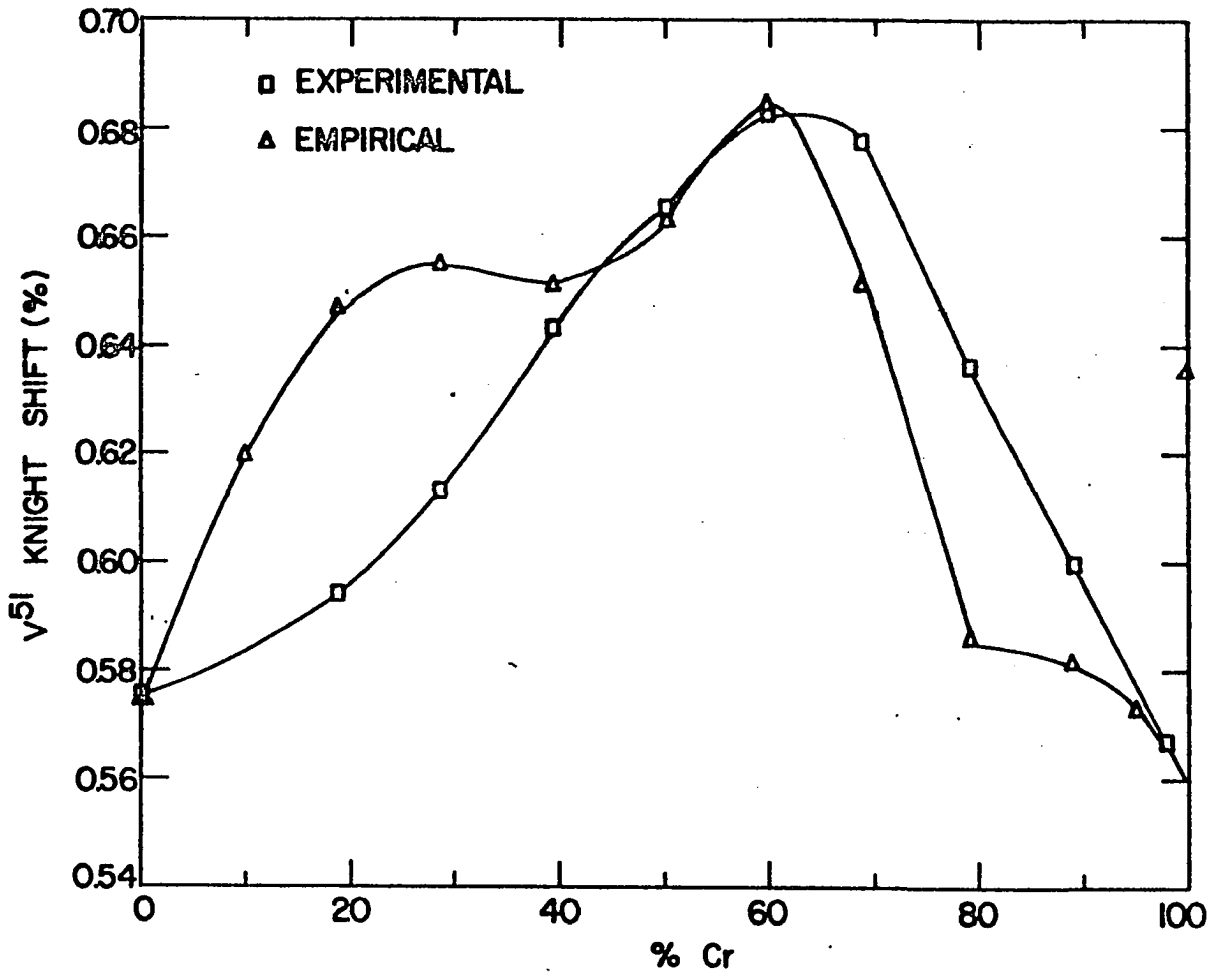
EXPERIMENTAL
EMPIRICAL
V^{51} KNIGHT SHIFT (%)
0.70
0.68
0.66
0.64
0.62
0.60
0.58
0.56
0.54
0
20
40
60
80
100
% Cr

Table 9. Calculated vanadium-51 Knight shifts

% Vanadium	$\chi_{sp\ ht}$[a]	χ_{meas}[b]	χ_{orb}	χ_d	k_s%	k_d%	k_{orb}%	k_V%
		10^{-4} emu/mole						
100	1.21	3.07	1.86	1.12	0.06	-0.218	0.733	0.575
90	1.02	2.90	1.88	0.93	0.06	-0.181	0.741	0.620
81.32	0.88	2.76	1.88	0.79	0.06	-0.154	0.741	0.647
71.57	0.78	2.63	1.85	0.69	0.06	-0.134	0.729	0.655
60.78	0.72	2.53	1.81	0.63	0.06	-0.123	0.714	0.651
49.93	0.67	2.49	1.82	0.58	0.06	-0.113	0.717	0.664
40.36	0.41	2.15	1.74	0.32	0.06	-0.062	0.686	0.684
31.30	0.31	1.92	1.61	0.22	0.06	-0.043	0.634	0.651
21.06	0.30	1.74	1.44	0.21	0.06	-0.041	0.567	0.586
11.10	0.30	1.73	1.43	0.21	0.06	-0.041	0.563	0.582
5.36	0.31	1.72	1.41	0.22	0.06	-0.043	0.556	0.573
0	0.21	1.73	1.52	0.12	0.06	-0.023	0.599	0.636

Note: $_s$ = 0.09 x 10^{-4} emu/mole using Equation 55 and the Y for copper (68).

[a]Using Equation 55 and the data of Cheng et al. (68).

[b]Reference (80).

and their difference which we attribute to the orbital interaction. $\chi_{sp\ ht}$ is analyzed into its s-electron and d-electron contributions by using the low temperature specific heat of copper to describe the s-electron contribution. This choice gives a constant χ_s and K_s throughout the system and the variation in density of states is due only to the variation of d-electron states. With this separation of the susceptibility, we can now determine the constants in Equation 51, $\alpha = 66.67$, $\beta = -19.46$ and $\delta = 39.41$ mole emu^{-1}. In Figure 16 we exhibit the various contributions to the calculated shifts. In our estimate of K_d, K_d^2 is involved and so there is an ambiguity in sign. In previous measurements of Knight shifts and internal fields, core polarization has been found to contribute a negative shift or field and so the minus sign was chosen.

In Table 9, we present the results of this analysis and in Figure 17 we compare the shifts obtained in this manner with the measured shifts. Fair agreement is obtained; the main feature of the measured shifts, the maximum around 62% chromium, is fairly well described. In view of the assumptions made, and the interpolations that were required in combining three different types of measurements made on different sets of alloys, more than qualitative agreement is not expected. The point calculated for 100% chromium deviates considerably from the general trend. Recently, Heiniger (84) measured the low temperature specific heat and Néel temperature of a large

number of dilute chromium alloys. He concluded that the specific heat constant, γ, for paramagnetic chromium is twice that which is actually measured. At low temperatures chromium is antiferromagnetic and according to the current understanding of this state, the Fermi surface is truncated by the magnetic zone boundaries. Thus only a fraction (50% according to Heiniger) of the electrons contribute to the specific heat at low temperatures. On this basis the point would lie somewhat below the experimental curve bringing it into general agreement. It might be noted that this procedure gives a smaller χ_{orb}, $\sim 130 \times 10^{-6}$ emu/mole, in better agreement with the rough estimate of $\sim 100 \times 10^{-6}$ emu/mole made by Denbigh and Lomer based on Equation 9 (83).

We have also attempted to determine the concentration dependence of T_1 on the basis of the estimates of the s-electron and d-electron contributions. We can write the total relaxation rate as

$$(T_1 T)^{-1}_{exp} = a\, N_s^2(E_F) + b\, N_d^2(E_F) + c\, N_d^2(E_F) \qquad (56)$$

The first term on the right can be determined from the contact part of the shift and the Korringa relation. We can lump the second and third terms together with a single constant and determine this constant by fitting the equation to the T_1 of vanadium. In terms of the specific heat constant the resulting equation (for a temperature of 300° K) is

$$T_1 = (28.2 + 1.77 \times 10^8\, \gamma_d^2)^{-1} \qquad (57)$$

where γ_d is obtained by subtracting out the γ for copper. This is plotted in Figure 10 and is seen to be in general agreement with the measured T_1's.

The relative importance of the various mechanisms can be estimated. Using Equations 15 and 19 in conjunction with K_s and K_d and assuming a spherically symmetric distribution for the d-electrons, $f = 3/5$, we find that the relaxation rate due to the contact interaction varies from 0.4 to 5 times the rate due to core polarization on going from the vanadium end to the chromium end of the system. Similarly, using Equations 16 and 19 and the β and δ from Equation 51, we find the orbital rate to be about 4 times that due to core polarization. So it appears that all the mechanisms are important.

The analysis presented here indicates that a rigid band approach can give a reasonable account of the data. The constants α, β and δ are probably not constant. We would expect some change in the wave-functions, the types of wave-function at the Fermi surface and $\langle r^{-3} \rangle$ but apparently these changes are not too drastic.

2. Impurity effects

As was mentioned previously, it is believed that the inhomogeneous Knight shift and quadrupole interactions are responsible for the line shapes of the vanadium resonances at the chromium end of the system. Based on the examples provided by the work of Rowland (39), it was thought that the scattering

theory approach to dilute alloys developed by Friedel (40) would give at least a qualitative description for the dilute chromium alloys.

Blandin and Daniel (41) have considered the scattering of Bloch functions from an impurity potential which they approximated by a spherical square well (or barrier). The symmetry of the lattice was ignored. They have shown that the relative change in Knight shift is related to the relative change in charge density of the electrons at the Fermi surface by

$$\frac{\Delta K}{K} = c \sum_R \frac{\Delta\rho(r)}{\rho(r)} \tag{58}$$

where c is the impurity concentration and the sum is over the lattice sites. They took as the periodic part of the Bloch function the wave-function at the bottom of the band and in forming the ratio, it drops out. So essentially one has a case of plane wave scattering from the well. Using the partial wave analysis, the relative change in charge density is related to the scattering phase shifts by

$$\frac{\Delta\rho(r)}{\rho(r)} = \sum_l (2l+1) \left[[n_l^2(kr) - j_l^2(kr)] \sin^2\delta_l - j_l(kr)\, n_l(kr) \sin 2\delta_l \right] \tag{59}$$

where δ_l is the phase shift of the l^{th} partial wave and $j_l(kr)$ and $n_l(kr)$ are spherical Bessel and Neumann functions respectively. The phase shifts are obtained from (86)

$$\tan\delta_l = \frac{kr_s j_l'(kr_s) - \gamma_l\, j_l(kr_s)}{kr_s n_l'(kr_s) - \gamma_l\, n_l(kr_s)} \; ; \; \gamma_l = \alpha r_s \frac{j_l'(\alpha r_s)}{j_l(\alpha r_s)} \tag{60}$$

Figure 18. The V^{51} Knight shifts measured at 15.235 MHz at the chromium-rich end of the alloy system as a function of the electron per atom ratio

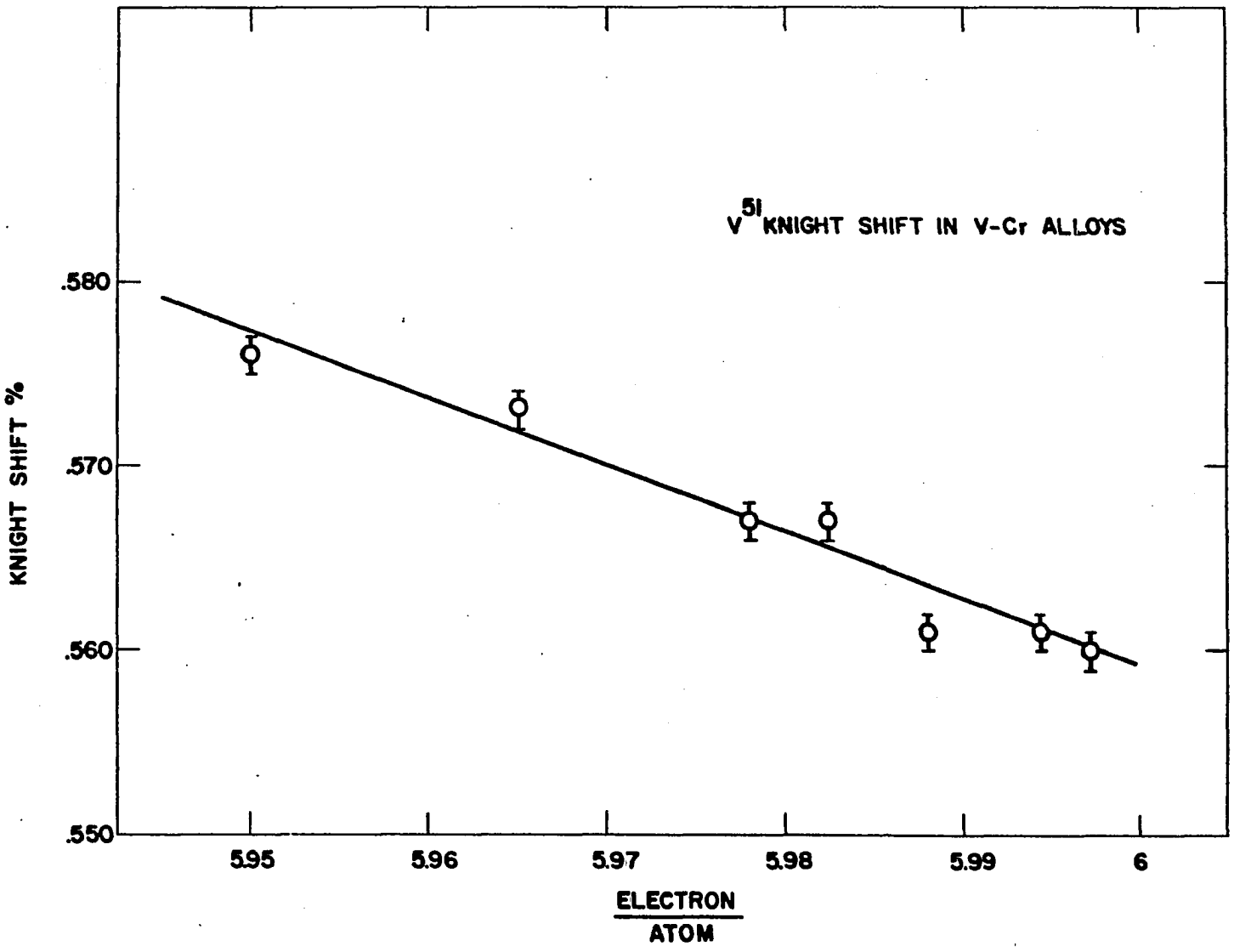
V^{51} KNIGHT SHIFT IN V-Cr ALLOYS
KNIGHT SHIFT %
.580
.570
.560
.550
5.95
5.96
5.97
5.98
5.99
6
ELECTRON
ATOM

where the primes indicate a derivative with respect to the argument and α is related to the scattering potential by

$$\alpha^2 = k^2 - \frac{2mV}{\hbar^2} \tag{61}$$

and r_s is the effective radius of the unit cell which is taken to be the radius of the potential.

The phase shifts are determined by varying the strength of the potential, i.e. α, until the phase shifts satisfy the Friedel sum rule (40)

$$Z = \frac{2}{\pi} \sum_l (2l + 1)\, \delta_l \tag{62}$$

Z is the difference between the number of valence electrons of the impurity and host atoms and is the charge to be screened by the conduction electrons. For the case at hand, Z = -1, and we take r_s to be 1.42 Å which is half the nearest neighbor distance in the chromium lattice. If one requires the screening to be due entirely to the d-electrons, the sum rule immediately gives $\delta_2 = -\frac{\pi}{10}$ with the rest zero. This corresponds to resonant scattering, i.e. the formation of a virtual d-state at the Fermi level. For potential scattering, we used $kr_s = 2.06$ to obtain the nonresonant phase shifts. A Fermi energy of 8.1 ev was estimated from data given by Shimizu et al. (87) and Wood (88) and the free electron dispersion rule used to obtain k. We find that the sum rule is satisfied when $\alpha r_s = 1.25$ by the phase shifts $\delta_o = -0.7555$, $\delta_1 = -0.2112$, $\delta_2 = -0.0331$ and $\delta_3 = -0.0026$, all in radians. Using Equation

59, $\sum_R \frac{\Delta\rho}{\rho}$ was evaluated for the first 21 shells of atoms around an impurity in the bcc chromium lattice with the results

$$\sum_R \frac{\Delta\rho(r)}{\rho(r)} = \begin{matrix} +0.54 & \text{nonresonant scattering} \\ -1.86 & \text{resonant scattering} \end{matrix} \qquad (63)$$

From the slope of the line in Figure 18, which shows the Knight shifts at the chromium end in detail, we obtain +0.65 for $\sum_R \frac{\Delta\rho}{\rho}$. Although the theory was developed for the resonance of the host and not of the impurity, the comparison we make is valid. It has been shown (42, 67) that the shift of the resonance of an impurity differs from its value in a pure metal because of the pileup of the screening charge on the impurity. This contribution to the ΔK should be the same for all the impurities. Since we can find K_v as the vanadium concentration approaches zero, we can measure ΔK with respect to it. Thus the changes in K will be those that result from the overlap of the oscillating charge density of neighboring impurities. If the orbital contribution is constant, then we expect that the comparison is meaningful. The value calculated on the basis of resonant scattering is seen to differ both in magnitude and sign. This is not unexpected since the alloys do not exhibit a local moment which is usually taken to be a manifestation of a virtual d-state in transition metals. The value calculated for the nonresonant case is in fairly good agreement with the observations. This agreement should be regarded as only qualitative in view of the simplifications made.

Figure 19. The relative change in charge distribution due to a vanadium impurity in chromium metal as a function of the radial distance from the impurity calculated for the case of nonresonant scattering as discussed in the text. The arrows denote the positions of the first 21 shells of neighbors in the chromium lattice

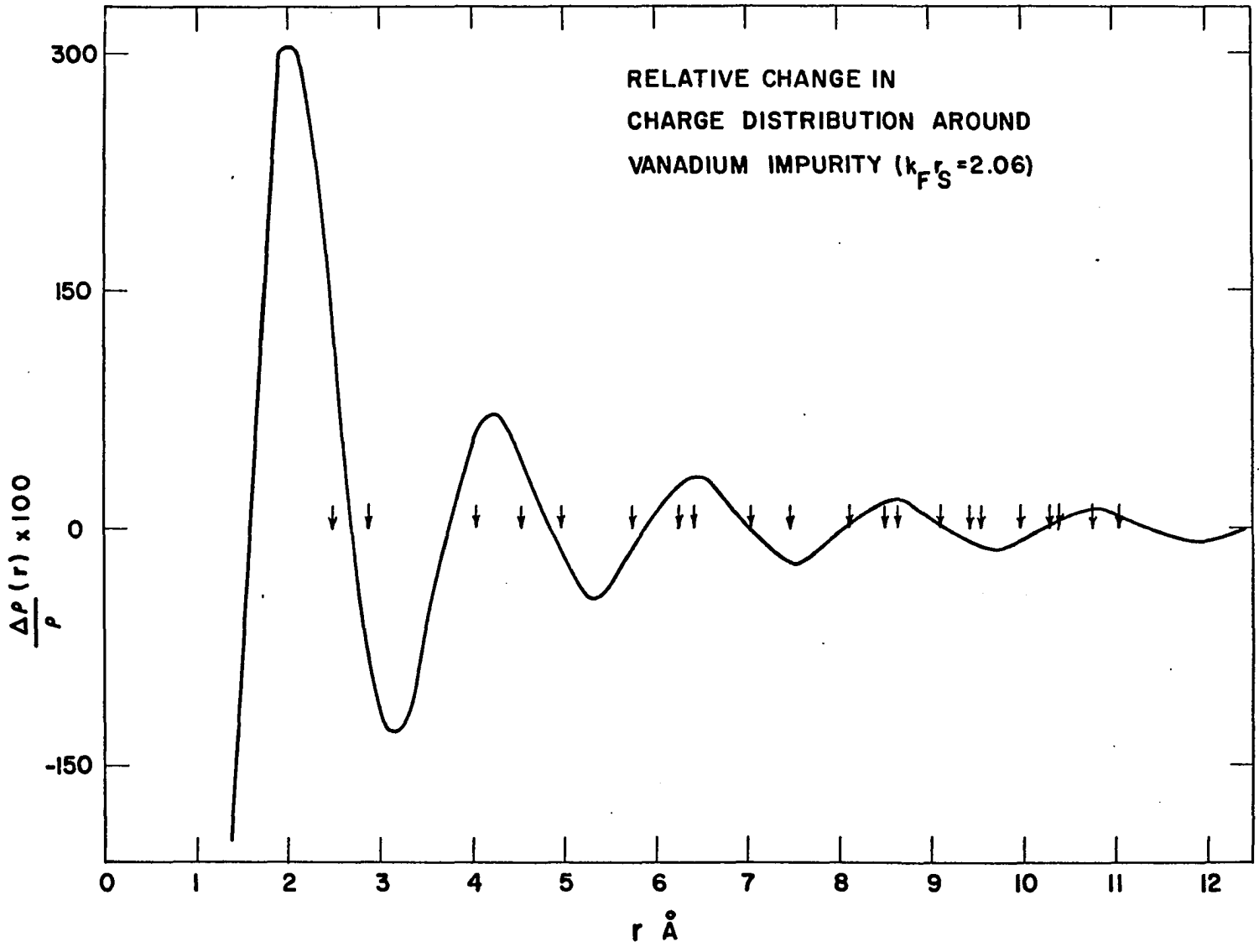
RELATIVE CHANGE IN
CHARGE DISTRIBUTION AROUND
VANADIUM IMPURITY ($k_F r_S$ =2.06)
300
150
0
-150
$\frac{\Delta\rho}{\rho}(r) \times 100$
0
1
2
3
4
5
6
7
8
9
10
11
12
r Å

Figure 20. The number of atoms in a shell around a vanadium impurity as a function of the relative change in charge density at the position of a given shell. The direction of decreasing field in this figure is from left to right

NUMBER OF ATOMS
10
20
30
40
50
-9
-6
-3
0
3
6
9
12
15
$\frac{\Delta\nu}{\nu}$

It is instructive to look at the dependence of the relative change in charge density as a function of the radial distance from the impurity. This is shown in Figure 19 for the case of nonresonant scattering. This curve is obtained from Equation 59 where the asymptotic forms of the Bessel and Neumann functions were used. The zeros of the resulting function could be obtained analytically and the maxima and minima graphically. The curve was sketched from these points. The arrows locate the distances of the various shells from an impurity in chromium. As can be seen, the charge density and hence the shift differs from shell to shell. In Figure 20 we have plotted the number in a shell vs. the relative change in charge density for the shell in order to get an idea of the line shape. (The number should be multiplied by the concentration since we are looking at the impurity.) To generate an actual line shape, one would superpose a line shape function describing the dipolar broadening at the resonance position for each shell and sum. The center of gravity of the resulting line in this example would be shifted in the direction of increasing shift as is observed. For an experiment done at constant frequency, the resonance is shifted to lower fields. We can see from the figure that the low field side of the resonance would have a "lump" on it and be more spread out than the high field side. This corresponds to what is observed in the dilute chromium alloys.

We can use the nonresonant phase shifts to estimate the relative strengths of the field gradient at the position of the shells. (Relative strengths because we lack information about the Bloch functions and the antishielding factor.) Using Equation 37 with

$$\tan \varphi = \frac{\sum_l (2l+1) \sin\delta_l \cos(\delta_l - l\pi)}{\sum_l (2l+1) \sin\delta_l \sin(\delta_l - l\pi)} \qquad (64)$$

we find that the magnitudes of the gradients for the first six shells are in the ratios

$$116 : 46 : 34 : 16 : 10 : 10 \qquad (65)$$

The gradients for the other shells are smaller due to the r^{-3} factor. It is thus possible that those nuclei in the first 2 or 3 shells experience gradients that eliminate their contributions to the resonance. This effect can qualitatively account for the intensity falling below 19% and the observed lineshapes.

The vanadium-51 Knight shift has also been measured in a chromium alloy containing 1.03% vanadium and 0.28% manganese. The shift was 0.568% at room temperature. This is about the same value as is obtained for a vanadium-chromium alloy with the same electron per atom ratio as would be expected on the basis of a rigid band model.

Table 10. Chromium-53 Knight shifts

% Vanadium	Knight shift %	Temperature (deg. C)	Comments
0	0.688 ± 0.020	114	UK
	0.690 ± 0.006[a]	89	UK
	0.682 ± 0.004[a]	93	A
	0.677 ± 0.004[a]	45	A
0.25[b]	0.688 ± 0.020	R.T.	UK
0.267	0.683 ± 0.003	R.T.	HA
0.50[b]	0.695 ± 0.020	R.T.	UK
0.556	0.684 ± 0.003	R.T.	HA
1.17	0.676 ± 0.004	R.T.	HA
1.5[b]	0.699 ± 0.020	R.T.	UK
1.72	0.683 ± 0.007	R.T.	HA
3.0[b]	0.690 ± 0.020	R.T.	UK

UK - Unannealed; K^{39} in HCOOK used as reference

A - Annealed

HA - Homogenizing anneal before filing; annealed after filing

[a]Chromium sample enriched to 98.5% Cr^{53}.

[b]Nominal concentration.

3. Chromium-53

The chromium-53 Knight shift was measured in pure chromium and in a few of the alloys containing small amounts of vanadium. The shifts were determined using the dispersion mode. The measurements are given in Table 10. The shift of the resonance in the enriched sample was 0.682% at 93° C, a temperature which is well above the antiferromagnetic transition region. The shift was essentially temperature independent down to the Néel temperature. The shift in the alloys was about the same as in the pure metal. The resonance intensity decreased very rapidly with the addition of vanadium and hence the range of alloy composition for which the shift could be measured was rather narrow. The decrease was more than one expects simply on the basis of the reduction of the number of chromium-53 nuclei and it is probable that the quadrupole interaction is responsible for the reduction in intensity. This may also account for the apparent constancy of the shift in the alloys. Those nuclei for which the shift is greatest are also subject to the largest gradients and do not contribute to the resonance.

The Knight shift in chromium is also probably made up of contributions from the orbital interaction, core polarization and the usual contact interaction. The T_1 of chromium has not been measured due to experimental difficulties and thus the Korringa relation cannot be checked. However, the disparity

between the measured susceptibility and the susceptibility calculated from the low temperature specific heat coefficient indicates a sizeable orbital contribution. In fact, if one scales the contributions to the vanadium shift at zero vanadium concentration, one obtains approximately the observed chromium shift. For vanadium we saw that the contact and core polarizations contributions essentially cancel at the chromium end of the system. Using Equation 8 we see the shifts should be in the ratio

$$\frac{K_V}{K_{Cr}} = \frac{\langle r^{-3} \rangle_{V \text{ metal}}}{\langle r^{-3} \rangle_{Cr \text{ metal}}} \sim 0.8 \qquad (66)$$

using the tabulated values of $\langle r^{-3} \rangle$ given by Freeman and Watson (89). We assume that the values $\langle r^{-3} \rangle$ are modified to the same extent in the metal for both vanadium and chromium. This gives a chromium shift of ~0.7% which is close to that observed.

4. Manganese-55

The manganese-55 Knight shift was measured in the alloy containing 1.03% vanadium and 0.28% manganese. The value was 0.342%. On the basis of the $\langle r^{-3} \rangle$ values (89), an estimate of the manganese shift is about three times the measured value. As noted, the vanadium shift in this alloy is consistent with the interpretation given on the basis of a rigid band. At about 15% manganese in chromium, a Curie-Weiss behaviour is observed which indicates that a localized moment has formed

Figure 21. Temperature dependence of the Cr^{53} resonance intensity in isotopically enriched (98.5% Cr^{53}) chromium

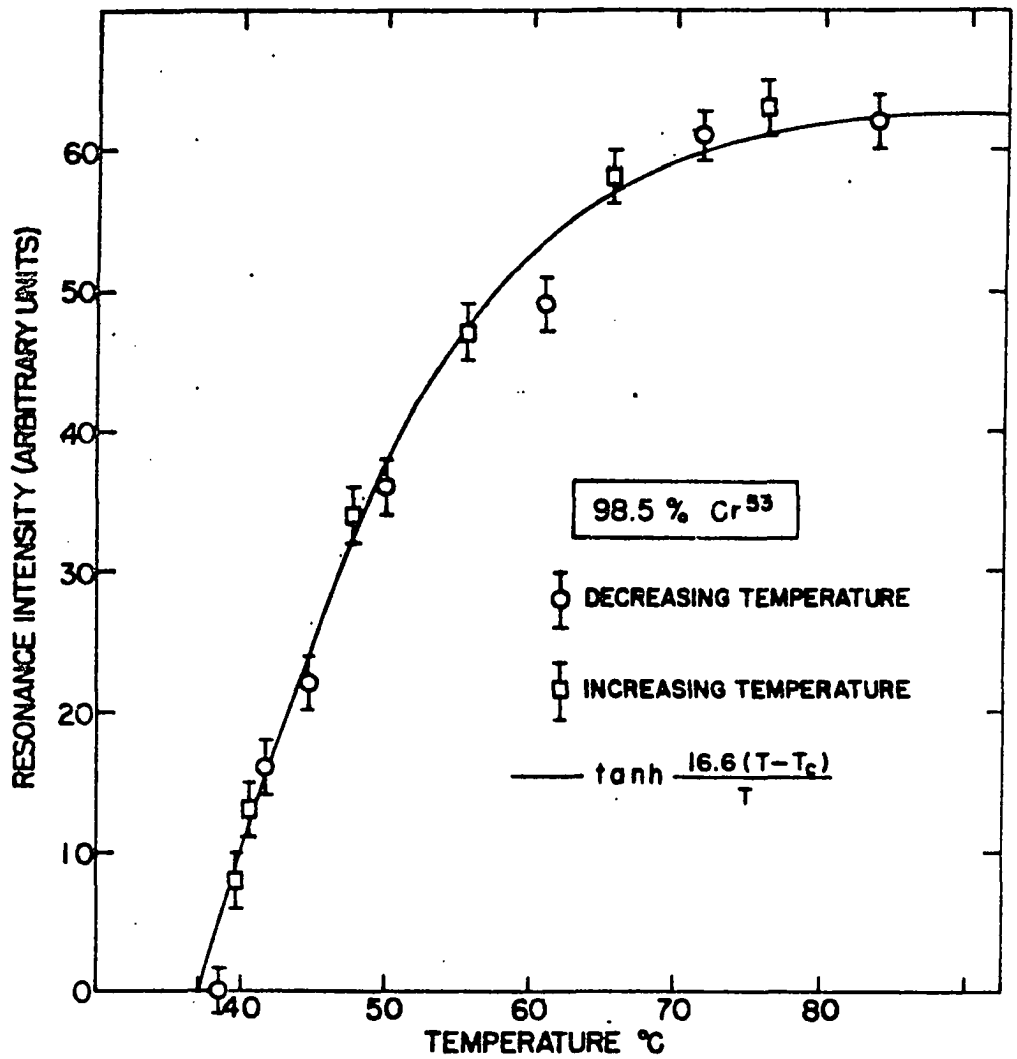
RESONANCE INTENSITY (ARBITRARY UNITS)
0
10
20
30
40
50
60
40
50
60
70
80
TEMPERATURE °C
98.5 % Cr53
DECREASING TEMPERATURE
INCREASING TEMPERATURE
tanh 16.6(T−Tc)/T

(90). The shift of manganese metal is approximately -0.13% (35) which indicates a considerable contribution from core polarization. If one assumes that in the alloy, the d-electrons are more or less localized on a manganese atom, a larger core polarization contribution could be expected. This would tend to make the shift more negative and produce better agreement with the measured shift.

E. Néel Temperatures of the Chromium-rich Alloys

As was previously mentioned, the vanadium-51 resonance could not be observed for a number of the dilute alloys of vanadium in chromium at 77° K. It was thought that this was due to the existence of an ordered antiferromagnetic state. To study the extinction of the resonance in these alloys, the resonance amplitude was monitored as the sample temperature was changed. The experiments were usually done with a magnetic field of about 13 KOe. In Figure 21 we show a plot of the peak-to-peak amplitude of the chromium-53 resonance from the sample of chromium enriched to 98.5% chromium-53 as a function of temperature. The amplitude is seen to vanish as the temperature is lowered through 39° C. The resonance position is essentially unshifted as the temperature is lowered as determined by the Knight shift measurements. The resonance line width broadens considerably (more than a factor of two) as the temperature of 39° C is approached from above. The diminution of resonance amplitude was taken as a measure of the

decrease in resonance intensity. The amplitude is the more convenient quantity to measure since the weakness of the resonance and broadening of the line make intensity measurements difficult. There is the possibility that, as the amplitude decreases, the line width increases such that the intensity remains constant. However, in one of the alloys (0.267% vanadium), this was checked by comparing amplitude measurements with intensity measurements (I α amplitude X line width^2) for the vanadium-51 resonance. The extinction temperature was the same in both cases indicating that the resonance does indeed "go away." This extinction temperature is within a degree of the Néel temperature as determined by neutron diffraction (10) and is in general agreement with the temperature at which various other anomalies in the properties of chromium occur. Thus we have chosen to regard the NMR extinction temperature as being identical with the Néel temperature T_N in chromium and also in the alloys. The field dependence, if any, of T_N of chromium could not be checked because of limitations on the frequency of the spectrometer. However, for one of the alloys (1.72% vanadium), measurements on the vanadium-51 resonance were made at 13.3 KOe and 3 KOe with no apparent difference in the Néel temperature. In Figure 21 the intensity data is well represented by the equation

$$I = I_o \tanh [K(1 - T_N/T)] \qquad (67)$$

Figure 22. Temperature dependence of the V^{51} resonance amplitude in a 1.72% vanadium-chromium alloy

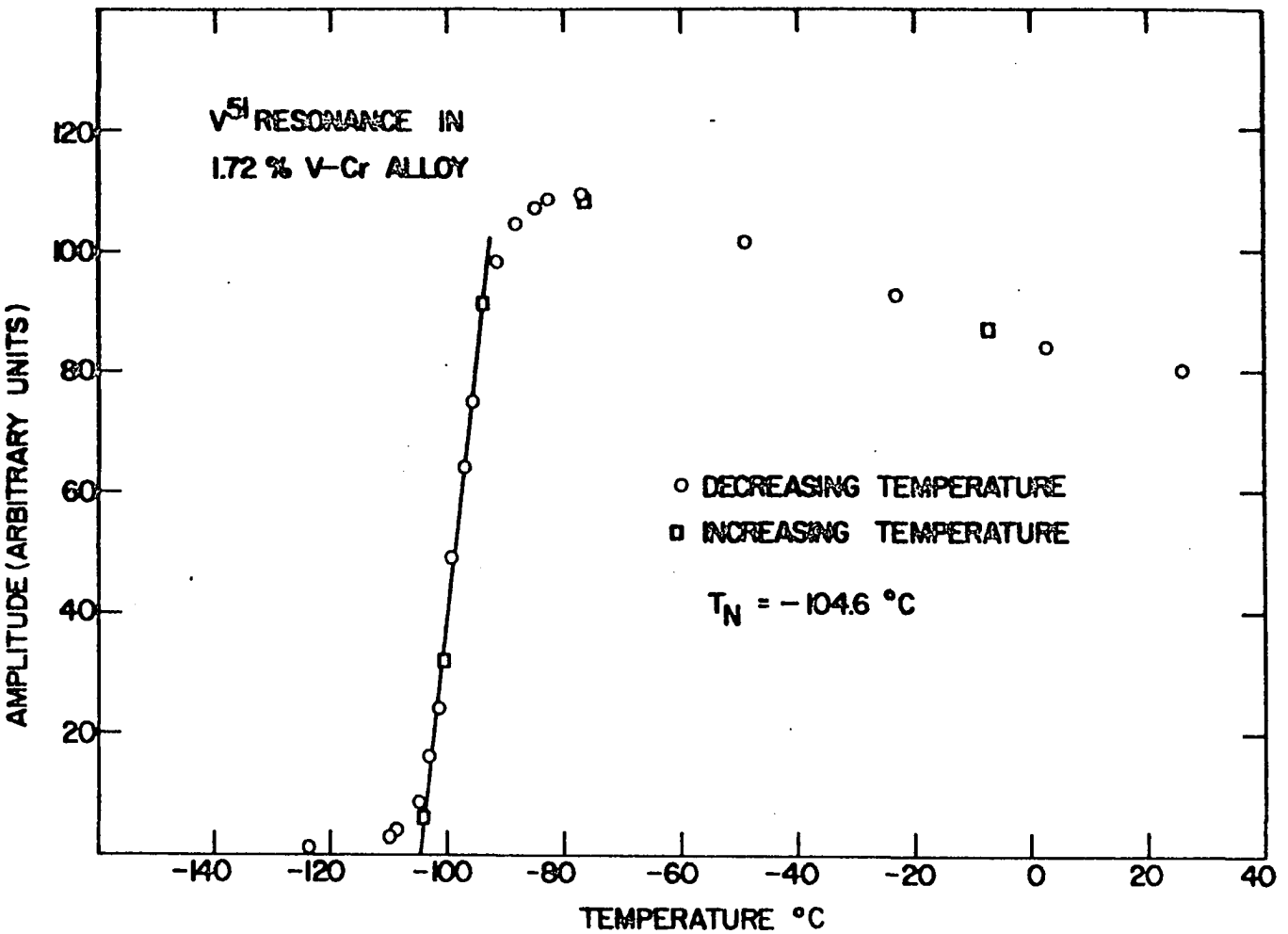
V^{51} RESONANCE IN
1.72 % V-Cr ALLOY
AMPLITUDE (ARBITRARY UNITS)
120
100
80
60
40
20
-140
-120
-100
-80
-60
-40
-20
0
20
40
TEMPERATURE °C
o DECREASING TEMPERATURE
□ INCREASING TEMPERATURE
T_N = −104.6 °C

Figure 23. Temperature dependence of the V^{51} resonance amplitude in a 2.16% vanadium-chromium alloy

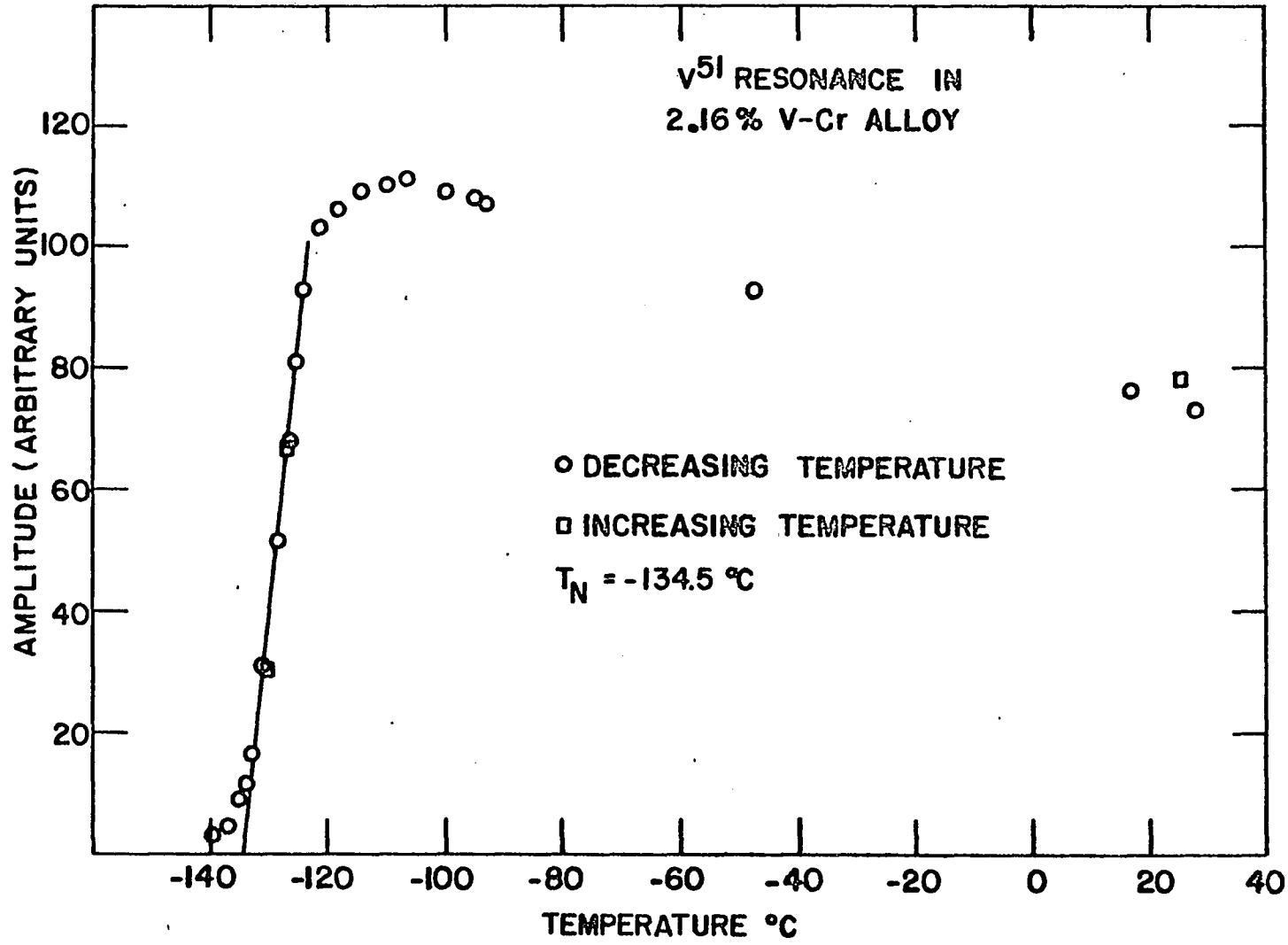
V51 RESONANCE IN
2.16% V-Cr ALLOY
AMPLITUDE (ARBITRARY UNITS)
120
100
80
60
40
20
-140
-120
-100
-80
-60
-40
-20
0
20
40
TEMPERATURE °C
O DECREASING TEMPERATURE
□ INCREASING TEMPERATURE
T_N = -134.5 °C

Figure 24. Temperature dependence of the V^{51} resonance amplitude in a 1.15% vanadium- 0.70% manganese-chromium alloy

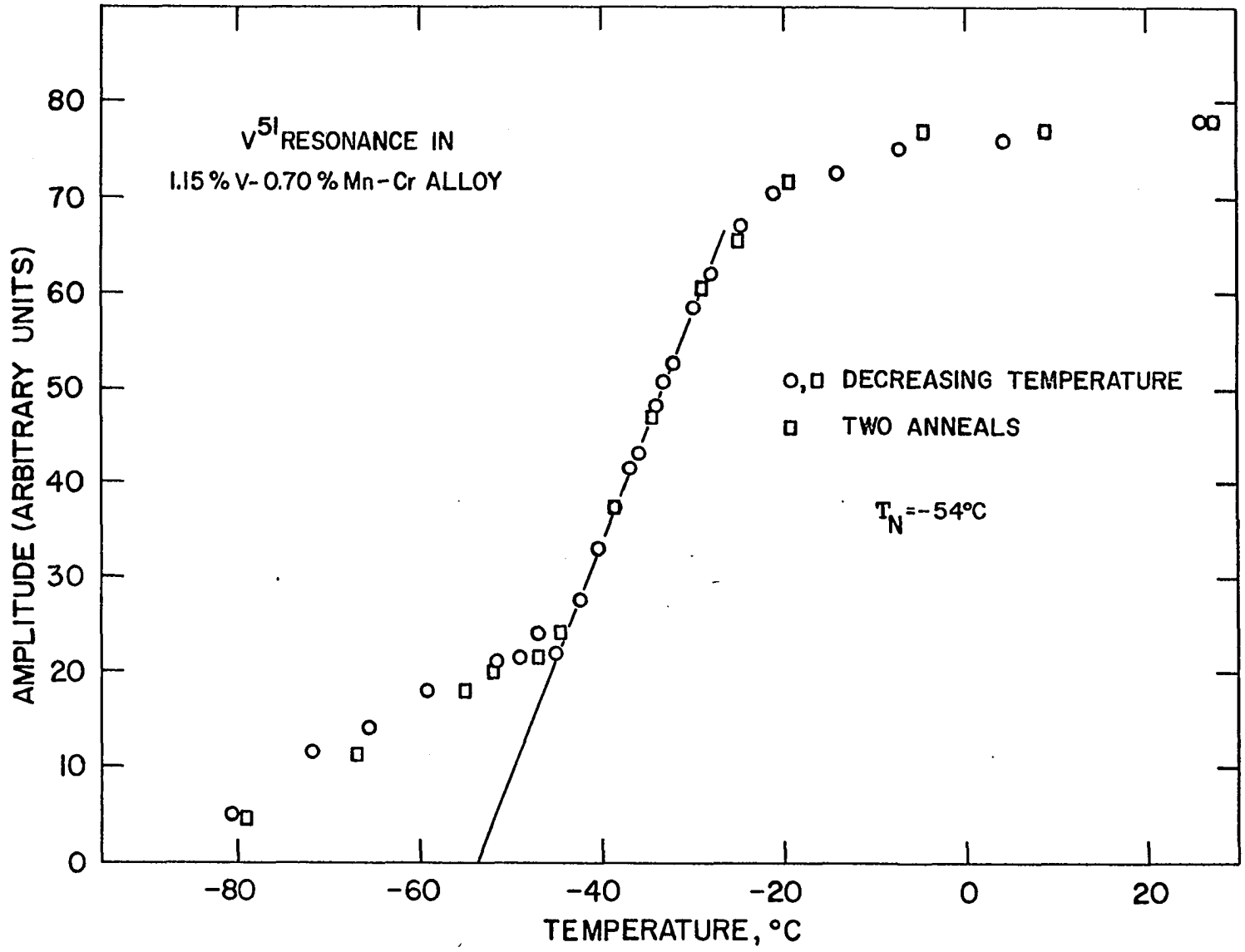
V^{51} RESONANCE IN
1.15 % V- 0.70 % Mn - Cr ALLOY
O, □ DECREASING TEMPERATURE
□ TWO ANNEALS
T_N = -54°C
AMPLITUDE (ARBITRARY UNITS)
TEMPERATURE, °C
0
10
20
30
40
50
60
70
80
-80
-60
-40
-20
0
20

Table 11. Néel temperatures in the chromium-rich alloys

Solute concentration %	e/a	T_N deg. K	Resonant nucleus	Particle size microns	Width of transition region deg. K
0[a]	6	310.7 ± 0.5	Cr^{53}	< 44	20
0.267 V	5.9973	277 ± 1.5	Cr^{53}, V^{51}	< 44	35
0.556 V	5.9943	244 ± 1	V^{51}	< 44	15
1.17 V	5.9881	203.8 ± 0.7	V^{51}	< 44	16
		190.7 ± 1.0	V^{51}	44-62	24
		192.8 ± 0.7	V^{51}	74-149	24
1.72 V	5.9824	168.0 ± 0.7	V^{51}	< 44	18
		168.0 ± 0.8[b]	V^{51}	< 44	16
		168.5 ± 0.6	V^{51}	44-62	20
		173 ± 1	V^{51}	74-149	20
2.16 V	5.9780	138.7 ± 0.7	V^{51}	< 44	20
		137.4 ± 0.7	V^{51}	44-62	20

[a]Enriched sample.

[b]Measured at 3 KOe.

Table 11. (Continued)

Solute concentration %	e/a	T_N deg. K	Resonant nucleus	Particle size microns	Width of transition region deg. K
2.83 V	5.9711	87.2 ± 0.8	V^{51}	< 44	35
3.41 V	5.9652	3	V^{51}	< 44	-
0.25 Mn	6.0024	350 ± 5	Cr^{53}	< 44	-
1.03 V & 0.28 Mn	5.9921	218.1 ± 0.7	V^{51}	< 44	25
		218.5 ± 0.7	V^{51}	44-62	25
1.15 V & 0.70 Mn	5.9949	219.0 ± 0.6	V^{51}	< 44	33

where I_o is the intensity at temperatures well above the transition region and K = 16.6. No theoretical significance has been attached to this equation, it was merely used as an aid in extrapolation. Similar measurements were also performed using a sample of natural chromium with a resulting T_N of about 40° C. Due to the weakness of the resonance, this result is not too precise. The number of nuclei is down a factor of ten from that of the enriched sample and consequently the signal to noise ratio is poor.

A number of dilute chromium alloys were studied by observing (usually) the temperature dependence of the vanadium-51 resonance. The Néel temperatures are tabulated in Table 11 and representative amplitude vs. temperature plots are shown in Figures 22, 23 and 24 for 1.72% vanadium in chromium, 2.16% vanadium in chromium and 1.15% vanadium and 0.70% manganese in chromium, respectively. As can be seen, the shape of the amplitude vs. temperature curve differs from that of pure chromium. This was generally true of the alloys with the exception of the 0.267% vanadium alloy. Probably small concentration differences among the powder grains is partly responsible for the differences in shape. No attempt was made to fit the shape by an analytic expression. In the transition region the curve is linear so the linear region was extrapolated to zero amplitude and the point of intersection with the temperature axis was taken to be T_N. The value for the

Figure 25. Dependence of the Neel temperature on the electron per atom ratio in chromium alloys with vanadium and manganese

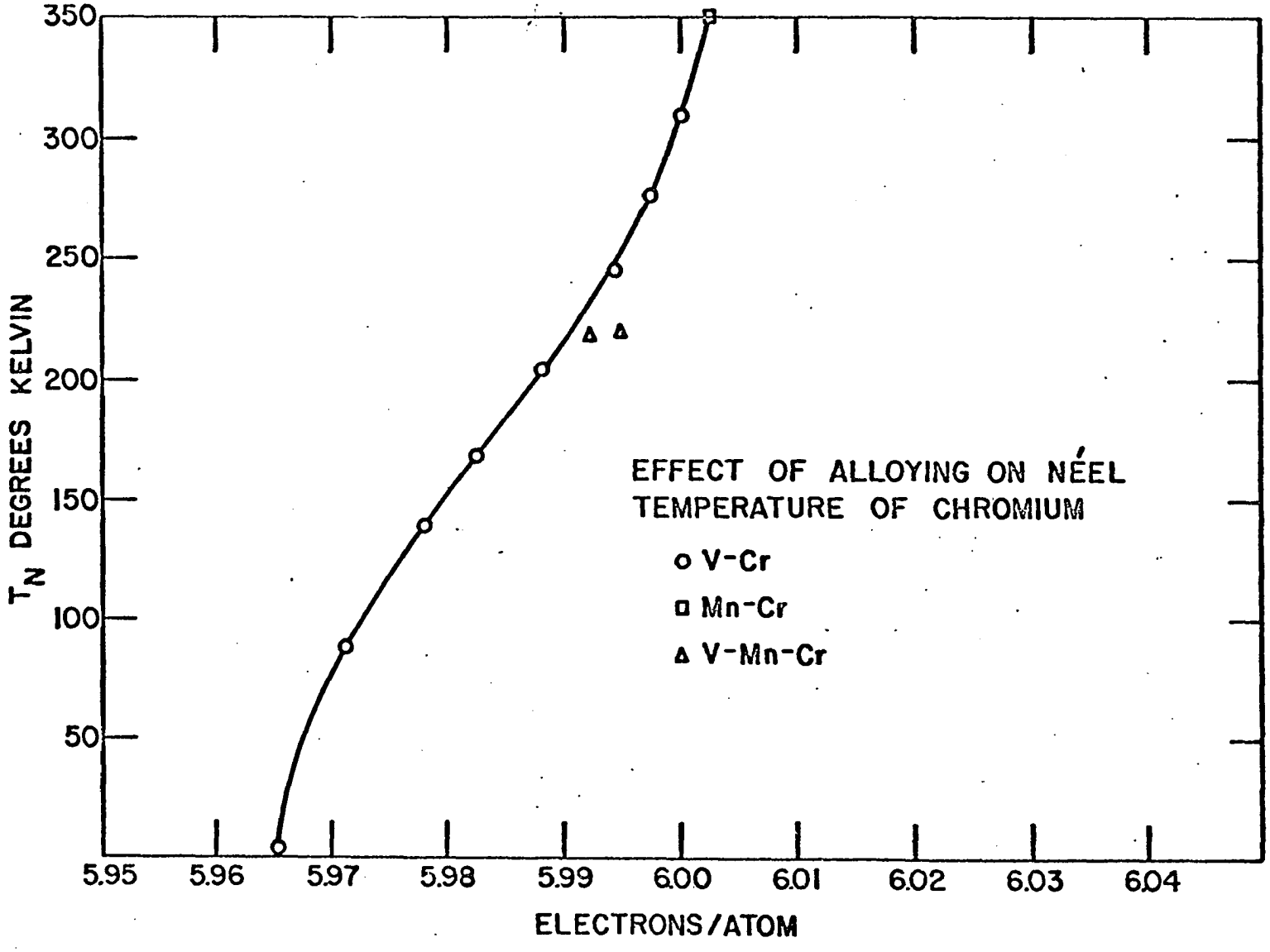
350
300
250
200
150
100
50
T_N DEGREES KELVIN
5.95
5.96
5.97
5.98
5.99
6.00
6.01
6.02
6.03
6.04
ELECTRONS/ATOM
EFFECT OF ALLOYING ON NÉEL TEMPERATURE OF CHROMIUM
o V-Cr
□ Mn-Cr
△ V-Mn-Cr

chromium-manganese alloy was obtained using the chromium-53 resonance which was quite weak and is not as reliable as the others.

The Néel temperatures determined for 325 mesh powders are summarized in Figure 25 where they are plotted as a function of the number of electrons per atom outside the argon core. With the equipment used it was not possible to control the temperature in the range 4.2° K to 77° K. The resonance in the 3.41% vanadium alloy was quite strong at 77° K whereas at 4.2° K it was all but extinguished. On this basis a Néel temperature of 3° K was chosen for this sample. Samples containing 4.92% and 5.35% vanadium exhibited strong vanadium-51 resonances at 4.2° K.

In some runs, the resonance amplitude above the transition differed depending upon whether the transition was approached from higher or lower temperatures. The amplitude was somewhat diminished when the temperature was increased through the transition. In his neutron diffraction studies of powdered chromium, Bacon (10) noted that some residual antiferromagnetic order persisted to temperatures well above the Néel temperature. The determination of the Néel temperatures was not affected by this hysteresis however, since the linear region was unaffected. Generally, for the alloys, a slight tail was observed below T_N. This is presumed to be due to a small fraction of the sample having a larger concentration of

solute than the average. The 1.15% vanadium, 0.70% manganese sample exhibited a large hump in its amplitude vs. temperature curve. The sample was reannealed but this did not result in any significant change. It is probable that the sample was not sufficiently homogeneous prior to filing. The actual position for this alloy on the e/a axis in Figure 25 is thus in doubt; presumably it should be shifted somewhat to the right. Some dependence of T_N on particle size was noted. Generally T_N differed only slightly for samples that had been passed through different sized sieves, however, the samples containing 1.17% vanadium exhibited a 14° K spread in their values of T_N. The width of the transition, as measured from T_N to the knee of the curve, increased with increasing particle size which seems to indicate a greater variation in solute concentration for the larger particles. The 325 mesh data was chosen for Figure 25 because the particle size--44 microns or less--best fulfilled the requirement that the particle size be less than the skindepth of the radio-frequency radiation. Eddy current effects, however, are not thought to be the cause of the differences in the Néel temperatures.

It appears that, at present, the most appropriate description of the transition to an antiferromagnetic state in chromium is in terms of a magnetic ordering of the electron gas. Overhauser (91) has suggested that in the ordered state there exists a "spin density wave" (SDW). In this state there are no localized moments, but the electrons in the electron gas

are coupled via exchange interactions in such a way that there is a sinusoidal spatial variation of electronic magnetic moment. Neutron diffraction studies (12) have confirmed this and have shown that the wavevector $\vec{q}$ of the magnetic modulation is parallel to a cube axis and is not commensurate with the lattice. Lomer (92) proposed that the main features of the Fermi surface of non-magnetic chromium consist of an octahedron of electrons at the center of the Brillouin zone and, in a second band, hole octahedra at the zone corners. Detailed calculations by Loucks (93) and Fermi surface studies (94) of the other chromium group metals molybdenum and tungsten, are in agreement. Lomer suggests that the states on the electron and hole surfaces connected by the wavevector $\vec{q}$ of the magnetic modulation are responsible for the magnetic ordering and consequently the coupling of these states produces energy gaps at the Fermi surface. The occurrence of these gaps is believed to be responsible for the anomalies observed in the transport, thermal and magnetic properties. Fedders and Martin (95) have discussed Lomer's model in some detail and have presented a simplified model for the antiferromagnetism in chromium with which they derive an expression for the Néel temperature. The various quantities in this expression, however, are not readily amenable to comparison with experimentally determined parameters. Hence we must restrict ourselves to a qualitative discussion of the effects of the antiferromagnetic ordering on the resonance properties.

Chromium has no localized moment above the Néel temperature (70) and hence exhibits only Pauli paramagnetism. This is consistent with the temperature independent Knight shift and the constant linewidth and amplitude observed above the transition region. Critical magnetic scattering of neutrons at temperatures above the Néel temperature (96, 97) indicate the presence of short range magnetic order. So, as the transition begins, some nuclei experience internal fields through their hyperfine coupling to the electrons. There should be a spectrum of hyperfine fields because the wavelength of the magnetic modulation is about 1.05 times the lattice constant (12). As the temperature is lowered, some nuclei experience large hyperfine fields and their resonance is shifted beyond the range of observation. Some of the nuclei can experience small fields at first and contribute to the line broadening. As the temperature is decreased further the internal fields increase and eventually shift the resonance contribution of all the nuclei beyond the range of observation. Hence the width of the resonance line and of the transition region can be pictured as resulting from a gradual 'turning on' of internal fields of differing magnitudes. It seems that, in principle, since some of the nuclei are near nodes of the SDW, these nuclei would be relatively unaffected by the magnetic ordering. This was not observed, possibly due to the fact that the resonances are rather weak to begin with. Another

contribution to the width of the transition can come from the spread in solute concentration from particle to particle and thus the possibility of different grains undergoing the transition at different temperatures. In addition, Overhauser (91) has indicated that in a polycrystalline powder the wavelength of the SDW may be partly determined by grain boundaries, the particle surface or other mechanical imperfections which may be present.

As can be seen from Figure 25, the Néel temperature is a rapidly decreasing function of vanadium concentration in the alloys. Various attempts were made to find a linear relation between the Néel temperature and other parameters, concentration and the low temperature specific heat constants for example, without success. On the basis of the Lomer model, one expects the Néel temperature to depend on the area of the Fermi surface for which the exchange interaction couples electron and hole states. To sketch the exact dependence of T_N on composition would require a detailed knowledge of the Fermi surface as a function of the solute concentration. Qualitatively we can see how the rapid change of T_N could come about. The Hall coefficients are positive for chromium, 1% vanadium in chromium and 1% manganese in chromium and their magnitudes are in the order $R_{1\%\ V} < R_{Cr} < R_{1\%\ Mn}$ at room temperature (11). This implies that the number of holes decreases and the number of electrons increases as the electron per atom ratio

is increased. This is also to be expected on the basis of Loucks' calculations (93). As the electron per atom ratio increases from about 5.95 to above 6, the electron surface is expanding while the hole surface is contracting. These surfaces have roughly the same shape except that initially the volume enclosed by the electron surface is less than the volume enclosed by the hole surface. As the electron concentration is increased, the surfaces become more identical and larger regions of the surfaces can be connected by the vector $\vec{q}$ and hence T_N increases. On this model T_N is correlated with the concentration but not in a simple fashion since only those electrons on certain protions of the Fermi surface are involved. Again, in our explanations we have used a rigid band model. We would thus expect dilute alloys with $e/a < 6$ to have $T_N < T_{N_{Cr}}$, those with $e/a > 6$ to have $T_N > T_{N_{Cr}}$ and those with $e/a = 6$ to have the same T_N as chromium. This is observed with the exceptions of iron, cobalt, molybdenum and tungsten which decrease T_N although less rapidly than does vanadium. This implies a breakdown in the rigid band model. However, according to Blatt (98), the effective valence of a solute which expands the lattice, as do molybdenum and tungsten, in chromium, is less than the valence assigned on the basis of the number of electrons outside a closed shell. On this basis the chromium alloys with molybdenum and tungsten would have an effective electron per atom ratio less than 6

and a T_N less than that of chromium, as is observed. Also since the atomic diameter of tungsten is larger than that of molybdenum we would expect tungsten to depress the Neel temperature to a larger extent, as is also observed. Using these ideas, DeSorbo (99) has found, for vanadium alloys, an improved correlation of superconducting transition temperatures with the effective e/a ratio rather than the usual e/a ratio. Similar considerations might also apply to iron and cobalt. However these cases would be complicated by the fact that they are known to exhibit localized moments in chromium. If one excludes the localized electrons when considering the number of electrons contributing to the band, the e/a ratio would be 6. In these cases, however, the effect of magnetic couplings would have to be considered.

Anomalies, similar to those found in chromium at the Néel temperature, have been observed in pure vanadium around 220° K. An antiferromagnetic transition has been proffered for their explanation. In addition to observing the vanadium-51 resonance between room temperature and 77° K, we monitored the resonance amplitude as a function of temperature down to about 160° K without observing any irregularities. Recently, distortions of the crystal structure have been observed by Suzuki around 230° K in single crystals of vanadium (100). The spacing between various planes changes sharply and the

thermal expansion coefficient differs for the three cubic axes below this temperature. This crystallographic change is probably responsible for the anomalies observed.

V. SUMMARY

Evidence has been presented for appreciable quadrupole interaction in the cubic vanadium-chromium alloys. This evidence consists primarily of the intensity measurements supplemented by the observation of the narrow echo widths. The apparent constancy of the Cr^{53} Knight shifts and the absence of the resonance with a few per cent vanadium present are also indicative of quadrupole interactions. The origin of the gradients producing these interactions has not been established. It was suggested that the changes induced in the charge distribution by solute atoms was the primary cause and that the change in the magnitude as one proceeds through the alloy system reflected the rather sharp change in the density of states around 60% chromium. This point of view is not entirely consistent with the line width measurements. There we found better agreement for the field independent width when the spin-flip term for nearest neighbors was included in the calculation of the second moment. The difficulty probably lies, to some extent, in attempting to use ideas conceived for dilute alloys for the more concentrated alloys. In the more concentrated alloys we also found a sizeable field dependent contribution of uncertain origin.

The Knight shifts and spin-lattice relaxation times of V^{51} have been found to be in qualitative agreement with the predictions based on a rigid band model. The rapid rise in

the relaxation times reflect the sharp decrease in the density of states as the chromium concentration increases beyond 60%. The variation of the Knight shift as a function of concentration results from the interplay of the orbital and core polarization contributions. In the region from 0 to 50% chromium, the orbital contribution is large, positive and relatively constant. In this region the core polarization contribution is approximately one-third the magnitude of k_{orb}, negative and slowly decreasing in magnitude. They combine to give an increasing Knight shift in this region. At higher concentrations, the orbital contribution decreases more rapidly than the core polarization contribution and causes the total shift to decrease at concentrations higher than about 62% chromium. A detailed fit is lacking but the general behavior is in agreement with the measurements. A slightly different analysis than ours, by Shimizu et al. (101), gives the same conclusions. By considering the contributions to the vanadium shift extrapolated to pure chromium, a value for the Cr^{53} Knight shift was estimated which was in good agreement with the observed shift. On this basis, the shift in chromium is almost entirely due to the orbital interaction.

The shapes of the vanadium resonances at the chromium-rich end of the system are in qualitative agreement with the line shapes expected from inhomogeneous Knight shift effects. A rather approximate, and perhaps naive, calculation of these

effects, based on the scattering of free electrons from a square well potential, gives fairly good agreement for the relative change in Knight shift as a function of concentration.

The Néel temperatures of chromium and of a series of dilute vanadium-chromium alloys were measured. The Néel temperatures decrease rapidly as the vanadium concentration is increased. These temperatures extrapolate to zero Néel temperature at a vanadium concentration of about 3.5%. The behaviour of the Néel temperatures is in qualitative accord with the current knowledge of the band structure of chromium and the interpretation of the antiferromagnetic state in terms of a sinusoidal modulation of the magnetic moment of the band electrons. The behavior of the resonance parameters in the vicinity of the transition is also consistent with these views.

VI. LITERATURE CITED

1. Carlson, O. N., D. T. Eash and A. L. Eustice, Reactive Metals 2, 277 (1958).

2. Burger, J. P. and M. A. Taylor, Phys. Rev. Letters 6, 185 (1961).

3. Collings, E. W., F. T. Hedgcock and A. Siddiqi, Phil. Mag. 6, 155 (1961).

4. Bolef, D. I., J. de Klerk and G. B. Brandt, Bull. Am. Phys. Soc. 7, 236 (1962).

5. White, G. K., Australian J. Phys. 14, 359 (1961).

6. Beaumont, R. H., H. Chihara and J. A. Morrison, Phil. Mag. 5, 188 (1960).

7. Mackintosh, A. R. and L. Sill, J. Phys. Chem. Solids 24, 501 (1963).

8. de Vries, G. and G. W. Rathenau, J. Phys. Chem. Solids 2, 339 (1957).

9. Arajs, S., R. V. Colvin and M. J. Marcinkowski, J. Less-Common Metals 4, 46 (1962).

10. Bacon, G. E., Acta Cryst. 14, 823 (1961).

11. de Vries, J. Phys. Radium 20, 438 (1959).

12. Koehler, W. C., J. W. Cable, A. L. Trego and A. R. Mackintosh, Phys. Rev. 151, 405 (1966).

13. Pake, G. E., Solid State Physics 2, 1 (1956).

14. Fermi, E., Z. Phys. 60, 320 (1930).

15. Knight, W. D., Phys. Rev. 76, 1259 (1949).

16. Townes, C. H., C. Herring and W. D. Knight, Phys. Rev. 77, 852 (1950).

17. Milford, F. J., Am. J. Phys. 28, 521 (1960).

18. Slichter, Charles P., Principles of Magnetic Resonance, Harper and Row, New York, N.Y. (1963).

19. Kubo, R. and Y. Obata, J. Phys. Soc. Japan 11, 547 (1956).

20. Clogston, A. M., V. Jaccarino and Y. Yafet, Phys. Rev. 134, A650 (1964).

21. Bloembergen, N. and T. J. Rowland, Acta Met. 1, 731 (1953).

22. Cohen, M. H., D. A. Goodings and V. Heine, Proc. Phys. Soc. (London) A73, 811 (1959).

23. Clogston, A. M. and V. Jaccarino, Phys. Rev. 121, 1357 (1961).

24. Yafet, Y. and V. Jaccarino, Phys. Rev. 133, A1630 (1964).

25. Bloch, F., Phys. Rev. 70, 460 (1946).

26. Korringa, J., Physica 16, 601 (1950).

27. Pines, D., Solid State Physics 1, 367 (1955).

28. Obata, Y., J. Phys. Soc. Japan 18, 1020 (1963).

29. Mitchell, A. H., J. Chem. Phys. 26, 1714 (1957).

30. Andrew, E. R., Phys. Rev. 91, 425 (1953).

31. Van Vleck, J. H., Phys. Rev. 74, 1168 (1948).

32. Holcomb, D. F. and R. E. Norberg, Phys. Rev. 98, 1074 (1955).

33. Abragam, A., The Principles of Nuclear Magnetism, Oxford, London (1961).

34. Kambe, K. and J. F. Ollom, J. Phys. Soc. Japan 11, 50 (1956).

35. Rowland, T. J., Progress in Materials Science 9, 1 (1961).

36. Knight, W. D., Solid State Physics 2, 93 (1956).

37. Mott, N. F., Proc. Camb. Phil. Soc. 32, 281 (1936).

38. Drain, L. E., Phil. Mag. 4, 484 (1959).

39. Rowland, T. J., Phys. Rev. 125, 459 (1962).

40. Friedel, J., Suppl. Nuovo Cimento 7, 287 (1958).

41. Blandin, A. and E. Daniel, J. Phys. Chem. Solids 10, 126 (1959).

42. Daniel, E., J. Phys. Chem. Solids 10, 174 (1959).

43. Drain, L. E., Proc. Phys. Soc. 80, 1380 (1963).

44. Ruderman, M. A. and C. Kittel, Phys. Rev. 96, 99 (1954).

45. Andrew, E. R., Nuclear Magnetic Resonance, Cambridge, London, England (1955).

46. Watkins, G. D. and R. V. Pound, Phys. Rev. 89, 658 (1953).

47. Bloembergen, N., Nuclear Magnetic Resonance in Imperfect Crystals. In Report of Conference on Defects in Crystalline solids, p. 1. Physical Society, London, England (1955).

48. Averbuch, P., F. DeBergevin and W. Muller-Warmuth, Compt. Rend. 249, 2315 (1959).

49. Rowland, T. J., Phys. Rev. 119, 900 (1960).

50. Kohn, W. and S. H. Vosko, Phys. Rev. 119, 912 (1960).

51. Sternheimer, R. M., Phys. Rev. 84, 244 (1951).

52. Poulis, N. J. and G. E. C. Hardenman, Physica 18, 201 (1952).

53. Jaccarino, V. and R. G. Shulman, Phys. Rev. 107, 1196 (1957).

54. Bloch, F., W. W. Hansen and M. Packard, Phys. Rev. 70, 474 (1946).

55. Hahn, E. L., Phys. Rev. 80, 580 (1950).

56. Reich, H. A., Phys. Rev. 129, 630 (1963).

57. Buchta, J. C., H. S. Gutowsky and D. E. Woessner, Rev. Sci. Instr. 29, 55 (1958).

58. Hultsch, R. A. and R. G. Barnes, Phys. Rev. 125, 1832 (1962).

59. Chapman, A. C., P. Rhodes and E. F. W. Seymour, Proc. Phys. Soc. (London) B70, 345 (1947).

60. Walchli, H. E. and H. W. Morgan, Phys. Rev. 87, 541 (1952).

61. Alder, F. and K. Halbach, Helv. Phys. Acta 26, 426 (1953).

62. Collins, T. L., Phys. Rev. 80, 103 (1950).

63. Rowland, T. J., Acta Met. 3, 74 (1955).

64. Lecander, Ronald G. Unpublished Ph.D. thesis. Ames, Iowa, Library, Iowa State University of Science and Technology. 1967.

65. Weinberg, D. L. and N. Bloembergen, J. Phys. Chem. Solids 15, 240 (1960).

66. Langer, J. S. and S. H. Vosko, J. Phys. Chem. Solids 12, 196 (1959).

67. Clogston, A. M., Phys. Rev. 125, 439 (1962).

68. Cheng, C. H., C. T. Wei and P. A. Beck, Phys. Rev. 120, 426 (1960).

69. Shull, C. G. and M. K. Wilkinson, Rev. Mod. Phys. 25, 100 (1953).

70. Wilkinson, M. K., E. O. Wollan, W. C. Koehler and J. W. Cable, Phys. Rev. 127, 2080 (1962).

71. Caroli, B., J. Phys. Radium 22, 356 (1961).

72. Van Ostenburg, D. O., D. J. Lamb, H. D. Trapp and D. E. MacLoed, Phys. Rev. 128, 1550 (1962).

73. Gutowsky, H. S. and B. R. McGarvey, J. Chem. Phys. 20, 1472 (1952).

74. Childs, W. J., L. S. Goodman and D. von Ehrenstein, Phys. Rev. 132, 2128 (1963).

75. Redfield, A. G., Phys. Rev. 130, 589 (1963).

76. Butterworth, J., Proc. Phys. Soc. (London) 83, 71 (1964).

77. Solomon, I., Phys. Rev. 111, 61 (1958).

78. Barnes, R. G. and T. P. Graham, Phys. Rev. Letters 8, 248 (1962).

79. Drain, L. E., J. Phys. Radium 23, 745 (1962).

80. Childs, B. G., W. E. Gardner and J. Penfold, Phil. Mag. 5, 1267 (1960).

81. Clogston, A. M., A. C. Gossard, V. Jaccarino and Y. Yafet, Phys. Rev. Letters 9, 262 (1962).

82. Shull, C. G. and R. P. Ferrier, Phys. Rev. Letters 10, 295 (1963).

83. Butterworth, J., Phys. Rev. Letters 5, 305 (1960).

84. Heiniger, F., Physik Kondensierten Materie 5, 285 (1966).

85. Dembigh, J. S. and W. M. Lomer, Proc. Phys. Soc. (London) 82, 156 (1963).

86. Schiff, Leonard I., Quantum Mechanics, McGraw Hill, New York, N.Y. (1955).

87. Shimizu, M., T. Takahashi and A. Katsuki, J. Phys. Soc. Japan 17, 1740 (1962).

88. Wood, J. H., Phys. Rev. 126, 517 (1962).

89. Freeman, A. J. and R. E. Watson, in Rado, G. T. and H. Suhl, eds. Magnetism IIA p. 167. Academic Press, Inc., New York, N.Y. (1965).

90. Lingelbach, R., Z. Physik Chem. (Neue Folge) 14, 1 (1958).

91. Overhauser, A. W., Phys. Rev. 128, 1437 (1962).

92. Lomer, W., Proc. Phys. Soc. (London) 80, 489 (1962).

93. Loucks, T. L., Phys. Rev. 139, A1181 (1965).

94. Brandt, G. B. and J. A. Rayne, Phys. Rev. 132, 1945 (1963).

95. Fedders, P. A. and P. C. Martin, Phys. Rev. 143, 245 (1966).

96. Moller, H. B., K. Blinowski, A. R. Mackintosh and T. Brun, Solid State Commun. 2, 109 (1964).

97. Werner, S. A., A. Arrott and H. Kendrick, J. Appl. Phys. 37, 1260 (1966).

98. Blatt, F. J., Phys. Rev. 108, 285 (1957).

99. DeSorbo, W., Phys. Rev. 130, 2177 (1963).

100. Suzuki, H., J. Phys. Soc. Japan 21, 2735 (1966).

101. Shimizu, M., T. Takahashi and A. Katsuki, J. Phys. Soc. Japan 18, 1192 (1963).

102. Andrew, E. R. and D. P. Tunstall, Proc. Phys. Soc. (London) 78, 1 (1961).

VII. ACKNOWLEDGEMENTS

The author wishes to express his gratitude to Dr. Richard G. Barnes for his guidance and patience during the course of this investigation.

Thanks are also extended to Dr. O. N. Carlson and his group for providing the metals and alloys used in this study and to Dr. C. V. Banks and his group for the chemical analyses of the alloys. The author is indebted also to Dr. D. T. Peterson for metallurgical advice; to Mr. R. D. Engardt for considerable aid in making the pulse measurements; and to Dr. B. R. McCart and Mr. D. R. Torgeson for helpful discussions and assistance.

My thanks go also to Dr. J. J. Kepes for his encouragement and to my wife, Madonna, for her support and understanding. Nor do I forget the moral support derived from the (usually) bright and shining faces of Mike and Tommy.

VIII. APPENDIX

A. Relaxation for the Case of Unequal Level Spacing

In this section we outline the spin-lattice relaxation behaviour of nuclei with spin I = 7/2 when the energy level spacings are rendered unequal by perturbations due to quadrupole interactions with a crystalline electric field. This is an extension to the spin 7/2 case of the results of Andrew and Tunstall (102). We consider the case of magnetic relaxation for the two different initial conditions, 1) all energy levels equally populated, 2) the central transition saturated while the remaining levels are in thermal equilibrium.

We can write, for the rate of change of population of the m^{th} level,

$$\frac{dn_m}{dt} = - n_m W_{m,m-1} - n_m W_{m,m+1} + n_{m+1} W_{m+1,m} + n_{m-1} W_{m-1,m} \qquad (A.1)$$

where $W_{i,j}$ is the probability of transition from the i^{th} to the adjacent j^{th} level and n_i is the population of the i^{th} level. The magnetic interaction connects only adjacent levels. The rate equation for the difference in population between adjacent levels can be written as

$$\begin{aligned}\frac{d(n_m - n_{m-1})}{dt} = &- n_m W_{m,m-1} - n_m W_{m,m+1} + n_{m+1} W_{m+1,m} \\ &+ n_{m-1} W_{m-1,m} + n_{m-1} W_{m-1,m-2} + n_{m-1} W_{m-1,m} \\ &- n_m W_{m,m-1} - n_{m-2} W_{m-2,m-1} \qquad (A.2)\end{aligned}$$

The probabilities for upward transitions are related to those for downward transitions by

$$W_{i,j} = W_{j,i} \frac{n_j^o}{n_i^o} \tag{A.3}$$

where the superscript denotes the equilibrium value of the population. If we assume that the quadrupole splittings are small compared to the Zeeman splitting, then the Boltzmann factors are the same for pairs of adjacent levels and the equilibrium population differences are the same, say n_o. The above equation can then be written in the form

$$\frac{d(n_m - n_{m-1})}{dt} = -2 W_{m,m-1} [n_m - n_{m-1} - n_o] + W_{m+1,m} [n_{m+1} - n_m - n_o] + W_{m-1,m-2} [n_{m-1} - n_{m-2} - n_o] \tag{A.4}$$

We define $N'_{i-1/2} = N_{i-1/2} - n_o$ where $N_{i-1/2} = n_i - n_{i-1}$. This allows us to write

$$\dot{N}'_{m-1/2} = -2 W_{m,m-1} N'_{m-1/2} + W_{m+1,m} N'_{m+1/2} + W_{m-1,m-2} N'_{m-3/2} \tag{A.5}$$

This is an equation for the population difference in excess of the equilibrium difference. For the spin 7/2 case this gives us a set of seven equations. Since we are discussing magnetic relaxation we have

$$W_{m,m-1} = W(I+m)(I-m+1) \tag{A.6}$$

and

$$W_{m,m-1} = W_{-m,-(m-1)} \tag{A.7}$$

The set of equations can then be reduced to four equations since $N_{m-1/2} = N_{-(m-1/2)}$ and the initial conditions are symmetrical. The equations are

$$\begin{aligned}
\dot{N}'_3 &= -14\ W\ N'_3 + 12\ W\ N'_2 \\
\dot{N}'_2 &= 7\ W\ N'_3 - 24\ W\ N'_2 + 15\ W\ N'_1 \\
\dot{N}'_1 &= 12\ W\ N'_2 - 30\ W\ N'_1 + 16\ W\ N'_o \\
\dot{N}'_o &= 15\ W\ N'_1 - 32\ W\ N'_o + 15\ W\ N'_{-1} \\
&= 30\ W\ N'_1 - 32\ W\ N'_o
\end{aligned} \tag{A.8}$$

This system has solutions of the form

$$N'_p = \sum_q a_{pq} e^{-\lambda_q t} \tag{A.9}$$

From Andrew and Tunstall we have the roots of the secular determinant

$$\lambda_{3,2,1,0} = 2W, 12W, 30W, 56W. \tag{A.10}$$

Using these roots to find the coefficients a_{pq} we have the solutions

$$\begin{aligned}
N'_3 &= a_{33}\, e^{-2Wt} + a_{32}\, e^{-12Wt} + a_{31}\, e^{-30Wt} + a_{3o}\, e^{-56Wt} \\
N'_2 &= a_{33}\, e^{-2Wt} + \tfrac{1}{6} a_{32}\, e^{-12Wt} - \tfrac{4}{3} a_{31}\, e^{-30Wt} \\
&\quad - \tfrac{7}{2} a_{30}\, e^{-56Wt} \\
N'_1 &= a_{33}\, e^{-2Wt} - \tfrac{1}{3} a_{32}\, e^{-12Wt} + \tfrac{1}{15} a_{31}\, e^{-30Wt} \\
&\quad + 7\, a_{30}\, e^{-56Wt} \\
N'_o &= a_{33}\, e^{-2Wt} - \tfrac{1}{2} a_{32}\, e^{-12Wt} + a_{31}\, e^{-30Wt} - \tfrac{35}{4} a_{30}\, e^{-56Wt}
\end{aligned} \tag{A.11}$$

The initial conditions for the first case, all transitions saturated, are $N_i' = -n_o$. Using this condition we find that the only non-zero coefficient is $a_{33} = -n_o$. Thus the approach to equilibrium is characterized by one relaxation time, $T_1 = (2W)^{-1}$ and the population difference between adjacent levels is governed by

$$N = n_o(1 - e^{-t/T_1}). \qquad (A.12)$$

In the second case we consider only the central transition saturated. So initially $N_o' = -n_o$, N_1', N_2', $N_3' = 0$. Solving for the coefficients we find that the regrowth of the central transition is governed by

$$N_o = n_o [1 - 0.21 \exp(-t/T_1) - 0.247 \exp(-6t/T_1) - 0.243 \exp(-15t/T_1) - 0.298 \exp(-28t/T_1)] \qquad (A.13)$$

The growth is characterized by four relaxation times and the initial rate is fourteen times faster than in the first case.